NUMERICAL MODEL AND EXPERIMENTAL BEHAVIOR OF CONCRETE BEAMS REINFORCED WITH PLAIN STAINLESS STEEL REBARS

MD. AHSAN HABIB

(*BSc Engg., WUB*)

A THESIS SUBMITTED FOR THE DEGREE OF

MASTER OF SCIENCE IN CIVIL ENGINEERING

DEPARTMENT OF CIVIL ENGINEERING
MILITARY INSTITUTE OF SCIENCE AND TECHNOLOGY

SEPTEMBER 2020

The thesis titled **"Numerical Model and Experimental Behavior of Concrete Beams Reinforced with Plain Stainless Steel Rebars"** submitted by **Md. Ahsan Habib**, Roll No: 1013110001, Session 2013-2014 has been accepted as satisfactory in partial fulfillment of the requirement for the degree of **Master of Science in Civil Engineering (Structure)** on 30th September, 2020.

BOARD OF EXAMINERS

1. …….....

   Lt Col Khondaker Sakil Ahmed, PhD, PEng — Chairman
   Associate Professor — (Supervisor)
   Department of Civil Engineering
   MIST, Dhaka

2. …….....

   Brig Gen Md Abul Kalam Azad, psc — Member
   Dean & Head — (Ex-Officio)
   Department of Civil Engineering
   MIST, Dhaka

3. …….....

   Maj Md Soebur Rahman, PhD, PEng — Member
   Associate Professor — (Internal)
   Department of Civil Engineering
   MIST, Dhaka

4. …….....

   Dr Nazrul Islam — Member
   Assistant Professor — (External)
   Department of Civil Engineering
   Bangladesh University of Engineering and Technology (BUET)

DECLARATION

I hereby declare that this thesis is my original work and it has been written by me in its entirety. I have duly acknowledged all the sources of information which have been used in the thesis.

This thesis has also not been submitted for any degree in any university previously.

_____

Md. Ahsan Habib

30 September, 2020

ABSTRACT

Stainless steel (SS) is gaining popularity as reinforcement of structural elements in Bangladesh mainly due to its enhanced corrosion resistance, improved performance against fire, and resilient behavior. This research investigates the flexural performance of concrete beam reinforced with locally manufactured stainless steel of the Grade 201 series. This experimental program included a total twelve reinforced concrete beams subjected four points bending test. Eight of them are SS reinforced concrete beams and the remaining four beams are reinforced by carbon steel (CS) as control specimens. Prior to conduct these tests, the mechanical properties of SS rebars and their bond strength in concrete are examined briefly. The tested beam specimens are divided into three categories based on their reinforcement ratio. Each group of beam consists of four specimens with low, medium, and high reinforcement ratios. The tested results of SS reinforced beams of each category are compared with that of the CS reinforced beams and also with the available codes. The experimental results in terms of the cracking moment showed a very good agreement with the code values as the differences of capacities within 10%. The ultimate moment capacity of tested SS reinforced beams also shows that theoretical value exceeds by a maximum of 30% compared to that of test results. Additionally, a series of finite element models are developed emulating the experimental program to understand the flexural response numerically. All twelve models are validated using finite element (FE) models in Abaqus v14.1. Crack propagation and damage patterns of experimental specimens matched well with that of the FE simulations. The outcome in terms of load-displacement relationships extracted from finite element analysis also supports the experimental results with minor deviance. The overall outcome of this study suggests that using SS as reinforcement of the beam is quite reasonable and can be used confidently as an alternative to CS.

ACKNOWLEDGEMENT

First and foremost, all praise and profound gratitude to the almighty Allah who is the most beneficent and the most merciful for allowing great opportunity and ability to bring this effort to fruition safely and peacefully.

The author conveys his heartiest gratitude to his supervisor, Lt Col Khondaker Sakil Ahmed, PhD, PEng., Associate Professor, CE Dept, MIST, for his systematic support and supervision in the dissertation. His guidance and suggestion worked as inspiration to unlock different new avenues for research. It was indeed a unique opportunity and special privilege for the authors to work with Dr. Ahmed, whose constant guidance made it possible to complete this study successfully. His active interest in this topic and valuable advice was the source of author's inspiration.

The author also appreciatively remembers the supports and encouragement of Assistant Professor Kamrul Islam, Maj Kamrul Reza and Mirza Mohaymenul Islam and everyone related to carry out the entire study. Finally, it is particularly important to thank my parents, siblings, intimate friends and relatives for their continuous support to finish my research. They are the key source of inspiration for all my achievements.

TABLE OF CONTENTS

LIST OF SYMBOLS, ABBREVIATIONS

Aa	Cross Sectional Area of Stainless-Steel Bar at the Bottom
A`a	Cross-Sectional Area of The Mild Steel Bar at the Top
- b	Width of The Beam Section
c	Distance to Neutral Axis Measured from Top Concrete Fiber
d	Effective Depth of the Beam Section
dc	Depth of Compression Reinforcement
Ea	Modulus of Elasticity of Stainless Steel Bar
Es	Modulus of Elasticity of Mild Steel Bar
f`c	Cylinder Compressive Strength of Concrete
f_t	Tensile Strength of Concrete
f_u	Ultimate Strength of Mild Steel Bar
f_{ua}	Ultimate Strength of Stainless Steel Bar
fy	Yield Strength of Mild Steel Bar
$f_{0.2}$	Nominal Yield Strength of Stainless Steel Bar
h	Depth of The Beam Section
Ig	Second Moment of Area of The Uncracked Section
k_m	Empirical Coefficient
k1, k2	Correction Factors
p	Longitudinal Reinforcement Ratio of Concrete Beam
M_c	Total Bending Moment Given By The Concrete with Respect to The Neutral Axis
M_{cr}	Cracking Moment of Concrete Beam
M_{cr},*p*	Predicted Value of Cracking Moment of Concrete Beam

$M_{cr,t}$	Test Value of Cracking Moment of Concrete Beam
M_u	Ultimate Moment of Concrete Beam
$M_{u,p}$	Predicted Value of Ultimate Moment of Concrete Beam
$M_{u,t}$	Test Value of Ultimate Moment of Concrete Beam
My	Yielding Moment of Concrete Beam
P	Concentrated Force Applied on The Distribution Beam
P_{cr}	Cracking Load
P_u	Ultimate Load
Δ_u	Midspan Deflection at P_u
Δ_y	Midspan Deflection at P_y
$\varepsilon`_a$	Strain in Compression Mild Steel Bar
ε_c	Concrete Strain at The Extreme Compression Fiber
ε_{cu}	Ultimate Strain of Concrete
ε_{ua}	Strain Corresponding to F_{ua}
ε_0	Concrete Strain at Peak Stress
$\varepsilon_{0.2}$	Strain Corresponding to $F_{0.2}$
FRP	Fiber Reinforced Polymer
SMA	Shape Memory Alloy
CRR	Corrosion Resistant Rebar
SS	Stainless Steel
ASTM	American Society for Testing and Materials
BS	British Standard
ACI	American Concrete Institute
AASHTO	American Association of State Highway and Transportation Officials
CHBDC	Canadian Highway Bridge Design Code

CEB FIP	European Committee for Concrete - International Federation for Pre-stressing
BNBC	Bangladesh National Building Code
CSA	Canadian Standards Association
GFRP	Glass Fiber Reinforced Polymer
SS	Stainless Steel
MS	Mild Steel
UTM	Universal Testing Machine
AISI	American Iron and Steel Institute
SAE	Society of Automotive Engineers

LIST OF FIGURES

CHAPTER 1 INTRODUCTION

CHAPTER 2 LITERATURE REVIEW

CHAPTER 3 EXPERIMENTAL PROCEDURES

CHAPTER 4 EXPERIMENTAL RESULTS

CHAPTER 5 NUMERICAL MODELING

LIST OF TABLES

CHAPTER 1

INTRODUCTION

1.1 General

The corrosion of steel reinforcement has been considered as the main cause for the deterioration of reinforced concrete structures,[1-3]. To increase the service life of concrete structures by preventing the corrosion of steel reinforcement, several protection measures such as increasing the concrete cover over the steel reinforcing bars, using low-permeability concrete, coating the steel bars with an epoxy polymer, and applying cathodic protection systems have been developed and implemented in real structures over the past decades[4, 5]. Although the adoption of these methods can reduce the corrosion problem in some cases, the corrosion of steel reinforcement is still a major problem for the concrete structures exposed to moist and aggressive environments. The use of non-corrosive reinforcement can be an effective strategy to overcome such corrosion problem in steel reinforcement. A promising class of non-corrosive materials is fiber reinforced polymers (FRPs), which consists of fibers in a polymer-based matrix[6]. Furthermore, the bond strength of FRP rebars varies with the manufacturing process and uncertainty of strength such weakness in shear is predominant [2, 7, 8]. The initial cost of FRP rebars are also very high compare to their alternatives in the local market.

Stainless steel reinforcing bars have also been considered as an alternative to carbon steel rebars to employ as a reinforcement in concrete structures [7-9]. Stainless steel contains a minimum of 10.5% chromium, which provides excellent resistance to corrosion by forming a very thin self-regenerating oxide layer[8]. Extensive research into the behavior of structural stainless steel has been reported in the literature including the flexural behavior[7-9] compressive behavior [10, 11] . and the mechanical characteristics [12-14].

Recently, stainless steels have become popular in load-bearing applications where durability, ductility, stiffness, and strength are required, as well as excellent fire resistance. Stainless steels are produced in different forms including sheet, plate, bar, tube, hot-rolled and cold-formed structural sections, fasteners, and fixings. Cold-formed sections fabricated from steel plates are the most commonly used products for structural members because they are the most readily available and are reasonably straight-forward to manufacture [12]

Fig 1. 1: Stonecutters bridge in Hong Kong. Adopted from Rabi, Cashell et al. 2019[15]

One of the earliest examples of the use of stainless steel reinforcement is The Stonecutters Bridge in Hong Kong and Sheik Zayed Bridge in Abu Dhabi, as shown in Figs. 1 and 2, respectively. These two bridges are reinforced with grade 1.4462 duplex stainless steel. Because of the relatively high initial cost, the stainless steel rebars are strategically placed and only used for the outer layer of the reinforcement in both projects, in the so-called splash zone. For example, austenitic grade 1.4301 stainless steel rebar was used to rehabilitate the pillars

Fig 1. 2 : Sheik Zayed bridge in Abu Dhabi. Adopted from Rabi, Cashell et al. 2019 [15]

and stone arches of the Knucklas Rail Bridge[16].Stainless steel reinforcement has also been used in another project, including the Progresso Pier in Mexico, as shown in Fig. 3, which was constructed in the early 1940s using grade 1.4301 austenitic stainless steel.

Fig 1. 3: The Progresso Pier in Mexico. Adopted from Rabi, Cashell et al. 2019 [15]

It has been in continuous service for over 70 years without any major repair or significant maintenance activities.

Many researchers have already been working on reinforcing material for concrete as a replacement of Mild Steel Rebar e.g. Fiber Reinforced Polymer (FRP), Shape Memory Alloy, etc. The importance of the usage of sustainable materials should be considered. Stainless steel (SS) can be a superior alternative of conventional mild steel and other reinforcing due to the fact that SS is already proved to be corrosion resistant, better performance against fire and most importantly recyclable. However, there are some key issues such as bonding, ductility, seismic performance, integration as a composite component and long term effect in applying SS as reinforcement of concrete that are needed to be addressed before their practical application.

Stainless steel industries in Bangladesh is still in developing stage and are expected to have an excellent prospect as the county is growing at a very high rate. Some of the available stainless-steel rebar available in Bangladesh stainless steel solid rebar is produced by Steel Tech which is cheaper than the other conventional stainless steel available in the international market due to low labor and operational cost. After investigating on its all properties, it is considered to be suitable for the following locations such as Hydraulic Structure (i.e., bridge, retaining wall, tunnels, harbor, and jetty) all over our country, where salinity problem occurs especially in the southern region of Bangladesh and where airborne of chlorides happens especially near the seaside area of Bangladesh. Since no research work on SS rebar has been planned or conducted earlier on this type of local stainless steel, there is a scope to work in this area and hence develop stainless steel industry where SS rebars can be employed as reinforcement of concrete.

1.2 Research Objectives

The specific objectives of this research work are:

1. To investigate the flexural behavior and mode of failure of concrete beams reinforced with Stainless and carbon steel rebars.

2. To determine the flexural performance of different stainless steel-reinforced concrete beams both experimentally and numerically (using finite element modelling tools).

3. To observe on Stainless and carbon steel reinforced concrete beam behaviour of reinforcement yielding, strength limit state, load-deformation response, and crack pattern.

1.3 Scope of Research

This research program consists of experimental investigations and numerical simulations. This experimental program included a total twelve reinforced concrete beams subjected four points bending test. Eight of them are SS reinforced concrete beams and remaining four beams are reinforced by carbon steel (CS) as control specimens. A total of twelve reinforced concrete beams were tested under four-point bending.

The numerical simulation of stainless steel reinforced concrete beams is performed using finite element program ABAQUS/CAE. The performance of the numerical model is studied by simulating several experimental beams from the literature. Comparisons are made between the finite element predictions and experimental results in terms of load versus deflection curves, ultimate capacities and failure modes of the beams.

1.4 Methodology

A total of twelve concrete beams reinforced were loaded under four point bending with a simple span of 1200 mm. Out of twelve beams, 4 specimens are controlled carbon steel and remaining 8 specimens are SS reinforced beams with an uniform cross section of 150 x 200 mm and the total length is 1500 mm long. All specimens have a same shear reinforcement ratio and carbon steel 4.5mm diameter stirrups were placed at spacing of 150 mm and 100 mm for the constant moment zone and the shear span zone as shear reinforcement, respectively. The concrete strength and longitudinal and shear reinforcement ratios were selected as the variable design parameters. There are five levels of longitudinal reinforcement ratios; low, moderate, beyond moderate, high, and extremely

high and the relative concrete strength between specimens having the same reinforcement ratio (1 = Lower, 2 = Higher) which can be translated to levels L, M,M', H and H' Letter (MS) refers to Mild steel as longitudinal steel reinforcement while letter (SS) refers to Stainless Steel as longitudinal steel reinforcement. All twelve samples will be validated numerically using finite element program ABAQUS/CAE.

1.5 Organization of the Thesis

The outcomes of the research carried out have been divided into different topics and presented in five chapters.

In chapter one, General remark with background, objectives, scope and methodologies of the present study are described briefly.

In chapter two, a through a chronological literature review on compressive strength, shear, and flexural behavior of different types of reinforced concrete beams are presented. The definition and various aspects of stainless steel are discussed in this chapter.

In chapter three, the experimental program is described in detail. In this chapter, the amount and type of material, properties, and mix design are mentioned. The experimental procedure is also mentioned in chapter three.

In chapter four, all experimental results including compressive strength, shear, flexural strength, mode of failure of concrete beams results are presented. In this chapter, the comparison among tests results is made and discussed in details.

In chapter five, All Experimental results are validated numerically using the finite element simulation by ABAQUS/CAE.

In chapter six, conclusions and relevant recommendations are mentioned for future analysis.

CHAPTER 2

LITERATURE REVIEW

2.1 General

Reinforcement corrosion is one of the most serious causes of deterioration of concrete structures, and thus reduced service life of the structures. Corrosion resistance plays a vital role in the stability of reinforced concrete structures[17, 18]. Stainless steel has emerged as a very attractive material for many applications including reinforcing potential in concrete structures. Stainless steel bars present a potential solution to this rebar corrosion problem. Few research studies on the behavior of structural stainless steel have been reported in the literature the flexural and behavior[11, 13, 14], compressive behavior [12, 19, 20], and the mechanical characteristics [21, 22]. This chapter summarizes The Mechanical properties, Chemical composition, and Specification of stainless steel used in this research are presented. This section focuses on past research performed on the behavior of reinforced concrete beams incorporating several reinforcements was also discussed. Finally. A chronological literature review is presented of previous research on the flexural behavior of reinforced concrete beams in this chapter.

2.2 Stainless Steel Reinforcement

Stainless steel (SS) was first produced in Germany and the UK in 1912 [23]. It was termed as rustless steel due to its high resistance to corrosion as compared to carbon steel. SS usually contains 10% chromium, which leads to the formation of a self-healing oxide layer [24]. Stainless-steel can tolerate chloride levels up to 7% as compared to 0.4% tolerated by carbon steel. The term stainless steel does not refer to a single metal. Instead, it is used for a group of corrosion-resistant alloys. The primary alloy in stainless steel is chromium with a minimum content of 10.5%. It forms a chromium oxide layer on the bar surface that provides corrosion protection. If this protective layer is damaged, oxygen enables its self-

healing [25]. Corrosion resistance can be further improved by adding other alloys including chromium, nitrogen, molybdenum, titanium, and nickel, which makes stainless steel suitable for use in acid media [26]. Other alloys include carbon and manganese. Manganese improves hot working properties, strength, and toughness [27]. The composition of stainless-steel bars defines their corrosion resistance, mechanical properties, and weldability [26]. Therefore, the excellent corrosion resistance and high chemical stability of SS lead their application for bridges, coastal equipment, and the marine environment. Corrosion resistance plays a vital role in the stability of reinforced concrete structures [17, 18] when exposing ordinary steel reinforcements and SS reinforcements to chlorides, the damage of ordinary steel reinforcements is more serious than that of SS reinforcements [28-30].

2.2.1 Specification of Stainless Steel

Widely used specifications for stainless steel are BS6744 and ASTM A955 [31, 32] Generally, the SS rebar diameter range is from 8mm to 25mm and produced in coils and straight bars cut up to 12 m in length. Earlier bar profile and strength classes specified in EN 10080 and ASTM A615/A615M but later on all the items adopted in BS 6744 and ASTM A955. The material designation is assigned differently in two codes like BS 6744 followed EN 10088-1 and materials in ASTM A955 are designated following ASTM A276 [33, 34]. Earlier the most common stainless steel used in construction is Grade 1.4307 (304L), Grade 1.4311 (304LN), Grade 1.4162 (LDX 2101), and Grade 1.4362 (2304). Day by day the specification and other details are changing based on the demand. Currently most widely used SS rebar is Grade 1.4307 (304L) and it is a low carbon, standard chromium-nickel austenitic stainless steel. Grade 1.4162 (LDX 2101) is low nickel duplex stainless steel, known as a lean duplex. Chemical composition difference between 304, 316, and 2205 are shown below in Table 2.1.

Table 2. 1: Chemical composition of different grades of SS. Adopted from Gardner et el. (2015) [Gardner et el. (2015)]

Chemical composition (% by mass)			
Element	Steel Designation (Number)		
	1.4301(304)	1.4401(316)	1.4462(2205)
Carbon (C)	< 0.07	< 0.07	< 0.030
Chromium (Cr)	17.00 to 19.50	16.50 to 18.50	21.00 to 23.00
Nickel (Ni)	8.00 to 10.50	10.00 to 13.00	4.50 to 6.50
Molybdenum (Mo)	-	2.00 to 2.50	2.50 to 3.50
Manganese (Mn)	< 2.00	< 2.00	< 2.00
Silicon (Si)	< 1.00	< 1.00	< 1.00
Phosphorus (P)	< 0.045	< 0.045	< 0.035
Sulphur (S)	< 0.015	< 0.015	< 0.015
Nitrogen (N)	< 0.11	< 0.11	0.10 to 0.22
Titanium (Ti)	5×C to 0.70	5×C to 0.70	-
Tungsten (W)	-	-	0.50 to 1.00

2.2.2 Type & mechanical properties of SS

Three types of stainless-steel bars are readily available in the construction market. These are austenitic, ferritic, and ferritic-austenitic (duplex). Ferritic stainless steel has a chromium content of about 30% and is characterized by possessing ferromagnetic properties. Its tensile strength is higher than that of austenitic stainless steel, but its workability is not as efficient as other types. It is not recommended to be used for applications requiring long-life span or exposure to chloride ions [26].

Austenitic stainless steel has 17 to 25 % chromium and 8 to 26 % nickel. It has excellent toughness, ductility, and weldability as compared to both ferritic and duplex stainless steel.

Additionally, its high ductility has promoted its use in seismic areas. Austenitic stainless steel is available as a low-carbon chromium-nickel alloy (grades 304, 304L, 316, and 316L), which contains up to 0.3% carbon. It is used in a chloride environment. It is also available as chromium-manganese-nitrogen alloy[26].

Ferritic-austenitic (duplex) stainless steel has a binary structure of ferrite and austenite. It contains up to 8% nickel, and between 22 and 28% chromium. Molybdenum improves its corrosion resistance. It has improved ductility and toughness as compared to ferritic stainlesssteel and has improved strength and corrosion resistance as compared to both austenitic and ferritic stainless steel [25]. Duplex stainlesssteel grades include 2205, 2304, and 2507.

The stress-strain relationship for different types of stainless steels is illustrated in Figure 2.1 [35]. Note that only the austenitic and the ferritic-austenitic (duplex) steel are relevant as reinforcement. Austenitic and duplex (and ferritic) grades of steels show early plastic deformation in the test, and continue to sustain increasing load with increasing strain. Cold working (cold-formed SS) will increase the strength of the steels and is therefore used to meet the requirements for use as reinforcement in concrete. Cold working usually results in martensite formation in 1.4301 types, whereas in 1.4401/1.4436 and duplex materials, this is not the case. For the austenitic types cold working results in a reduction of the elongation from 40% to 20- 25%. For small dimensions (<16 mm) also warm working (at a temperature somewhat lower than normal for such process) may be used for increasing the strength, resulting in mechanical. Another way of increasing strength is the addition of nitrogen (0.15-0.2%). This is however not sufficient to reach the required strength and must therefore be combined with either cold or warm working properties similar to those obtained by cold working.

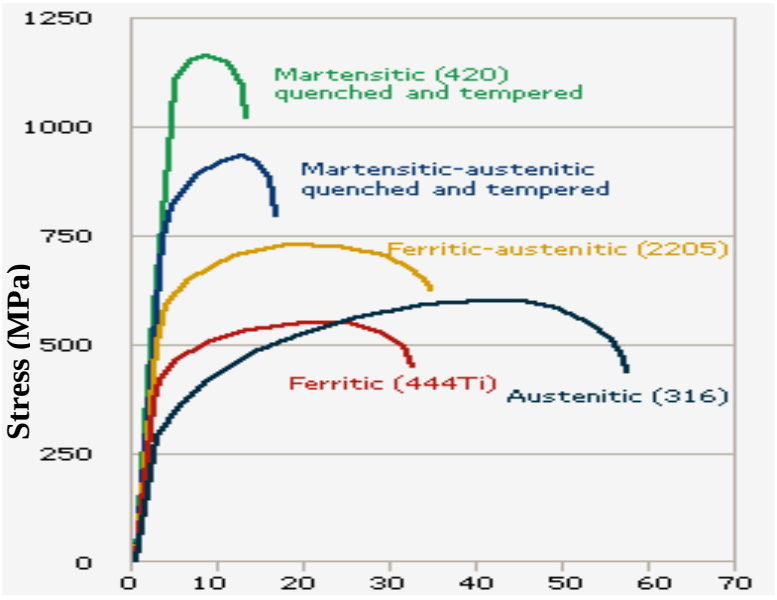

Fig 2. 1: Stress-strain curves for different stainless steels at room temperature, Adopted from Outokumpu (2006)

To characterize the design strength of such strain hardening materials, proof strength is defined and determined as the tensile stress (RBP0, 2B) at elongation (strain) 0.2 %., stainless steels can be produced as ribbed bars within the normal range of strength and deformability required for application in concrete. The modulus of elasticity (E) for the relevant SSR is about 200 kN/mm^2 in the same range as for carbon steel reinforcement (210 kN/mm^2). Owing to their excellent mechanical properties in the as-rolled conditions, duplex steels are of particular interest as material for reinforcement. For example, the duplex steel of grade 1.4462 (X2CrNiMoN 22-5) as cold-rolled, has a proof strength of 950 MPa, the tensile strength of 1059 MPa, and elongation of 14 % for 10 mm bars.

2.2.3 Influence of Chromium

Stainless steels are chromium containing steel alloys. The minimum chromium content of the standardized stainless steel is 10.5%. Steel with lower chromium content should not be termed "stainless". Chromium is the main alloy which provides the steel with

improved corrosion resistance and increased ductility. This improved corrosion resistance can be seen in Figure 2.2.

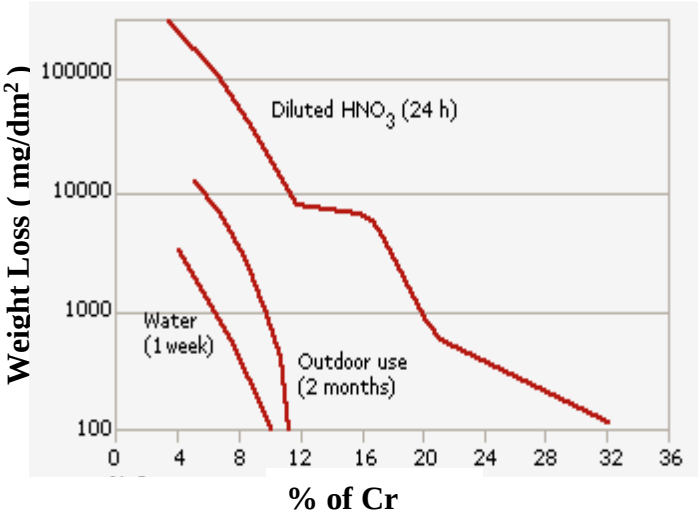

Fig 2. 2 : Influence of chromium on the corrosion resistance of stainless steel, Adopted, from Outokumpu (2006)

The improved corrosion resistance is due to a thin chromium oxide film that is formed on the steel surface and creates a so-called passive condition. It is important to realize that oxygen is required for the oxide film to form. The passivity is a dynamic process that is influenced by the surrounding environment, and especially temperature and humidity. The extremely thin chromium oxide film is also self-repairing under the right conditions, which includes the presence of oxygen. Besides chromium, typical alloying elements are molybdenum, nickel, and nitrogen. Nickel is mostly alloyed to improve the formability and ductility of stainless steel. Alloying these elements brings out different crystal structures to enable different properties of the steel for machining, forming, welding, etc.

2.3 Alternative Reinforcements of Concrete Beams

Usually, carbon steel with different grades is widely used as reinforcement of concrete structures. However, other reinforcement such as alloy steel, carbon fiber reinforced polymer, glass fiber reinforced polymers are also used as potential alternatives of carbon

steel after recent development. This section focuses on past research performed on the behavior of different hybrid reinforcements are discussed.

2.3.1 Epoxy-Coated Reinforcing Steel

Currently, the primary corrosion protection system for bridge decks in the United States is epoxy-coated reinforcing steel. Epoxy-coated reinforcing steel has been used in approximately 20,000 reinforced concrete bridge decks since the early 1970s and is estimated to have saved taxpayers billions of dollars in rehabilitation costs [36]

Epoxy-coated reinforcement was developed in the early 1970s, in response to the need for better corrosion protection on reinforced concrete bridge decks. However, epoxy-based coatings are not impermeable to water [37] Epoxy coatings reduce the magnitude of macrocell currents, which are responsible for extensive deterioration when they develop in bridge decks [38] Because the protective ability of epoxy coatings depends on their ability to act as both a physical and electrical barrier, effective quality control measures must be taken during coating of the bars and subsequent handling, shipping, and storage of the bars [38] If, when chloride ions arrive at the surface of the reinforcement and corrosion will take place under the coating. This corrosion will occur at a rate similar to that of a bare reinforcing bar in an acidic environment, which is faster than the corrosion of bare steel in concrete. Other studies have found that reinforcement in concrete with high moisture content generally suffers reduced adhesion of the [39-41] unfortunately, epoxy-coated reinforcement is never entirely free of defects. However, the question remains open as to whether epoxy-coated steel provides adequate long-term protection to reinforced concrete highway structures that are exposed to moisture and chlorides.

2.3.2 FRP Reinforcement

The idea of making composite materials by combining two different materials is not new and can be dated back to the ancient Egyptians when they used a straw to reinforce their

mud and make a stronger composite material. The fiber-reinforced polymer is just a later version of this idea [42].

In the 1980s in the USA a protrusion company entered the FRP reinforcing bar industry under the name of International Grating, Inc [43]. They developed sand coated glass FRP bars followed by the development of deformed FRP bars by Marshall Composites Inc in the 1990s. These experiments started to be undertaken with carbon FRP with deformed and sand coated surfaces [44]. In Europe, particularly in Germany, FRP was first used as concrete reinforcement in the construction of a prestressed FRP bridge in 1986 [45]. From 1991 to 1996 the European BRITE/EURAM project has undertaken extensive research on testing and analysis of FRP [45].

Currently, different types of Fibre Reinforced Polymer (FRP) rebar for reinforcing concrete structures are available, which are classified by fiber type as shown in Figure 2.3.

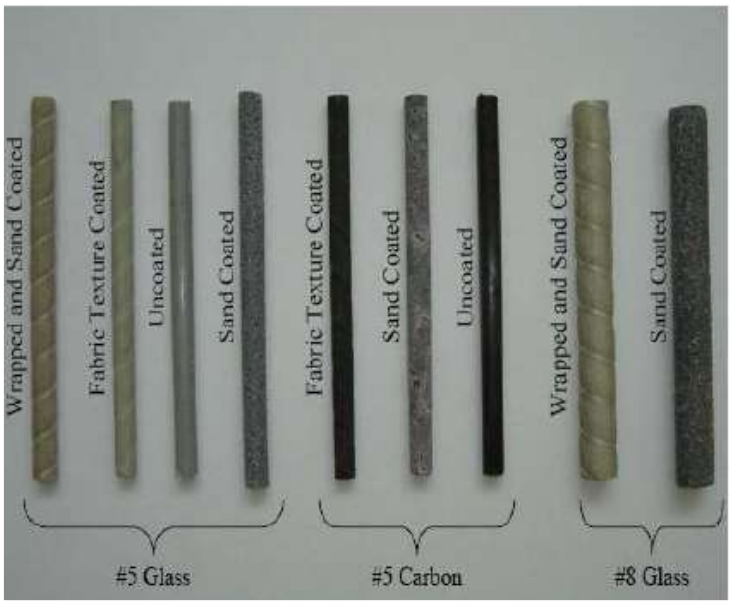

Fig 2. 3 : Samples of FRP Reinforcement Configuration, Adopted from Virmani and Clemena 1998 [36]

2.3.3 Metallic Coatings and Solid Metallic Reinforcing Bars

Solid metallic bars made of corrosion-resistant materials such as stainless steel have also been used in reinforced concrete structures. These materials must be able to serve as

reinforcement as well as resist aggressive environments. For years, metallic coatings have been used successfully to prevent corrosion of steel in environments other than concrete, leading to the anticipation that they could also protect steel in concrete. Metallic coatings for reinforcing steel can be divided into two categories, sacrificial or noble. Sacrificial coatings are made up of metals that have a more negative corrosion potential than steel, such as zinc. If the sacrificial coating is broken, a galvanic cell is set up and the coating corrodes while protecting the steel. Noble coatings such as copper and nickel do not corrode in concrete, but if the coating is broken, any exposed steel becomes anodic and will corrode [46] Galvanized steel was tested as part of a study of the effectiveness of corrosion inhibiting admixtures published by the Virginia Transportation Research Council in 1999 [36] Galvanized steel was observed to be providing good protection in the higher quality concrete. The specimen reinforced with galvanized steel seemed to be performing well for concrete with a w/c ratio of 0.45, with no cracks from corrosion visible at the time of inspection. The other galvanized steel specimen had a w/c ratio of 0.71 and exhibited excessive cracking.

Results of both laboratory and field studies on galvanized reinforcement have been conflicting [47]. A panel was formed in 1982 to resolve this discrepancy and came to the following conclusions[18]. Laboratory studies with aqueous solutions have shown that zinc has a higher chloride concentration level than steel at the onset of corrosion. This higher threshold helps to explain why galvanizing can delay the onset of corrosion in outdoor specimens. Stainless steel and stainless steel-clad reinforcement have been used in several structures in the past 15 years, but none of these structures is old enough that corrosion damage would be expected, even if no protection measures had been used. So far, stainless steel reinforcement is performing satisfactorily.

2.3.4 Shape Memory Alloy

Recently, a new group of alloys known as Shape Memory Alloys (SMAs) has emerged in the research community. Shape memory alloys (Fig:2.4) can sustain large deformations; Besides, SMAs can dissipate energy through hysteretic damping and be heat-treated to attain comparable strength to conventional deformed reinforcement. The unique properties of SMAs can address some of the shortcomings of conventional deformed reinforcing bars; specifically by controlling permanent strains. There are some disadvantages, including high cost, which leads to optimization of the material and the use of mechanical couplers to connect to conventional steel; difficulty in machining the material; the super elastic properties on the operating temperature, and the low elastic modulus that can result in larger displacements under service loads (Fig: 2.5). Nickel–Titanium (NiTi), consisting of approximately 56% nickel and 44%titanium alloy, is the most common type of SMA investigated for structural applications. [18]. Several studies have focused on material characterization and mechanical properties of super elastic NiTi bars and wires to evaluate the material for use in structural applications. Des Roches et al.[48]

Fig 2. 4: SMA and conventional reinforcement samples. Adopted from Cramer, Covino Jr et al. (2002) [17]

demonstrated that SMA in wire form experienced higher strength and damping properties compared to SMA bars; However, the re-centering capabilities based on residual strains

were not affected by the form of the SMA. A study by Tyber et al.[49] on large diameter NiTi bars revealed that transformation temperatures and hardness depended on bar heat treatment and not bar diameter. McCormick et al. [17] studied the deformation behavior of large-diameter super elastic bars.

Fig 2. 5: Larger Displacements, Adopted from Pérez-Quiroz, Terán et al. 2008 [18]

2.4 Existing Experimental Work of Concrete Beams

Concrete beams reinforced with alternative reinforcing steel have been studied for the last few decades. A chronological literature review of the research work conducted on concrete beams with different hybrid reinforcement is presented briefly in this section.

2.4.1 Robert F. Mast, Mina Dawood, Sami H. Rizkalla and Paul Zia (2008)

This paper presents a methodology for the flexural strength design of concrete beams reinforced with high-strength reinforcing steel that conforms to the requirements of ASTM A1035-07. The design method is based on simple analysis techniques that satisfy the fundamental principles of equilibrium and compatibility. Strain limits for tension-controlled sections and compression-controlled sections are proposed that are consistent with the approach of the current and past ACI 318 Codes. The stress-strain characteristics of the reinforcement are quite different from conventional Grade 60 (400 MPa) steel reinforcement. The new steel is considerably stronger than conventional reinforcing steel

and lacks a well-defined yield point. The flexural behavior of concrete beams reinforced with high-strength reinforcing bars has been investigated experimentally by several researchers. The research indicates that, when properly designed, beams reinforced with high-strength reinforcing bars will achieve similar but higher strength characteristics to beams reinforced with conventional steel reinforcements [50].

2.4.2 Issa, M.S., Metwally, I.M., and Elzeiny, S.M., (2011)

The experimental program consisted of seven concrete beams having the same concrete dimensions and reinforcement. The tested beams were classified into four groups according to the internal fiber types used. The first type of beams had no internal fibers, the second type had polypropylene fibers, the third type had glass fibers and the fourth type had steel fibers. The major aim of this paper was to improve the ductility of beams reinforced with FRP rebars. The experimental results of tests showed that using GFRP as the main reinforcement for the concrete beams achieved reasonable flexural strength. Also, the theoretical results calculated using ACI 440 code showed good agreement with the experimental results with an error of about 20%. The results of the current research indicated that all types of fibers used improved the ductility of FRP- reinforced concrete beams. It was found that the span-to-experimental service load deflection ratio is relatively high when compared to the usually accepted ratio of about span/250 [2].

2.4.3 Tejaswi and Ram (2015)

The authors present a comprehensive study of Two plain concrete beams, Six Reinforced concrete beams used in this investigation. To observe the first crack at which load and corresponding deflection this process is continued for all beams and also note the ultimate load with the corresponding deflection for all beam sections. The main objective of this study is to obtain the relation between loading and the corresponding deflection of a simply supported beam when it is subjected to a point load. To predict the flexural behavior of any brittle material like concrete, the load-deflection method on three points was essential. The

three-point method is the way to compute the deflections due to applied loads to analyze the flexural behavior. In this study the experimental set up was made to investigate the following:a) Loads and corresponding deflections, b) The effect of length and cross-sections on deflections per unit load. The following conclusions can be stated based on the evaluation of the analyses of the calibration model. 1. From the analytical investigation, it was observed that under reinforced ratio is the best type of reinforcement ratio among the others since it shows the greatest warning zone before failure.[51].

2.4.4.Rabi, M., K. Cashell, and R. Shamass, (2019)

In this study, the author reported results from The FE model is validated using five reinforced concrete beams from different experimental programs, Beams were reinforced with austenitic and duplex stainless steel rebars in grade 1.4311 and 1.4362, respectively. As these are the only two stainless steel reinforced concrete beam tests that have been found in the literature, three other beams containing carbon steel reinforcement are also included in the validation exercise for additional robustness. The details of geometry and reinforcement of these beams. All of the beams were tested under monotonic loading, in displacement control. It is concluded that the proposed analytical models provides a reliable solution for predicting the capacity of concrete beams reinforced with stainless steel[15]

Here also discuss the other inventor’s invention in this sector against eliminating the problem of steel corrosion in reinforced concrete structures

2.4.5 Qingfu Li, and Wei Guo (2020)

The authors present a comprehensive study of the flexural characteristics of stainless steel (SS) reinforced concrete beams. They conducted experimental work on six concrete beams reinforced with SS as shown in Figure 2.6

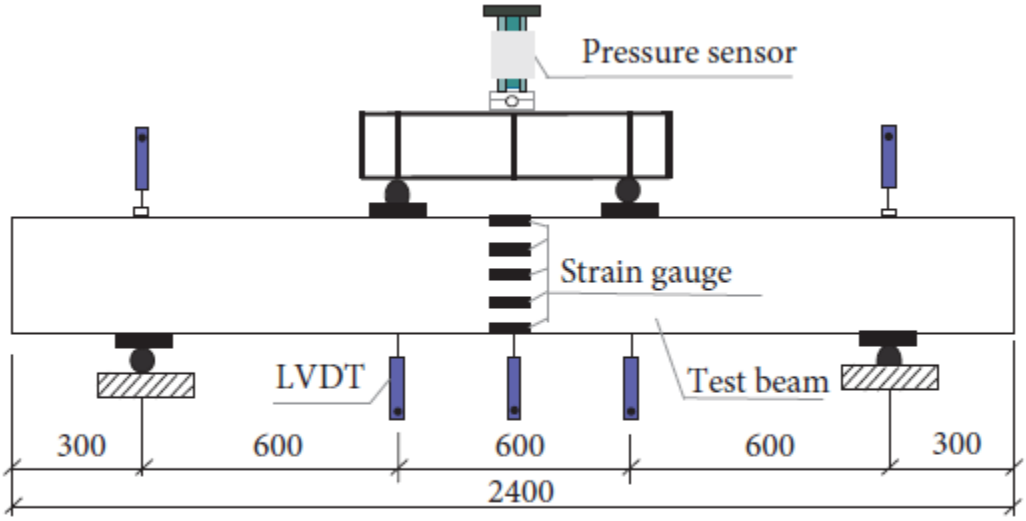

Fig 2. 6 : Instrumentation setup and load distribution (all dimensions in mm), Adopted from Qingfu Li,and Wei Guo (2020) [71]

The test results indicated that the failure mode of SS reinforced concrete beam can be divided into three stages: elastic stage, cracking stage, and failure stage as presented on Figure 2.7. Under the same reinforcement condition, load-bearing capacities of the SS reinforced concrete beams (the normal section and the oblique section) are significantly higher than those of the ordinary reinforced concrete beams. In addition, the prediction of the cracking moment and bearing capacity calculated by ACI 318-14.

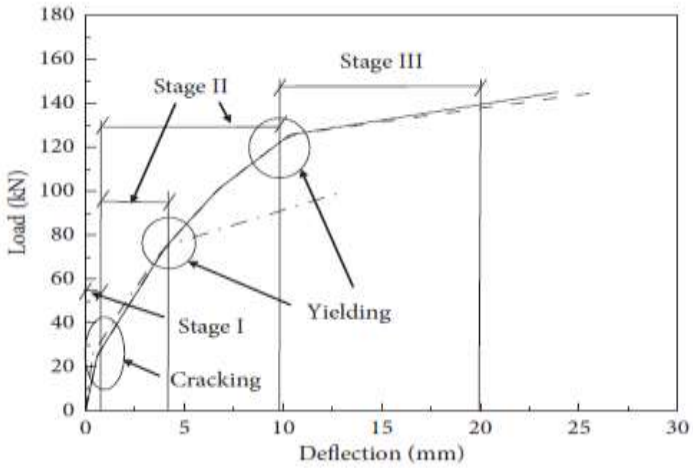

Fig 2. 7 : Typical load-deflection curves of all flexural beams tests Adopted from Qingfu Li,and Wei Guo (2020) [71]

Cracking Moment calculation of the cracking moment in the Chinese code and the American code is different. Equation (3) shows the calculation method of the theoretical concrete cracking moment in ACI 318-14.

$$M_{cr,c}^{A} = \frac{f_{r} I_{g}}{y_{t}} \quad \text{(2.1)}$$

In equation: 2.1, where $M^{A}_{cr,c}$ is the theoretical value of the concrete cracking moment. f_r is the flexural tensile strength of concrete, $f_{r0.62}$ $f_{c'}$, $f_{c'}$ are the compressive strength of the concrete cylinder test block, and its conversion relationship with the cubic compressive strength f_{cu} is $f_{c'}$ $0.8f_{cu}$. I_g is the sectional resistance moment on the centroid axes, regardless of the area of the reinforcement. y_t is the distance between the centroidal axis and the edge of tensile concrete [24].

2.5 Motivation and Research Gap

Over the years, many researchers have performed various works to prove their attention to improving corrosion problems in concrete structures. The corrosion of steel reinforcement has been considered as the main cause for the deterioration of reinforced concrete structures. Prioritizing this problem, locally made SS which is considered as the most economical stainless steel available in Bangladesh is taken into consideration to be applied as the potential alternative of carbon steel. Currently, SS is found available in round shape with a smooth finish in Bangladesh. So, it has been planned to evaluate the flexural behavior of concrete beams reinforced with plain stainless steel rebar which is expected to have higher corrosion resistance and improved mechanical properties. Moreover, no flexural test was conducted using this type of rebar earlier. Material properties of this rebar are also unknown and no codes or specifications are available for their application as rebar. Therefore, this research program performs the experimental studies and numerical analyses on the flexural behavior of concrete beams reinforced with plain stainless-steel rebar.

2.6 Summary

Previously conducted experimental investigations on the materials like CFRP, GFRP, conventional high strength steel, and SS and their application as reinforcement of concrete beams are presented in this chapter. The common findings in all the studies were improved load carrying capacity or ductility, reduced mid-span deflection, and improved ductility and hence more resilient applications. In our present study, the targets remained the same in a sense to find an alternative of conventional steel that may show improve performance against corrosion and seismic events. SS is expected to show desired qualities as reinforcement of concrete structures. Because of finding the proof of its performance, a test program of SS reinforced concrete beams with a comparative study with the conventional steel may give the light in the application SS as reinforcement. In addition, numerical models of SS reinforced concrete beams using FE method may further strengthen the proposed work through the validation. The research work on the application of stainless steel in concrete beams is very limited. This study is expected to be a new contribution that may help to improve the design guideline and practitioners to build confidence in applying SS as a reinforcing bar of concrete structures.

CHAPTER 3

EXPERIMENTAL PROCEDURES

3.1 General

To accomplish the aspiration of investigating the flexural behaviour of Stainless Steel (SS) reinforced concrete beams, a test program consisting of 12 beams was planned. These beams were reinforced with plain Stainless Steel (SS) rebars. All of the beams possessed enough transverse reinforcement to prevent shear failure, thus the desired failure mode was consistently flexural (either top concrete crushing or bottom reinforcement rupturing). The major variables in this program were concrete strength, type of SS bars, and hence the longitudinal reinforcement ratio. The detailed arrangement of the Mild Steel (MS) and Stainless Steel (SS) bars and material properties of concrete, individual test specimens, and test setup are presented in this chapter. In brief, this chapter presents the beam specimen preparation, experimental program, research strategies, test setup, data acquisition system and processes and overall methodology.

3.2 Material Properties

This section highlights the properties of the materials used in this experimental procedure. Various types of tests were performed on stone chips, sand, and cement to determine the material specification. Sieve analysis was conducted to get the gradation of aggregate. Aggregate properties such as specific gravity, absorption capacity, unit weight were also illustrated.

3.2.1 Cement

All cement used for the casting of concrete beams was ordinary Portland cement (CEM I) conforming to the requirements of the ASTM C 150. All concrete beams with different reinforcement arrangements and types were casted with the same brand of cement. All

types of cement were delivered from the same shipment so that their manufacturing dates are the same. Subsequently, they were stored in the laboratory with necessary precautions to carefully protect them against moisture and exposure to air.

3.2.2 Water

Water is a key ingredient of concrete. The property of water used in the concrete work was potable, free from oil and other organic impurities. Ordinary tap water was used as mixing water throughout the mixing procedure.

3.2.3 Aggregate

3.2.3.1 Sand as Fine Aggregate

Best quality coarse sand (brown) locally known as 'Sylhet sand' as shown in Figure 3.1 (d) was used as the fine aggregate. The sieve analysis was carried out as per ASTM C136 (ASTM 2006)[52]. The sieve analysis result indicated that the fine aggregate is well-graded having fineness modulus (F.M) 2.5.

Different basic tests were performed on coarse and fine aggregate such as water absorption capacity, moisture content, unit weight and specific gravity. ASTM C128 is followed as a standardized procedure for determining the specific gravity of the fine aggregate that passes the 4.75-mm (No. 4) sieve, using a water pycnometer. The specific gravity of sand was found 2.60.

3.2.3.2 Specific Gravity Test of Coarse Aggregates

This method is a modification of ASTM C 127 that provides a standardized procedure for determining the specific gravity of coarse aggregate as shown in figures 3.1a, 3.1b, & 3.1 c that retains the 4.75-mm (No. 4) sieve. The specific gravity of the stone aggregate was found 2.64, respectively.

a b c d

Fig 3. 1 : Types of aggregate used in research, here (a) ½" passing and ¼" in retained, (b) ¾ " passing and ½ " in retained, (c) 1" passing and ¾ " retained, (d) Stack of Sylhet Sand

3.3 Properties of Steel Reinforcement

Both mild steel and stainless steel were used in this research program. Locally produced well established 72.5 grade mild steel was used as the main flexural reinforcement of 4 beam specimens. In addition, shear reinforcement of all beam specimens was also planned to be mild steel though 8 beam specimens contained SS as main reinforcement. Properties of both types of reinforcement were determined through tensile tests using universal testing machine (UTM) before the rod binding of the proposed beam specimens.

3.3.1 Conventional Steel Reinforcement

Locally produced Mild Steel bars grade 72.5 were tested in UTM to find their exact mechanical properties. The stress-strain behavior of both 10mm and 12mm MS bar is presented in Figure 3.2. As per the test result, the yield of MS rebar was found to be 527MPa which is quite reasonable for 500-grade carbon steel rebars. The ultimate strength of CS rebars was found to be 713 MPa. Both rebars showed identical mechanical properties of 500 grade (72.5 grade) mild steel rebar. The elongation of the rebars varies in a range of 20 to 24%.

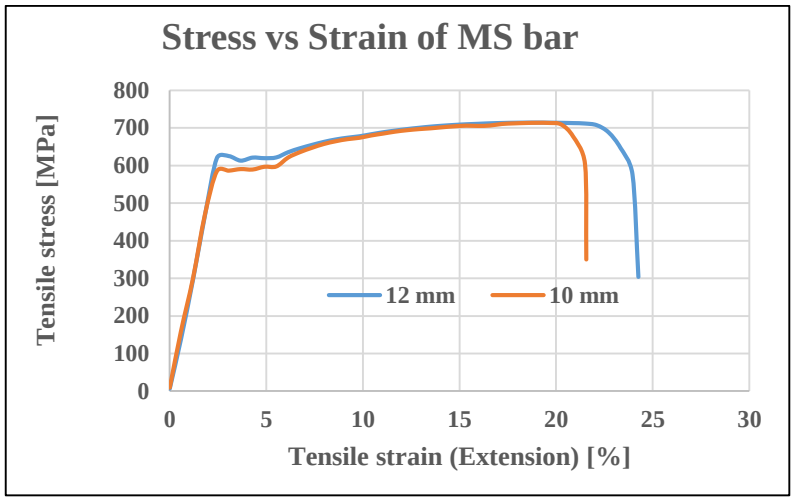

Fig 3. 2 : Stress-strain behaviour for mild steel

3.3.2 Mechanical Properties of Stainless Steel

In order to investigate the mechanical properties of this local stainless steel rebar's, tensile strength tests are conducted on both the 10mm and 12mm dia rebar samples using the universal testing machine as shown in Fig. 3.3, 3.4 and 3.5. Based on the tensile strength test data, the mechanical properties of SS rebar is presented in Table 3.1. The experimental results show that the yield strength at 0.2% strength is 888 MPa with an ultimate strength of over 1000 MPa whereas the strain at the ultimate strength of the SS rebar is 20% higher than that of the carbon steel. This data has been further used in the numerical analysis of the beams conducted in this study.

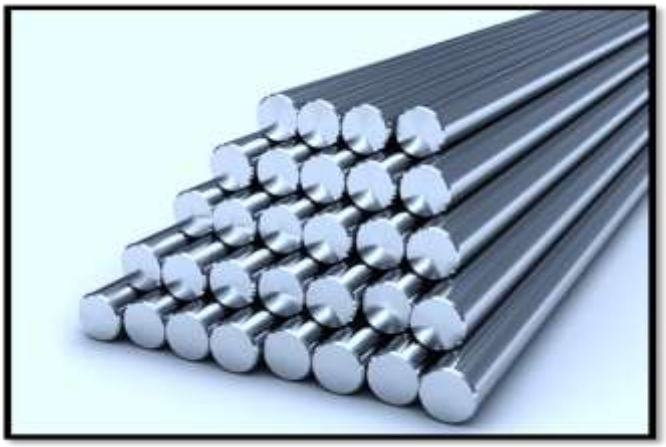

Fig 3. 3: Plain Stainless Steel Rebar. Adopted from Google.com (2020) [69]

Fig 3. 4 : Plain Steel Stainless Steel Rebar samples

Fig 3. 5 : Photographs of Tensile Strength Test ASTM A955

Table 3. 1: Mechanical properties of reinforcement

Mechanical properties of Mild steel and Stainless Steel bars.								
Dia. (mm)	Mild Steel bar(M.S)			Stainless Steel Bar(S.S)				
	Yield strength fy (MPa)	Ultimate strength fu (MPa)	Modulus of elasticity Es (GPa)	Nominal yield strength f0.2 (MPa)	Strain Ɛ 0.2 corresponding to f0.2 (%)	Ultimate strength *fuss* (MPa)	Strain Ɛ ua corresponding to *fss* (%)	Modulus of elasticity E*ss* (GPa)
12	527.49	709	205	887	0.461	1015	13.58	**192**
10	592.88	713	205	889	0.449	1110	20.0	**198**

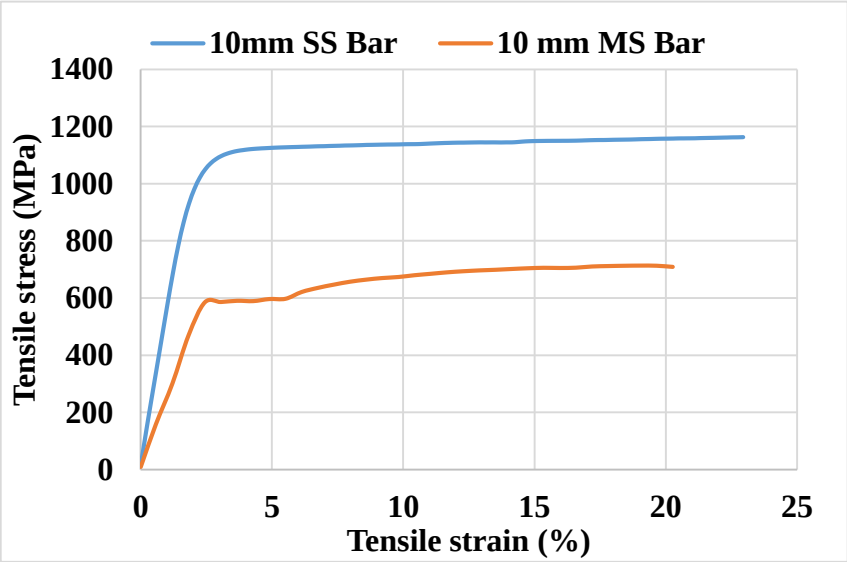

Fig 3. 6 : Tensile tests results comparison between MS and SS bar

3.3.3 Chemical Composition

Local industries of Bangladesh manufactures stainless steel whose grade is quite different than other neighboring countries. The chemical composition of the SS rebars is presented in Table 3.2 which is obtained from the composition test at the laboratory. The chemical of the stainless steel reflects that such properties and proportions of ingredients lie in 200 series SS (grade 201).

Table 3. 2 : Alloy composition of Stainless-steel rebar

Name of the Alloy	Composition of alloys. (Weight, %), 10mm	Composition of alloys. (Weight, %), 16mm
Carbon (C)	0.0929	0.0918
Silicon (Si)	0.213	0.25
Manganese (Mn)	09.36	09.70
Phosphorus (P)	0.0465	0.0415
Sulfur (S)	<0.0005	<0.0005
Nickel (Ni)	1.37	1.47
Chromium (Cr)	13.60	12.92
Copper (Cu)	1.44	0.997
Nitrogen (N)	0.0838	0.101
Iron (Fe)	73.49	74.07
Molybdenum (Mo)	0.0238	0.0125
Aluminum (Al)	0.0020	0.0030
Cobalt (Co)	0.0870	0.134
Niobium (Nb)	0.0133	0.0091
Titanium (Ti)	0.0033	0.0034
Vanadium (V)	0.0701	0.0961
Tungsten (W)	0.0192	0.0186
Lead (Pb)	<0.0050	<0.0050
Tin (Sn)	0.0105	0.0083
Boron (B)	0.0007	0.0010
Calcium (Ca)	0.0005	0.0007
Selenium (Se)	0.0123	0.0110
Antimony (Sb)	0.0050	0.0061
Tantalum (Ta)	0.0567	0.0541

3.4 Experimental Program and Data Acquisition

The strength and serviceability of structural components largely depend on the concrete strengths, reinforcement, and environmental parameters like temperature, relative humidity which mostly control the deboning behaviors. Considering all the above mentioned factors, this research program was planned to investigate flexural capacity of SS reinforced concrete beam with different reinforcement arrangement. This section includes the geometric properties, reinforcement arrangement, instrumentation and data acquisition system of the test program.

3.4.1 Test Specimens

In this section, the design of the specimens, flexural reinforcements, top compression reinforcements, and shear reinforcements are discussed.

3.4.1.1 Sectional Dimensions of Beam Specimens

All beam specimens were designed to have uniform dimensions to simulate the typical practical behavior of concrete beam applications. All beams were rectangular of 150 mm wide by 200 mm deep. The nominal length of all beams was 1500mm with a clear span of 1200 mm. The concrete dimensions of the test specimen are shown in Figure 3.7.

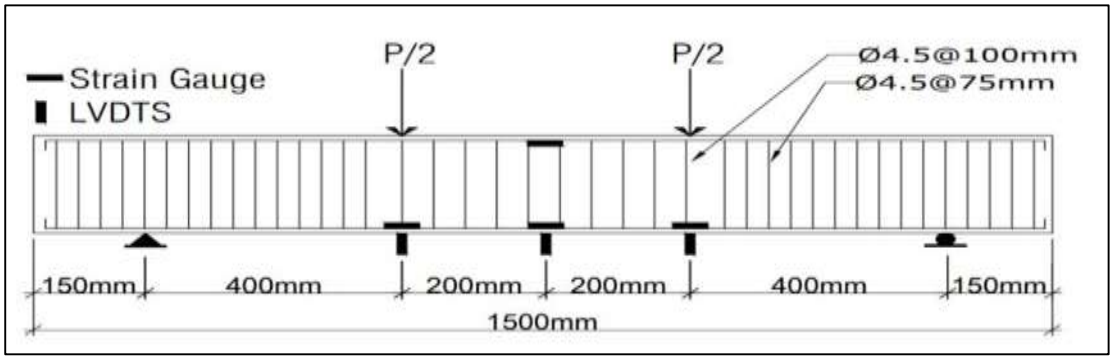

(a) Elevation

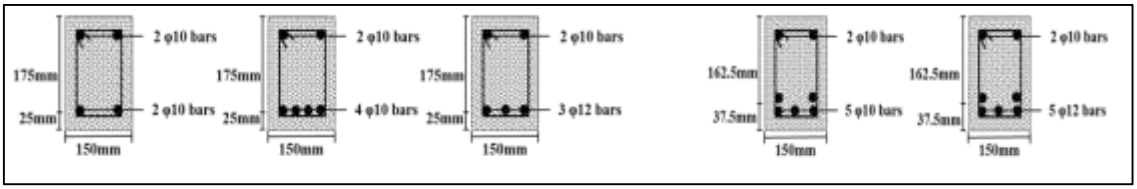

(b) Cross-Section

Fig 3. 7 : Test specimen; (a) Elevation (b) Cross-Section

3.4.1.2 Labeling of Test Specimens

The labeling on the specimen was used for specimen's identification. There are five levels of longitudinal reinforcement ratios; low, moderate, beyond moderate, high, and extremely high (Low, L, ρ = 0.59%; Moderate, M, ρ = 1.2%; Moderate, M', ρ = 1.3%; High, H, ρ = 1.6%; Extremely high, H', ρ = 2.32%) and the relative concrete strength between specimens having the same reinforcement ratio (1 = Lower, 2 = Higher) which can be translated to levels L, M,M', H and H' Letter (MS) refers to Mild steel as longitudinal steel

reinforcement while letter (SS) refers to Stainless Steel as longitudinal steel reinforcement. Specimens were marked as MSL-1, MSL-2, MSH-1, MSH-2, SSL-1,SSL-2, SSM-1, SSM-2, SSM'-2, SSH-1, SSH-2, SSH'-1.

3.4.2 Design of Test Specimens

Overall concrete dimensions were kept constant for all specimens. All beams were designed to achieve a minimum strain in the steel of 0.4 %. The reinforcement ratios for all beams satisfied the minimum and maximum value recommended by ACI 318-02[53]. The target compressive strength of concrete was 50 MPa. All specimens were loaded statically up to failure using a four-point bending scheme. Beams MSL-1, MSL-2, MSH-1, MSH-2, SSL-1, SSL-2, SSM-1, SSM-2, SSM'-2, SSH-1, SSH-2, and SSH'-1 had reinforcement ratios of 0.59, 0.59, 1.60, 1.60, 0.59, 0.59, 1.2, 1.2, 1.3, 1.6, 1.6, 2.32 %, respectively. Beams MSL-1, MSL-2, MSH-1and MSH-2 were the only beams reinforced with Mild steel (MS) bars on the tension side as controlled beams. Beams SSL-1, SSL-2, SSM-1, SSM-2, SSM'-2, SSH-1, SSH-2 and SSH'-1 were constructed to observe and evaluate Stainless Steel properties as reinforcement and hence they are compared to conventional steel Carbon steel bars.

3.4.3 Top & Bottom Reinforcement

Two Ø 10 mm MS longitudinal bars were used as the bottom reinforcement for Beam MSL-1 and MSL-2. FiveØ10 mm MS longitudinal bars were used as the bottom reinforcement for Beam MSH-1 and MSH-2. Two Ø 10 mm SS longitudinal bars were used as the bottom reinforcement for Beams SSL-1and SSL-2. Five Ø 12 mm SS longitudinal bars were used as the bottom reinforcement for Beams SSH'-1. Beam SSM-1 and SSM-2 were reinforced with four Ø10 mm SS steel rebars. Three Ø 12 mm SS longitudinal bars were used as the bottom reinforcement for Beams SSM'-2. Beams SSH-1 and SSH-2 were reinforced with five Ø 10 mm and five Ø 10 mm SS rebars respectively. Two Ø 10 mm MS longitudinal

bars were used as the compression reinforcement bars for all Beams. Typical detailing of reinforcement for all twelve specimens is shown in Figure 3.7 (a) and (b).

3.4.4 Shear Reinforcement

To prevent undesired shear failure in the beams, adequate shear reinforcement was provided. All beams had an identical stirrup arrangement as shown in Figure 3.1(b); Ø 4.5 mm mild steel bars were used as stirrups for all the twelve specimens, being spaced at 75 mm and 100 mm respectively in the shear span region and the constant moment region. Stirrup's spaced zone detail is shown in fig: 3.8. Shear reinforcements were provided in such a manner to ensure that the flexural behavior governed and that shear failure was prevented.

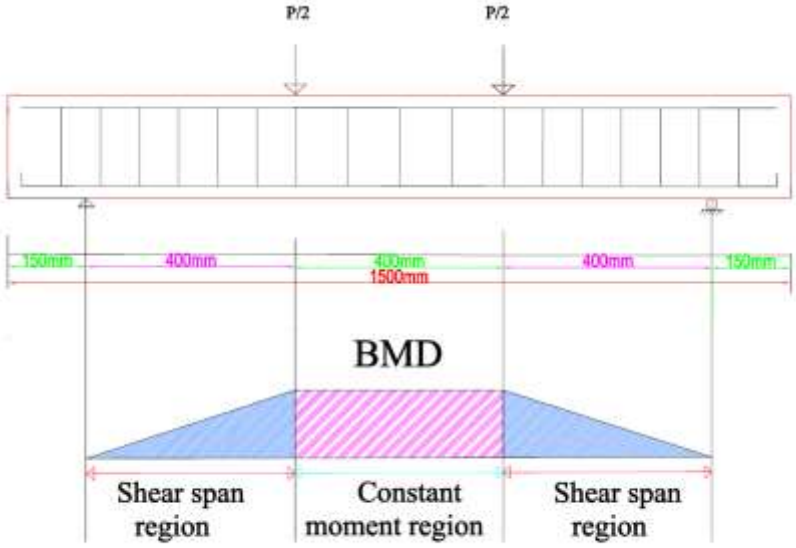

Fig 3. 8: Stirrup's spaced at different zones

3.5. Concrete Mix Design

A mix-design was prepared to conduct the experimental program as presented in Table 3.4 for two target strengths of concrete which are 45 and 50MPa as evaluated from the ACI 211 method (ACI 2002). For mix design, 36 cylinders (4" x 8") were prepared to conduct compressive strength tests at 28 days. Mix design details are shown in Table 3.3, 3.4 and Fig.3.9. The figure shows that (a, b, and c) both coarse and fine aggregates used in this

study at Saturated Surface Dry (SSD) condition just before mixing. Thereafter, twelve simply supported beams with rectangular cross-section were designed based on the guidelines of the ACI design code.

Table 3. 3 : Material properties of concrete

Properties	Materials		
	Stone aggregate	Cement (CEMII)	Sand
Specific gravity(SSD)	2.64	3.00	2.60

Table 3. 4 : Concrete mix design (weight basis) (Quantity for $1m^3$concrete)

	Weight (kg)					
Materials	**Target strength(MPa)**	**w/c**	**OPC**	**Coarse aggregate**	**Fine aggregate**	**Water**
Stone aggregate concrete	45	0.45	360	1041.216	742.560	180.00
	55	0.40	460	984.051	701.792	184.00

3.5.1 Concrete Mixing

Before the mixing of the concrete, cement was kept dry and placed in a moisture-proof container to prevent the initiation of hydration and difficulties in handling. The fine and coarse aggregate was maintained in a saturated surface-dry condition 24 hours before use. All the concrete materials were stored at room temperature in the range of 20° to 30° C by ASTM C 192-90a (1990) [54] 'Making and Curing Concrete Test Specimens in the Laboratory'. It is important to have proper mixing to ensure all surfaces of the aggregate particles were coated with cement paste, and the ingredients were blended into a uniform mass. In this study, the drum type mixer was used. The workability tests adopted in this investigation were the slump test for the concrete. The slump test was carried out following ASTM C143-90a (1990) 'Test Method for Slump of Hydraulic Cement Concrete'. Fresh Concrete mixing is prepared are shown in the figure: 3.9

(a) (c) (b)

Fig 3. 9 : (a) Casting Area (b) prepared fresh concrete and (c) Cylinder specimen

3.6 Specimen Preparation

3.6.1 Formwork

Smooth wooden formworks were used for casting the specimens. The wooden formwork consists of two sets, the base set and the side set. The base set consisted of 37.5 mm thick and 150mm wide wooden plates. The side set consisted of wooden plates of the same thickness and 200mm breadth. All formworks were strengthened by steel nail to fix the sides in place during casting. The sides were fixed at the base set utilizing nail to ease assembling and disassembling of the formwork. The formwork is shown in Figure 3.10. To determine the strain properties of rebars, strain gauges were fixed with the rebars as shown in Fig 3.10 (b) and Figure 3.10 (c) shows the curing of the beam specimens where d, e, and

f highlights the fresh beam specimens, paining, and gridline preparation of the beam samples.

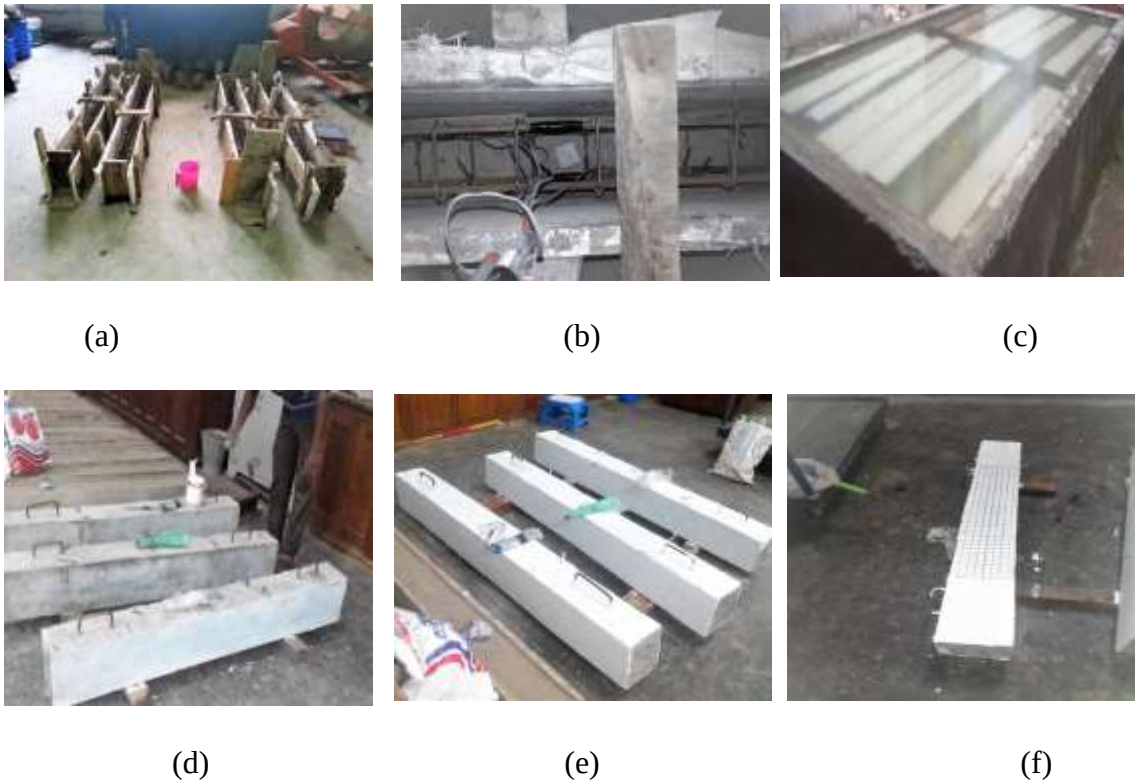

(a) (b) (c)

(d) (e) (f)

Fig 3. 10 : Photographs of tests specimen preparation (a) Test specimens formworks,(b) Strain Gauge Fixing,(c) Curing of Specimen (d, e, f) Surface preparation for the draw to grid line

3.6.2 Curing

Special care was taken to cure the reinforced concrete so that the desired mechanical strength can be achieved. After molding, the specimens were immediately covered with wet gunny sack to prevent the evaporation of water from the un-hydrated concrete. The specimens were removed from the molds after 24 ± 8 hours (ASTM C192, 1990) and moist cured at 23˚ ±1.7˚ C until the age of 28 days. After the completion of moist curing, the specimens were loaded for compressive strength test and flexure test.

3.6.3 Compressive Strength of the specimens

Mix design was established to get the required strength of concrete based on the test results, which were counter checked by the compressive strength test of cylinders which was prepared during the beam casting. Cylinder specimens were in a size of 4-inch diameter

and 8-inch height. The test was conducted as per ASTM C39-86. The specimens prepared were tested at the age of 28 days. The compressive strength test results including the other parameters of the beam specimens are listed in Table 3.5.

Table 3. 5 : Details of test beams.

Specimen	b x h (mm)	d (mm)	ρ (%)	Bottom reinforcement	Top reinforcement	Stirrup		Concrete strength f_{cu} (MPa)	Target Strength (MPa)
						At Midspan	At support		
MSL-1	150 x 200	175	0.59	2φ10	2φ10	φ4.5@100	φ4.5@75	48	45
MSL-2	150 x 200	175	0.59	2φ10	2φ10	φ4.5@100	φ4.5@75	50	55
MSH-1	150 x 200	162.5	1.60	5φ10	2φ10	φ4.5@100	φ4.5@75	45	45
MSH-2	150 x 200	162.5	1.60	5φ10	2φ10	φ4.5@100	φ4.5@75	52	55
SSL-1	150 x 200	175	0.59	2φ10	2φ10	φ4.5@100	φ4.5@75	50	45
SSL-2	150 x 200	175	0.59	2φ10	2φ10	φ4.5@100	φ4.5@75	60	55
SSM-1	150 x 200	175	1.2	4φ10	2φ10	φ4.5@100	φ4.5@75	46	45
SSM-2	150 x 200	175	1.2	4φ10	2φ10	φ4.5@100	φ4.5@75	67	55
SSM'-2	150 x 200	175	1.3	3φ12	2φ10	φ4.5@100	φ4.5@75	54	45
SSH-1	150 x 200	162.5	1.6	5φ10	2φ10	φ4.5@100	φ4.5@75	45	45
SSH-2	150 x 200	162.5	1.6	5φ10	2φ10	φ4.5@100	φ4.5@75	56	55
SSH'-1	150 x 200	162.5	2.32	5φ12	2φ10	φ4.5@100	φ4.5@75	48	45

3.7 Test Setup And Procedures

3.7.1 Instrumentation

One of the major test outputs in the present setup is the imposed displacements. In addition, the strain of the reinforcements is important parameter to measure since the SS rebar strain may vary from the other conventional steel. Electrical measurement devices were used in the appropriate locations, to measure the displacement as well as the strain in reinforcement bars. All the LVDTs and strain gauges were connected to a channel box. All the data was recorded by the data acquisition device, shown in Figure 3.11(b).

All beams were fully instrumented to measure the applied loads on the beams, deflections associated with each loading, and strains in steel as shown in Figure 3.11(b). Displacement transducers were the main devices used for measuring the imposed and resulting displacements in the test. Due to the relatively wide range of displacements measured, the transducers had minimum no-linearity and were capable of detecting small displacements.

Four linear variable displacement transducers (LVDTs) of maximum gauge length of 100mm and precision of 1/100 of mm were used to measure the displacement for Two LVDTs at loading points along the beams. Two LVDTs were placed side by side at the bottom of mid-span to measure the maximum deflection. Deflections at the location of the point loads were measured to plot the deflection distribution along beam length. LVDTs' locations on specimens are shown in Figure 3.11(a)

(a) (b)

Fig 3. 11: (a) LVDTs' locations, (b) Data acquisition device, and channel box

3.7.2 Experimental procedure

All beams were simply supported over two rigid supports and subjected to monotonic loading up to failure using a hydraulic actuator with a capacity of 2000 kN. Two concentrated loads were applied at 150 mm apart on either side of midspan in a force-controlled manner with a loading rate of 1mm/min (Fig. 3.12 and 3.13). After reaching the ultimate strength of each specimen, the concrete beams were loaded continuously by increasing the midspan displacement until a stable force was achieved for each step up to the specimen failed.

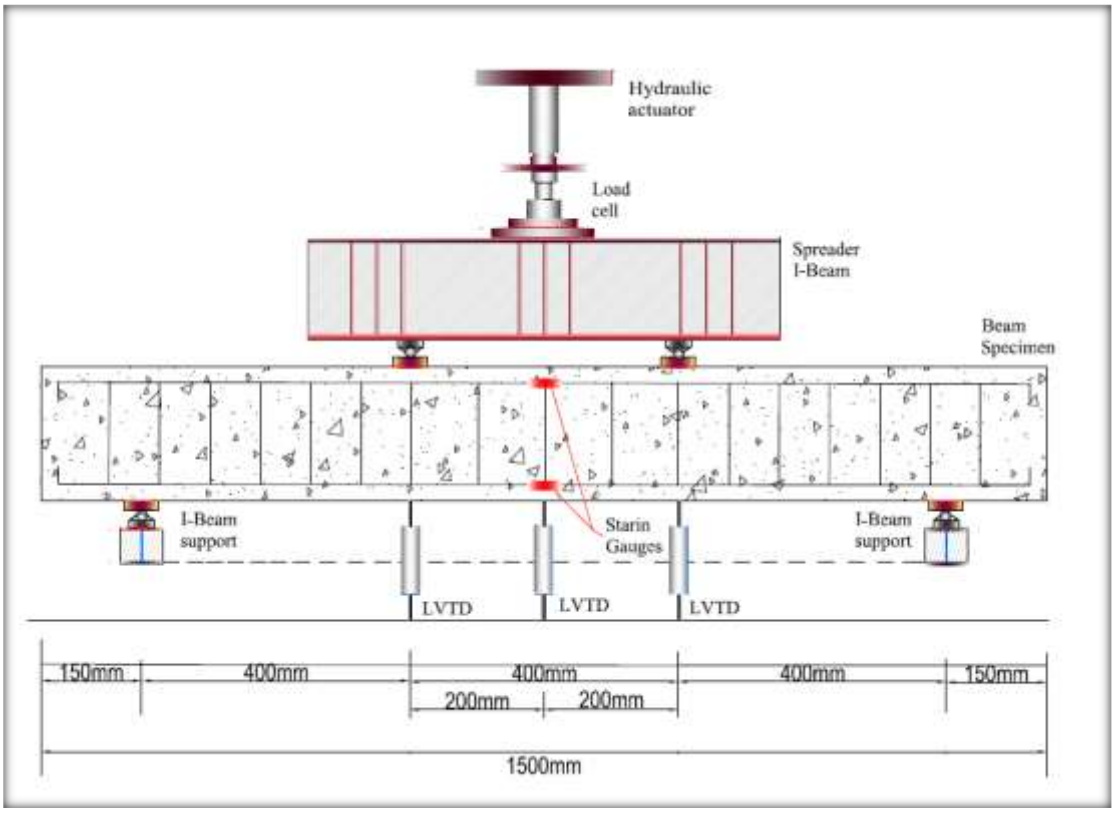

Fig 3. 12 : Four Point Static Bending Test setup (Schematic diagram)

Deflections were measured at 400mm and 800mm distance from the support and also at the mid-span using linear voltage displacement transducers (LVDTs). Strains were monitored at load points and midspan using electrical resistance strain gage transducers. All instruments were connected to a high-speed data acquisition system, which can monitor the response of the test specimens throughout the experimental investigation. Therefore, all data were set to record automatically on a computer except for the crack width readings, which were recorded manually at each loading step. The crack formation was marked on the two sides of each beam and the applied loads were recorded automatically in the data acquisition system of UTM. The actual beam set up at the SM lab is shown in Fig.3.13.

Fig 3. 13 : General view of the specimens test setup

3.8 Summary

Details of the experimental program are presented in this chapter in which eight Stainless Steel and four mild steel reinforced concrete beams were constructed to investigate their flexural behavior. All beams were of a constant size (150 mm wide by 200 mm high by 1500mm long) with the major variables being the type of SS bars, longitudinal reinforcement ratio (0.59%, 1.2%, 1.3%, 1.6%, or 2.32%) and variable concrete strength in arrangement of 45 MPa to 67 MPa where the target strength was 45 and 55 MPa. All twelve beams were tested under four-point loading with a 400 mm shear span. Details of instrumentation including internal strain gauges, LVDT' are highlighted in this chapter.

CHAPTER 4

EXPERIMENTAL RESULTS

4.1 General

This chapter presents the experimental results of the twelve concrete beams as described in chapter 3. Among them four beams were made as controlled concrete beam reinforced by mild steel. The remaining eight beams were made with stainless steel with different reinforcement ratio. Experimental results of the twelve beams including the cracking load, crack pattern, deflection, ultimate flexural strength and failure modes were evaluated. The response parameters include data from linear variable displacement transducers (LVDTs), strain gauges, visual inspection of specimen behavior, crack patterns and modes of failure.

The contribution of each response parameter to the behavior of specimens was enumerated. Primarily, plots of load versus midspan deflection for all specimens were prepared. During the analysis of test results, the test specimens were classified according to the type of steel reinforcement used, steel reinforcement ratios, and concrete compressive strength. The cracking moment and ultimate moment capacity of the SS reinforced beams were compared with that of the mild steel. In addition, results coming from different reinforcement ratio are also examined to understand the reinforcing effect of SS in concrete beams.

4.2 Experimental Investigation

A total of twelve concrete beams with constant cross-sectional dimensions were constructed and tested under four-point bending. The parameters that varied in the design were the longitudinal tensile reinforcement ratio. The overall performance of the tested specimens was evaluated based on the overall flexural behaviour. The different limit states used to evaluate flexural performance were:

1) Flexural cracking load
2) Crack pattern
3) Deflection under load
4) Ultimate flexural strength
5) Failure mode

4.2.1 Beams with Low Reinforcement

Based on the experimental investigation on tested beams having low reinforcement, results are presented in terms of crack pattern, failure mode and load-deflection responses. The reinforcement ratio for these beam sections are kept to be 0.59 %. Cracking behavior for low reinforcement ratios (0.59%), SS reinforced beams SSL-1, SSL-2 and MS reinforced beams MSL-1 and MSL-2 are discussed and compared.

4.2.1.1 Crack Pattern & Failure Mode

The crack pattern of the tested beams SSL-1, SSL-2, MSL-1 and MSL-2 are presented in figures from Figure 4.1 to 4.4.

Fig 4. 1: Crack Pattern for beam SSL-1

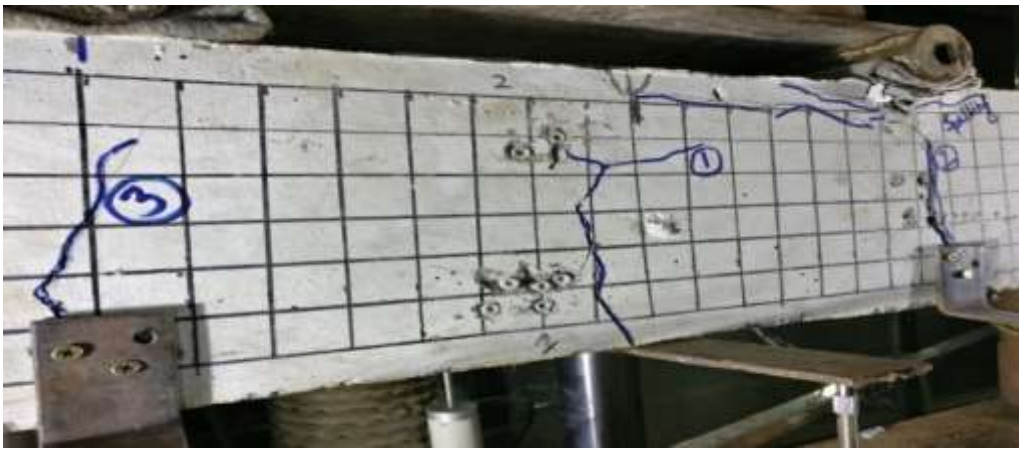

Fig 4. 2 : Crack Pattern for beam SSL-2

Fig 4. 3 : Crack Pattern for beam MSL-1

Fig 4. 4 : Crack Pattern for beam MSL-2

It is evident that the cracks at the constant moment region occurred at an earlier stage and continued to propagate after the yielding of the steel. On the other hand, cracks located

within the constant shear region initiated at a later stage. As the applied load increased, the flexural cracks started to appear outside of the constant moment region.

Therefore, it can be concluded that, due to the mechanical characteristics of SS bar, as the load increases, more cracks were formed rather than widening of the initially formed cracks. It should be noted that more crack formation in SS beams is recognized than the conventional steel reinforced beams with same reinforcement ratios. The figures showed that the cracks and failure of the concrete SS reinforced beams are more prominent in l/3 distance from the supports whereas for MS reinforced beams the cracks and failure were more prominent at the middle of the beams. Similar observations were found for both grades of concrete. This may have happened due to the fact that smooth SS rebars samples were used as reinforcement.

The failure mode of the beams SSL-1, SSL-2, MSL-1 and MSL-2 was crushing of the concrete in the constant moment zone after considerable deflection following yielding of the tension reinforcement. Flexural failure mode was observed for all low steel ratio beams. The failure patterns for these beams are shown in figures from Figure 4.5 to Figure 4.8. Another significant finding of these crack patterns and failure modes are that no significant concrete crushing was found in the compression zone for low SS reinforced concrete beams. However, for MS reinforced beams concrete crushing was observed in the compression zones.

Fig 4. 5: Failure Mode for beam SSL-1 due to concrete crushing

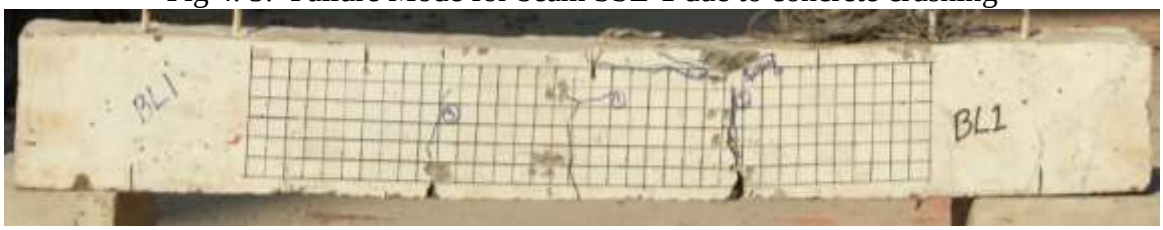

Fig 4. 6: Failure Mode for beam SSL-2 due to concrete crushing

Fig 4. 7: Failure Mode for beam MSL- 1 due to concrete crushing

Fig 4. 8: Failure Mode for beam MSL- 2 due to concrete crushing

4.2.1.2 Flexural Behavior on load vs deflection responses

Load-displacement responses of the beams having lower reinforcement ratios with both MS and SS bars are presented in Figure 4.9. It is evident from the figure that linear behavior was observed till cracking at a load level of 17.4 kN and 15.5 kN respectively. This behavior is attributed to the same elastic modulus for the reinforcing materials and the same reinforcement ratio. Yielding of conventional steel rebars Grade 72.5 was observed at a loading level of 42.34 kN and 44.60 kN with a corresponding midspan deflection of 4.77 mm & 3.88mm as presented in the Figure 4.9.

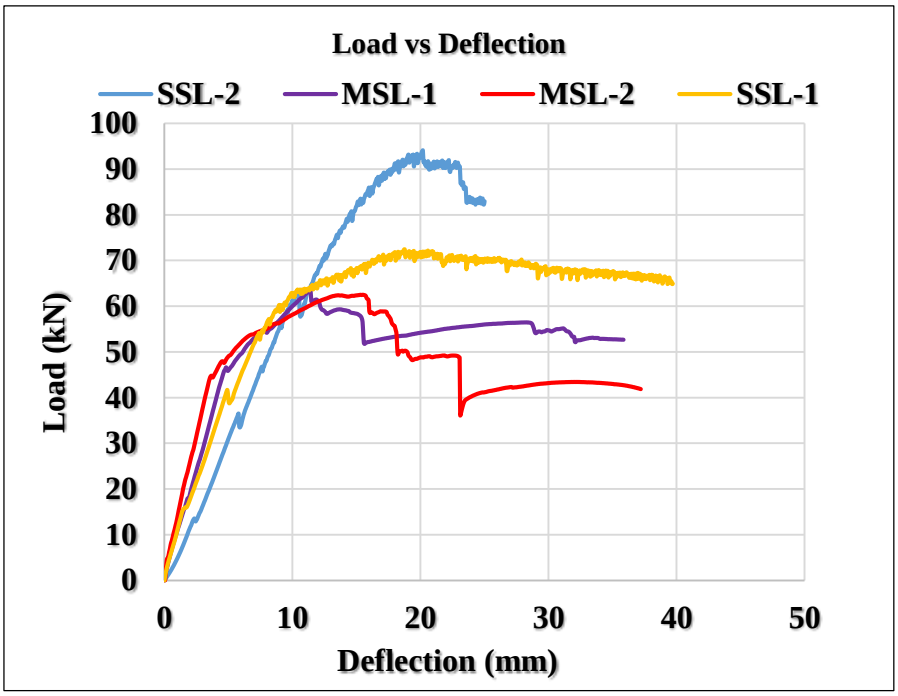

Fig 4. 9: Load-midspan deflection behaviour for beams SSL-2, SSL-1, MSL-1 & MSL-2

The ultimate capacity of the SS beams were observed at deflection of about 11.42mm and 15.70 mm with a peak load of 63.32 kN & 62.20 kN. Whereas for stainless steel (SS) beam SSL-1 & SSL-2 the ultimate capacity of beams occurred at deflection of about 18.77 mm and 24.80 mm with a peak load of 72.42 kN &102.13 kN respectively. The difference of ultimate strength between SS concrete beams and MS concrete beams was caused from the difference of concrete strength. The results indicate that the SS concrete beams showed 38% higher ultimate capacity than MS concrete beams for low reinforcement ratio. It is also notable that the stiffness (slope of the load vs deformation curve) of the SS beams are lower than the MS beams. This phenomenon can be explained by the fact that the modulus of elasticity of SS is less than the MS rebars and the smoothness of the SS rebars may result in slippage at the SS-concrete interface.

4.2.2 Medium Reinforcement Ratio

Based on the experimental investigations the figure below shows crack pattern, failure mode and the experimental midspan load-deflection responses of SS reinforced concrete

beams with 1.2 % and 1.3% steel ratios. These reinforcement percentage for the beams are termed as medium reinforced beam specimens.

4.2.2.1 Crack Pattern & Failure Mode

The crack pattern for tested beam specimens SSM-1, SSM-2, and SSM'-2 are presented in figures from Figure 4.10 to Figure 4.12.

Fig 4. 10 : Crack Pattern for beam SSM-1

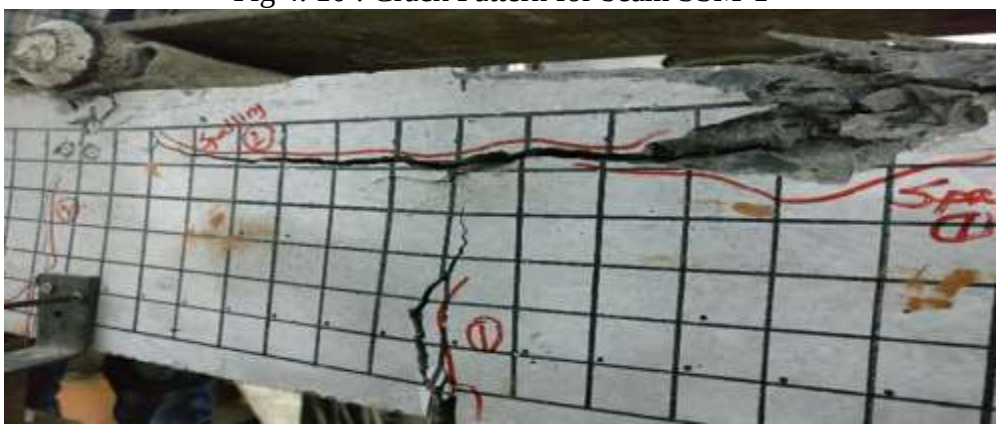

Fig 4. 11: Crack Pattern for beam SSM-2

Fig 4. 12 : Crack Pattern for beam SSM'-2

Cracking behavior for Medium reinforcement ratios (1.2%) beams SSM-1, SSM-2, and SSM'-2 with SS reinforced are discussed and compared to the beams reinforced with MS beams. It was observed that the cracks at the constant moment region occurred at an earlier stage and continued to propagate after the yielding of the steel. On the other hand, cracks located within the constant shear region initiated at a later stage. As the applied load increased, the flexural cracks started to appear outside of the constant moment region.

The failure mode of the beams of SSM-1, SSM-2, and SSM'-2 was due to crushing of the concrete in the constant moment zone after considerable deflection following yielding of the tension reinforcement. The failure patterns for these beams are shown in figures from Figure 4.13 to Figure 4.15.

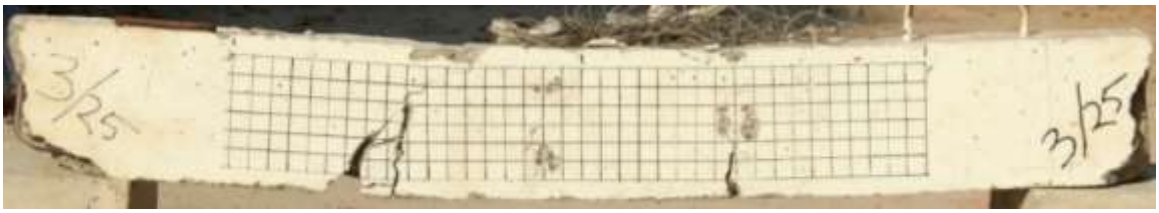

Fig 4. 13: Failure Mode for beam SSM- 1 due to concrete crushing

Fig 4. 14: Failure Mode for beam SSM- 2 due to concrete crushing

Fig 4. 15: Failure Mode for beam SSM- 2 due to concrete crushing

4.2.2.2 Flexural Behavior on Load vs Deflection responses

Stainless Steel concrete Beams SSM'-2 and SSM-1 exhibited same behavior described below as shown in Figure 4.16 where deflection increases linearly with the increase of the applied load prior to cracking. After the initiation of the first crack, at a load level of 23.05 kN and 11.67 kN, yielding of Stainless Steel rebars for SSM'-2 and SSM-1 beams was observed at a loading level of 117.54 kN and 83.74 kN with a corresponding midspan deflection of 13.9mm & 7.21mm respectively as shown in Figure 4.16. The beam SSM-2 showed reduced stiffness, yielding of the reinforcement at a load of 120.70 kN with a corresponding midspan deflection of 12.19 mm,

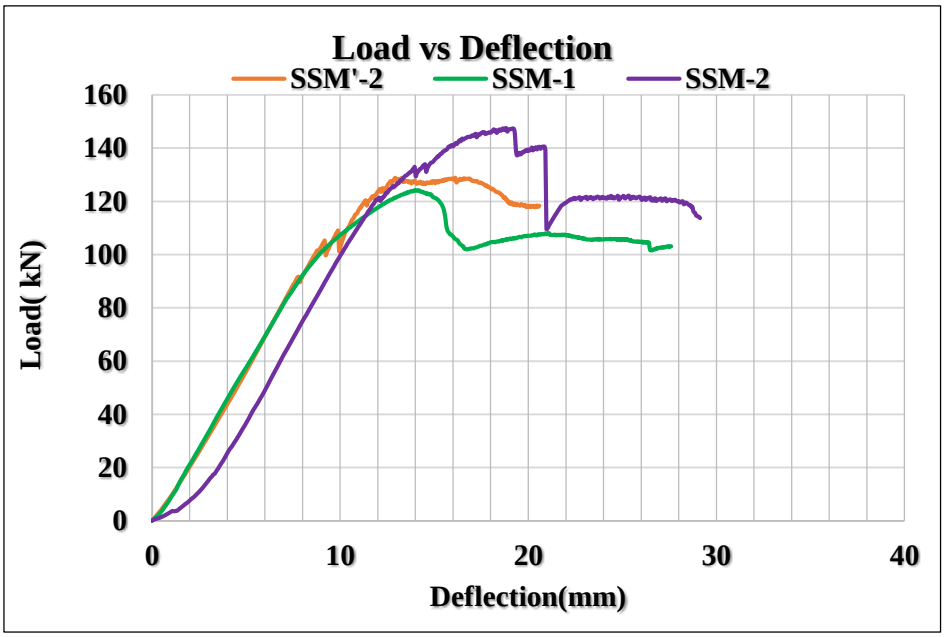

Fig 4. 16 : Load-midspan deflection behaviour of the beams SSM-1, SSM-2 & SSM'-2

The peak load was 146.71 kN with corresponding midspan deflection of 18.73mm. The specimens with the medium longitudinal reinforcement exhibited both the largest deflection and ultimate capacity.

4.2.3 High Reinforcement Ratio

This section incorporates the test results in terms of crack pattern, failure mode and the experimental midspan load-deflection responses of MS and SS reinforced concrete beams with 1.6 % and 2.32% steel ratios.

4.2.3.1 Crack Pattern & Failure Mode

The crack pattern for SSH-1, SSH-2, SSH'-1, MSH-1 and MSH-2 are given in figures from Figure 4.17 to Figure 4.21 for high reinforcement steel ratios. These 5 beams had reinforcement ratios 1.6 % and 2.32%.

Fig 4. 17 : Crack Pattern for beam SSH-1

Fig 4. 18 : Crack Pattern for beam SSH-2

Fig 4. 19 : Crack Pattern for beam SSH'-1

Fig 4. 20 : Crack Pattern for beam MSH-1

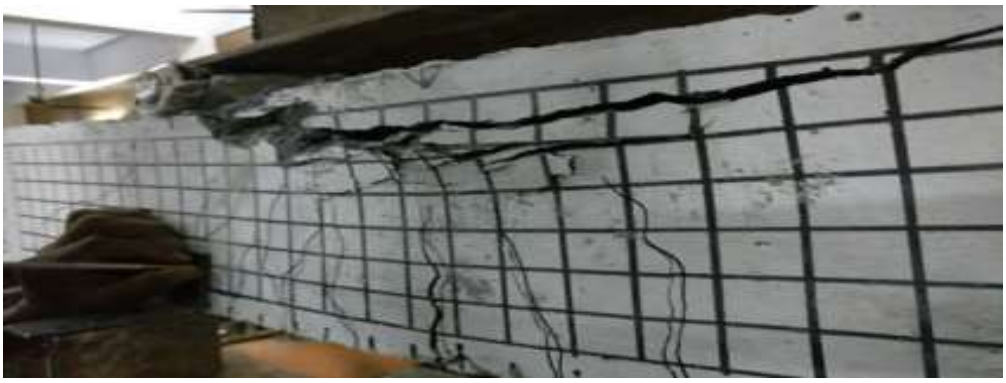

Fig 4. 21: Crack Pattern for beam MSH-2

Cracking behavior of beams having higher reinforcement ratios, beams SSH-1, SSH-2 and SSH'-1 with Stainless Steel and MSH-1 and MSH-2 beams with Mild Steel are discussed and compared in this section. It is evident that the cracks at the constant moment region occurred at an earlier stage and continued to propagate after the yielding of the steel. On the other hand, cracks located within the constant shear region initiated at a later stage. As the applied load increases, the flexural cracks started to appear outside of the constant moment region.

Therefore, it can be concluded that, due to the mechanical characteristics of SS bar, more cracks are formed rather than widening the existing cracks as the load increases. It should be noted that more crack formation was observed in SS beams than the conventional steel reinforced beams having same reinforcement ratios.

4.2.3.2Flexural Behavior on Load vs Deflection responses

It is evident in Figure 4.22 the load-midspan deflection behavior of MSH-2 and MSH-1 showed that linear behavior was observed till cracking at a load level of 25.3 kN and 20.14 kN respectively. This behavior is attributed to the same elastic modulus for the reinforcing materials and the same reinforcement ratio. Yielding of conventional steel rebars of Grade 72.5 was observed at a loading level of 144.8 kN and 136.00 kN with a corresponding midspan deflection of 8.23 mm & 8.52 mm. as shown in Figure 4.22

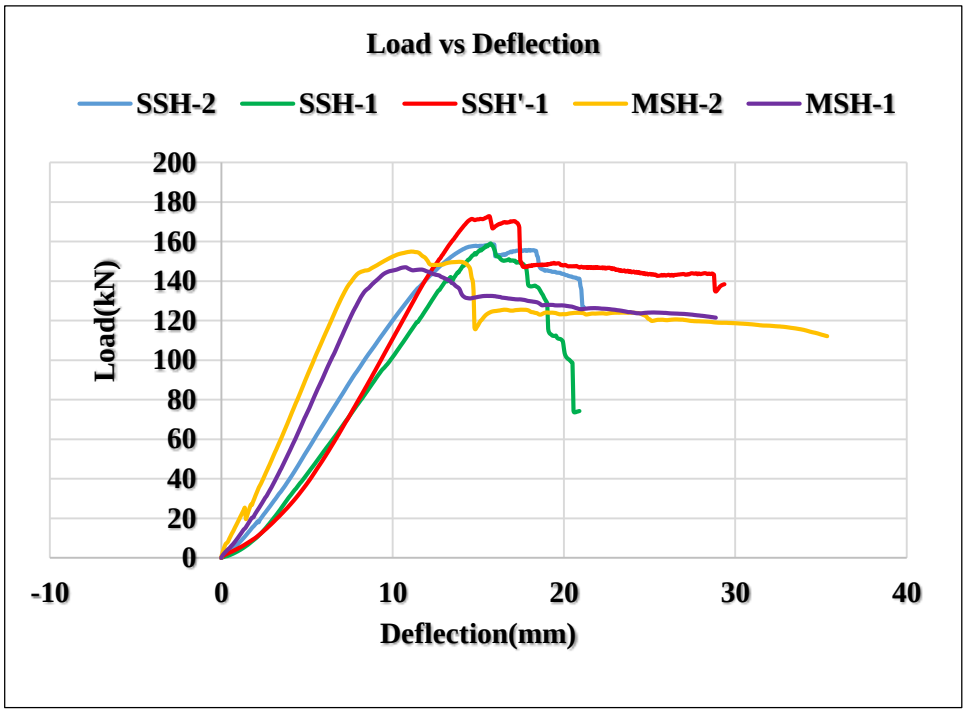

Fig 4. 22 : Load-midspan deflection behaviour for beams SSH-2, SSH-1, SSH'-1, MSH-2 & MSH-1

The ultimate capacity of beams occurred at deflection of about 11.30 mm and 10.65 mm with a peak load of 154.8 kN & 146.90 kN respectively. Whereas for stainless steel (SS) beam SSH-2, SSH-1& SSH'-1 the ultimate capacity of beams occurred at deflection of 18.86 mm and 15.78 mm and 15.67 mm with a peak load of 165.41 kN &158.27 kN and 172.63 kN respectively. Increasing the amount of reinforcement ratio results in higher load carrying capacity for the beams reinforced with Stainless Steel bars. These also shows comparatively low deflection amount than the beams having medium reinforcement ratios. The failure mode of the beams was due to crushing of the concrete in the constant moment zone after considerable deflection following yielding of the tension reinforcement. The concrete strength was recorded 50 MPa, 65 MPa, 48 MPa and 50 MPa for beams SSH-1, SSH-2, SSH'-1, MSH-1 and MSH-2 respectively. The failure modes for these beams are shown in figures 4.23 to 4.27.

Fig 4. 23: Failure Mode for beam SSH- 1 due to concrete crushing

Fig 4. 24: Failure Mode for beam SSH- 2 due to concrete crushing

Fig 4. 25 : Failure Mode for beam SSH'- 1 due to concrete crushing

Fig 4. 26 : Failure Mode for beam MSH- 1 due to concrete crushing

Fig 4. 27 : Failure Mode for beam MSH- 2 due to concrete crushing

4.3 Overall key experimental results

Based on the experimental investigation on twelve concrete beams, schematic diagram of crack patterns are presented on figure 4.28. The outcome of the other key design parameters are also tabulated in Table 4.1. The table highlights the yield and ultimate loads of the beam

specimens, midspan deflections, ductility and failure modes. The beam deflections along the length at different loading are presented on the figure 4.29.

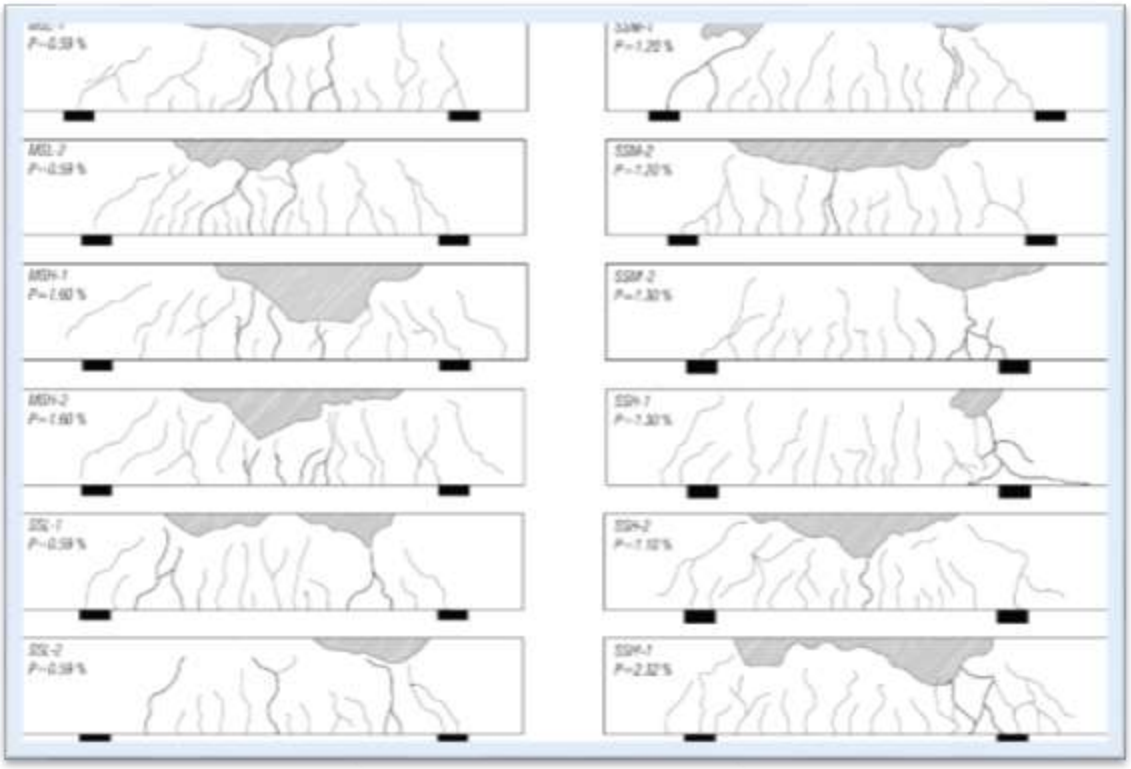

Table 4. 1: Details of Experimental Results

Specimen	Load, kN			Midspan deflection, mm			Ratio			Failure mode
	Cracking, P_{cr}	Yielding, P_y	Ultimate, P_u	Yielding, Δ_y	Ultimate, Δ_u	Failure, Δ_{max}	Load P_u/P_y	Displacement Δ_u/Δ_y	Δ_{max}/Δ_y	
MSL-1	17.4	46.34	63.32	4.77	11.42	35.86	1.37	2.39	7.51	Flexural
MSL-2	15.5	44.6	62.2	3.88	15.70	37.2	1.39	4.05	9.59	Flexural Shear
MSH-1	20.14	136	146.9	8.52	10.65	28.86	1.08	1.25	3.38	Flexural
MSH-2	25.3	144.8	154.8	8.23	11.30	35.37	1.06	1.37	4.29	Flexural
SSL-1	15.83	53.83	72.42	7.35	18.77	39.67	1.34	2.55	5.4	Flexural
SSL-2	21.04	71.44	102.13	15.12	24.80	25.01	1.43	1.64	1.65	Flexural
SSM-1	11.67	83.74	123.98	7.21	14.11	27.56	1.48	1.96	3.82	Flexural
SSM-2	18.48	120.7	146.71	12.19	18.73	29.13	1.21	1.54	2.39	Flexural
SSM'-2	23.05	117.54	154.73	13.9	18.97	26.57	1.31	1.36	1.91	flexural
SSH-1	23.28	119.23	158.27	11.46	15.78	20.9	1.32	1.38	1.82	Shear
SSH-2	24.96	137.45	165.41	13.86	18.87	24.1	1.2	1.36	1.74	Flexural
SSH'-1	27.71	144.04	172.63	12.18	15.67	29.32	1.2	1.23	2.4	Shear

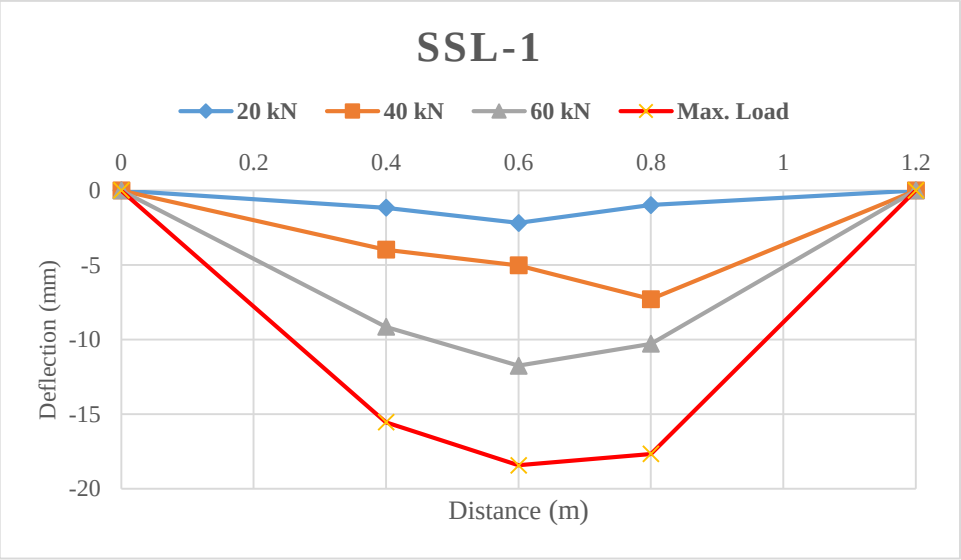
SSL-1
20 kN
40 kN
60 kN
Max. Load
0
0.2
0.4
0.6
0.8
1
1.2
0
-5
-10
-15
-20
Deflection (mm)
Distance (m)

SSL-2

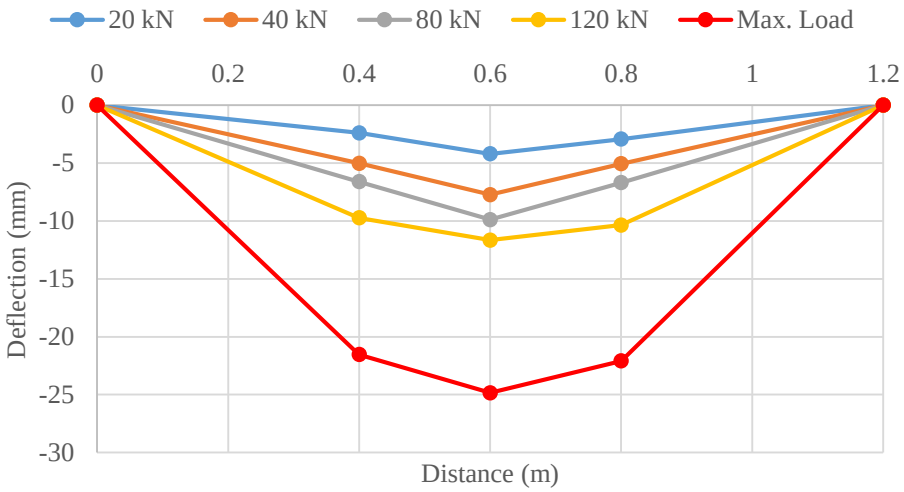
20 kN
40 kN
80 kN
120 kN
Max. Load
0
0.2
0.4
0.6
0.8
1
1.2
0
-5
-10
-15
-20
-25
-30
Deflection (mm)
Distance (m)

SSM-1

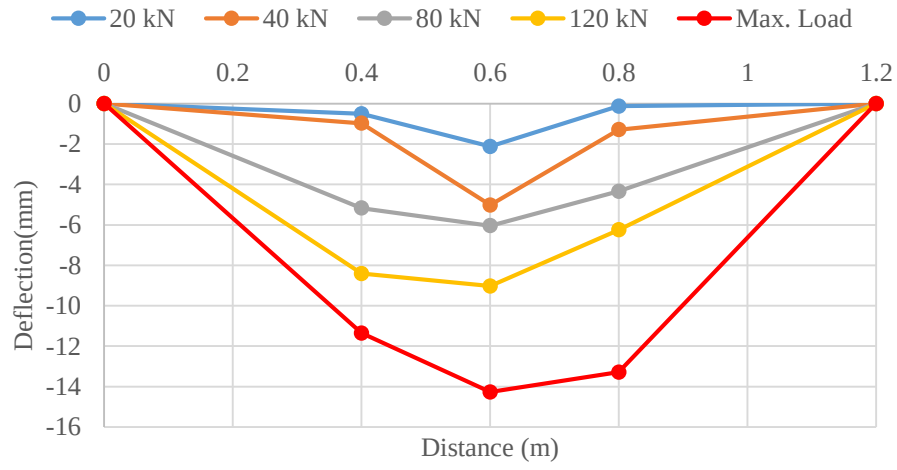
20 kN
40 kN
80 kN
120 kN
Max. Load
0
0.2
0.4
0.6
0.8
1
1.2
0
-2
-4
-6
-8
-10
-12
-14
-16
Deflection(mm)
Distance (m)

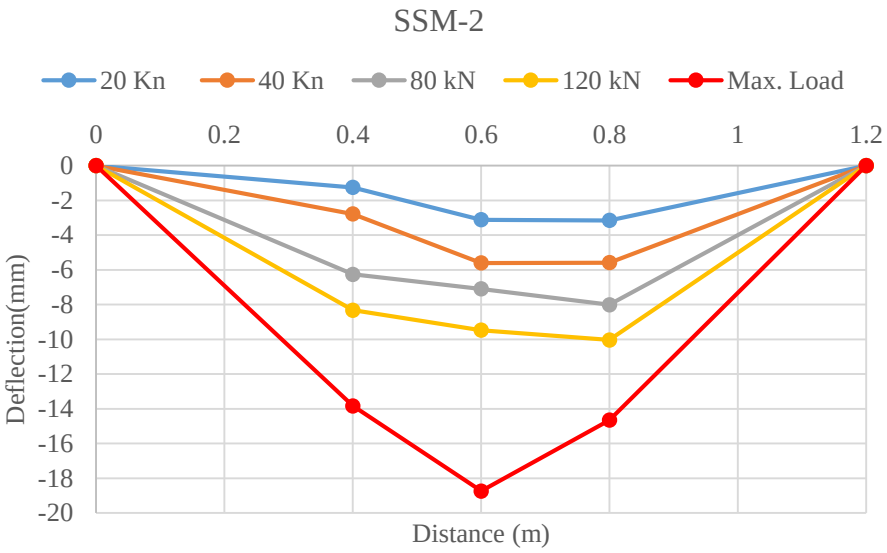
SSM-2
20 Kn
40 Kn
80 kN
120 kN
Max. Load
0
0.2
0.4
0.6
0.8
1
1.2
0
-2
-4
-6
-8
-10
-12
-14
-16
-18
-20
Deflection(mm)
Distance (m)

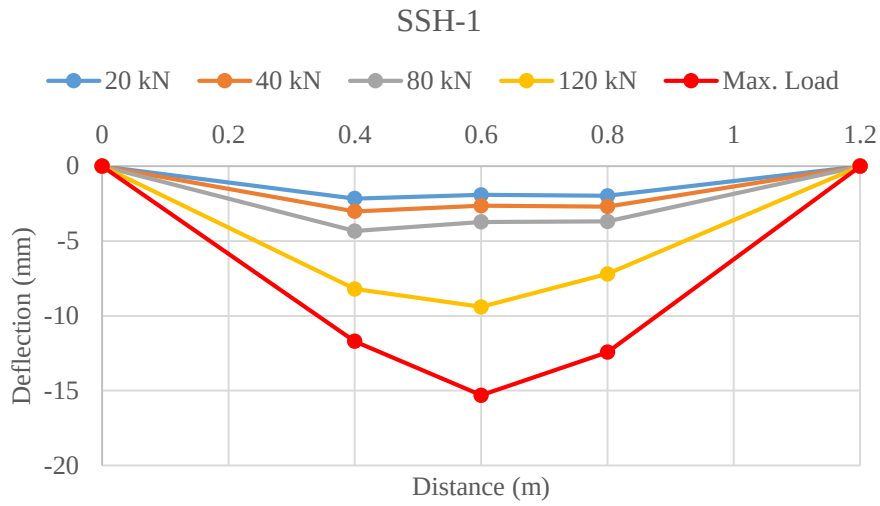
SSH-1
20 kN
40 kN
80 kN
120 kN
Max. Load
0
0.2
0.4
0.6
0.8
1
1.2
0
-5
-10
-15
-20
Deflection (mm)
Distance (m)

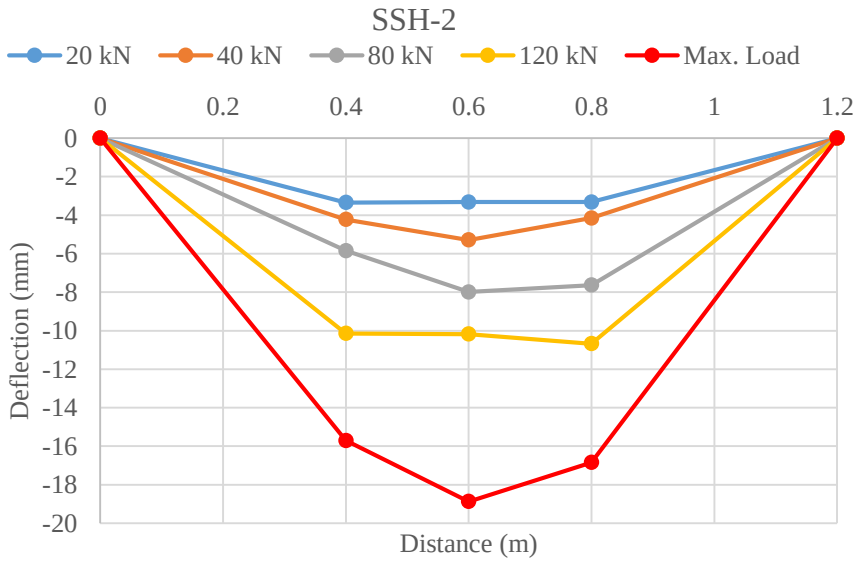
SSH-2
20 kN
40 kN
80 kN
120 kN
Max. Load
0
0.2
0.4
0.6
0.8
1
1.2
0
-2
-4
-6
-8
-10
-12
-14
-16
-18
-20
Deflection (mm)
Distance (m)

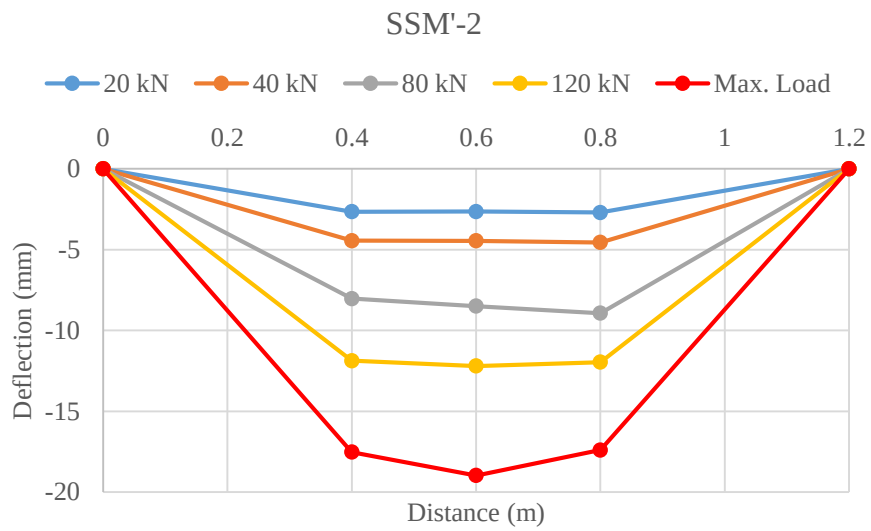
SSM'-2
20 kN
40 kN
80 kN
120 kN
Max. Load
0
0.2
0.4
0.6
0.8
1
1.2
0
-5
-10
-15
-20
Deflection (mm)
Distance (m)

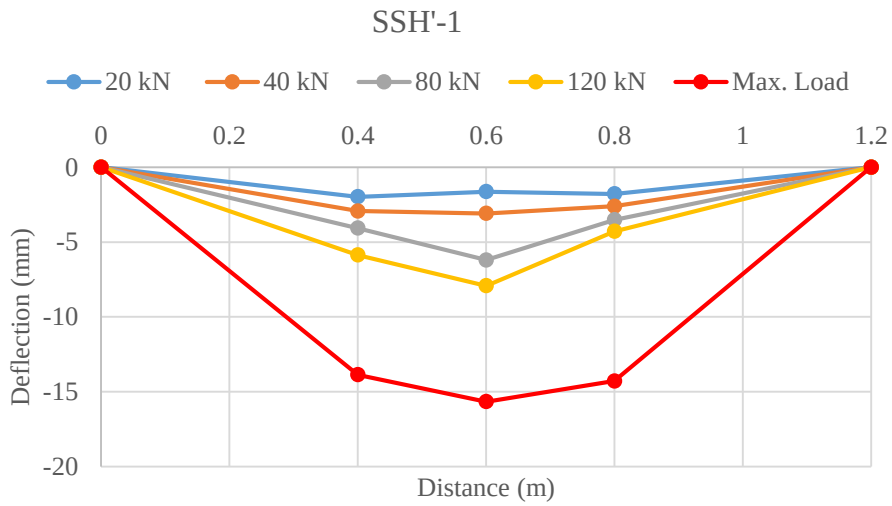
SSH'-1
20 kN
40 kN
80 kN
120 kN
Max. Load
0
0.2
0.4
0.6
0.8
1
1.2
0
-5
-10
-15
-20
Deflection (mm)
Distance (m)

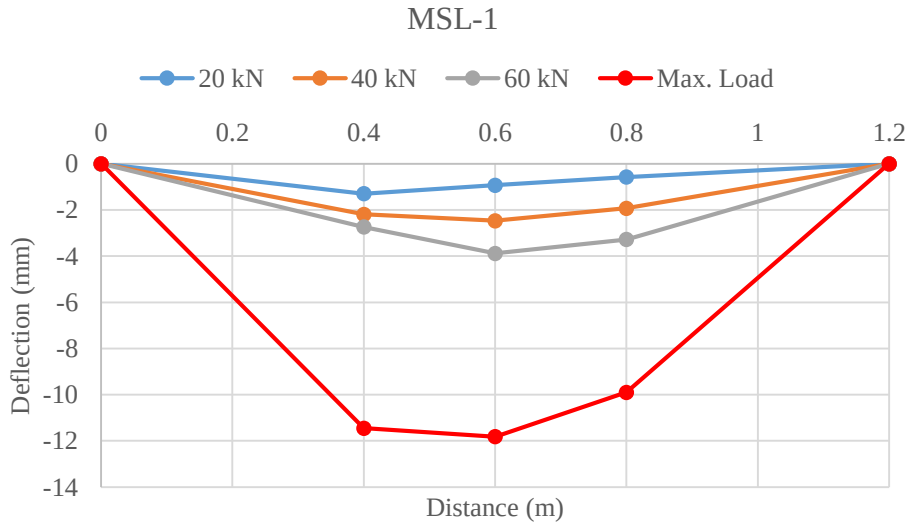
MSL-1
20 kN
40 kN
60 kN
Max. Load
0
0.2
0.4
0.6
0.8
1
1.2
0
-2
-4
-6
-8
-10
-12
-14
Deflection (mm)
Distance (m)

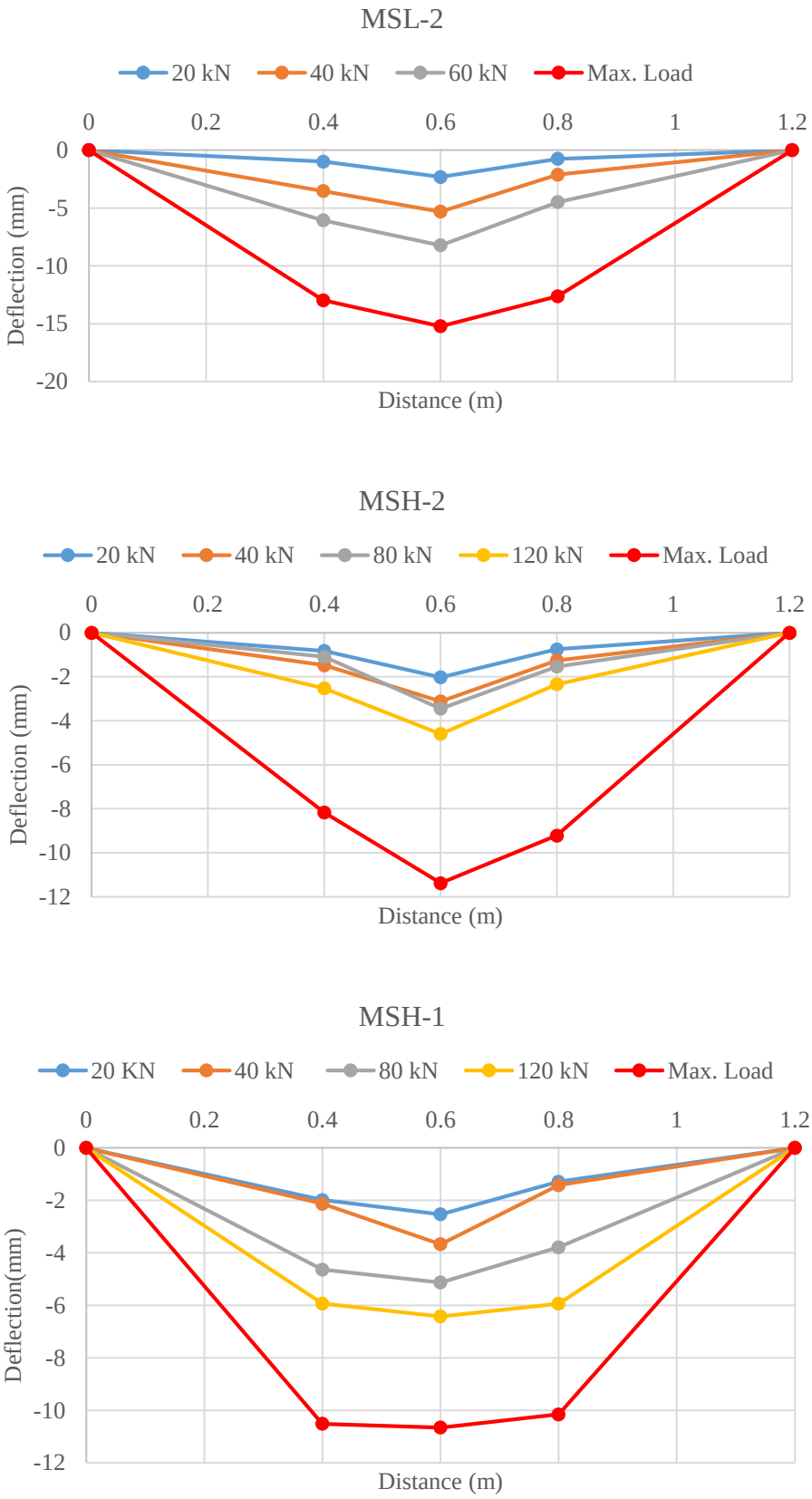

Fig 4. 29: The beam deflections at different loads from the LVDTs

4.5 Analytical Results & Code Comparison

This part of the study deals with the analytical capacities of tested beams as per different code comparison and hence comparing them with the experimental results in terms of cracking moment and ultimate moment capacity of the beams. Three different codes are studied for this comparison.

4.5.1 Cracking Moment Calculation

The cracking moment capacity of beam specimens as per ACI 318 guideline may be presented as [55]:

$$M_{cr}^{theo} = f_r \frac{I_g}{y_t} \quad \text{.....(4.1)}$$

Where $f_r = 0.62\lambda \sqrt{f'_c}$ for normal-weight concrete; λ is taken as equal to 1 for normal-density concrete and 0.85 for lightweight concrete; y_t is the distance from centroid axis of the cross section to the extreme tension fiber; and I_g is the second moment of area of the cross section neglecting the steel bars.

Canadian Standard Association CSA recommends the following equation for the cracking moment of beam specimens [56]:

$$M_{cr}^{theo} = f_r \frac{I_g}{y_t} \quad \text{.....(4.2)}$$

Where $f_r = 0.6\lambda \sqrt{f'_c}$ for normal-weight concrete; λ is taken as equal to1 for normal-density concrete and 0.85 for semi-low-density concrete (density ranged from 1850 to 2150 kg/m^3).

As per EC2, the cracking moment capacity of the beam may be written as [57]:

$$M_{cr}^{theo} = f_{ctm} \frac{I_u}{(h - x_u)} \quad \text{.....(4.3)}$$

where f_{ctm} is the mean value of axial tensile strength of concrete = $0.3 f_{ck}^{0.67}$ is the characteristic compressive cylinder strength of the concrete; I_u is the second moment of

area of the uncracked transformed section; x_u is the distance from the neutral axis of the section to the extreme top fiber and h is the height of the cross section of the beam.

Based on the stated equations of three different guideline the cracking moments are presented in Figure 4.30. From the figure it is evident that the 12 tested beams show a very good agreement with the codes, particularly with the ACI and CSA. Therefore, the results are clear enough to reflect the acceptable conformity between the theoretical results of several Code's and experimental data. The cracking moments for the experimental results are slightly higher than the analysis. As an example, the cracking moment of the beam MSH-1 was 4.028 kN, which is about 26% higher than that of the Theoretical Results. It is interesting to highlight that the tested cracking moments of high steel ratio SS beams were observed to be higher than the cracking moments computed from the codes. This may happen due to the fact that with the increase of steel, the beam become stiffer and capacity increases.

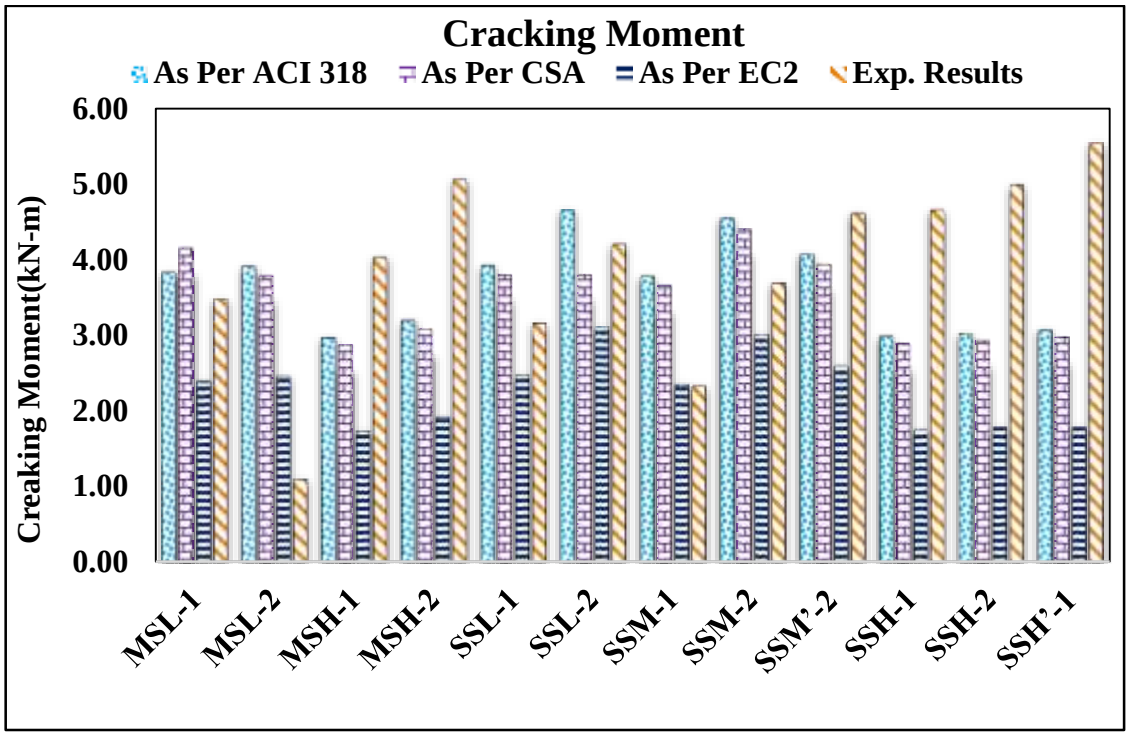

Fig 4. 30 : Comparison of Cracking Moment Capacity with Several Codes'

4.5.2 Ultimate Moment Calculation

The ultimate moment capacity of tested beam specimens as per ACI 318 guideline may be presented as follows ACI 318 [55].

$\rho_s = \frac{A_s}{bd}$; α=0.85

$$M_u = \rho_s f_s b d^2 \left(1 - \frac{\rho_s f_s}{2 \times \alpha_1 f_c'}\right) \quad \text{(4.4)}$$

If steel yields:

$f_s = f_y$

α = 0.85

β = 0.85 per $f'_c \leq$ 28 MPa

β = 0.85-0.05(f'_c-28)/7 ≥ 0.65 per $f'_c >$ 28 MPa

In this study, the experimental ultimate moment (M_u exp.) of each tested beam was compared to the theoretical design moments (M_{theo}) predicted using analytical formula

resulting from the rectangular stress block, as recommended by CSA[56], ACI 318[55] and EC2[57].

All design codes recommend a rectangular stress block with a height of ‘‘$\beta\, c$” and a width of ‘‘$\alpha\, f'_c$ ”in which f'_c concrete compressive strength, a and b are defined as stress block parameters. Eqn. (4.9)-(4.12) show the proposed values of stress block parameters for each design code. The ACI 318 and EC2

$\rho_f=\frac{A_f}{bd}$ α=0.85-0.0015$f'_c \geqslant 0.67$

$$M_u=\rho_f f_f bd^2\left(1-\frac{\rho_f f_f}{2\alpha_1 f'_c}\right) \quad (4.5)$$

α = 0.85-0.0015$f'_c \geq 0.67$

β = 0.97-0.0025$f'_c \geq 0.67$

AS 3600 [50]:

α_2=0.85-0.0015f'_c ... $\alpha_2 \geqslant 0.67$

γ =0.97-0.0025f'_c ... $\gamma \geqslant 0.67$

$k_u=\frac{A_{st}f_{sy}}{\alpha_2 f'_c \gamma Bd+A_{sc}f_{sy}}$

$$M_u = A_{st}f_{sy}*\left(D-\frac{\gamma k_u d}{2}\right) \quad (4.6)$$

α = 1-0.003f'_c where 0.67 ≤α ≤ 0.85 (4.7)

γ (=β) = 1.05-0.007f'_c where 0.67 ≤γ ≤ 0.85 (4.8)

EC2:

η (=α) = 1.0 per $f'_c \leq$ 50 MPa (4.9)

η (=α) = 1.0 - $\frac{f'_c-50}{200}$ per 50 <$f'_c \leq$ 70 MPa (4.10)

λ (=β) = 0.8 per per $f'_c \leq$ 50 MPa (4.11)

λ (=β) = 0.8 - $\frac{f'_c-50}{400}$ per 50 <$f'_c \leq$ 70 MPa (4.12)

Assuming that the nominal flexural strength of member is reached when the maximum strain at the extreme compression fiber reaches a strain limit of 0.003, while the CSA and EC2 specify a value of 0.0035 for ultimate concrete strain as shown in Fig.4.31, the comparison reveals that all investigated design codes (ACI, CSA and EC2) underestimated the flexural capacity SS reinforced tested beams.

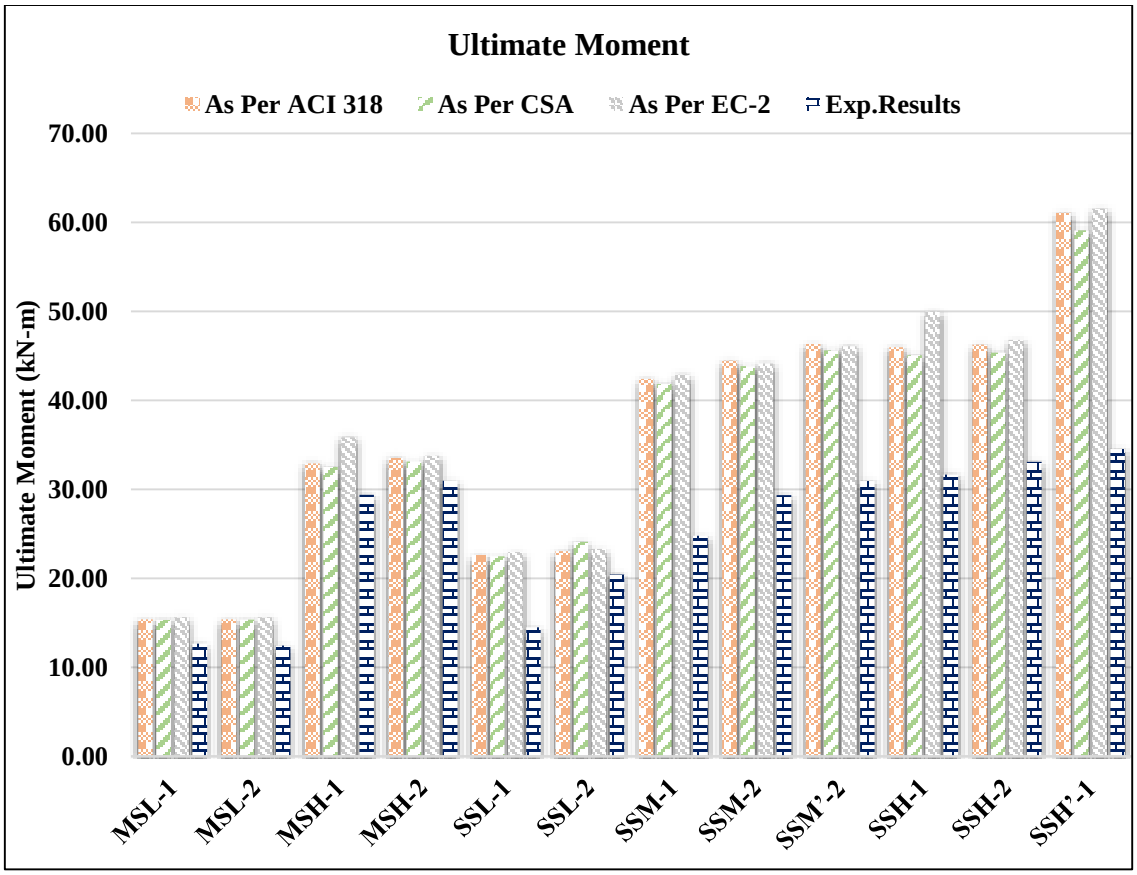

Fig 4. 31: Comparison of Ultimate Moment Capacity with Several Codes

Fig.4.31 shows the comparison of moment capacity of the tested beams with the theoretical ultimate moments calculated as per three design codes. It is observed from the figure that the results for all the experimental values of moment capacities of the beams having MS deformed rebar of both of Low and high reinforcement ratio, are quite close to the theoretical moment capacity; the difference between them is within 10%. The figure also shows that the ultimate capacity of SS reinforced beam with low steel ratio shows a good agreement with the codes. As an example, for SSL-2, the difference between experimental

and theoretical values are within the 10% of the predicted code recommended values. However, the predicted values by different codes for high SS steel ratios are approximately 25-40% higher than that of the experimental results of the beams. It is also important to note that the theoretical values of ultimate capacity as per different established codes are usually higher than the experimental results which is quite similar to the results presented in in Fig. 4.31.

4.6 Summary

In this chapter, the test results for flexural behavior of RC beams are presented. A total of twelve reinforced concrete beams were tested under four points bending test. Eight of them were SS reinforced concrete beams and remaining four beams were reinforced by carbon steel (CS) as control specimens. The variables during the tests were concrete compressive strength, rebar diameter and rebar types, steel ratio of the RC beam specimens. The key findings from the study can be summarized as:

1) The failure mode of most beams was classified as flexural failure accompanied by yielding of the tension reinforcement preceding the crushing of the concrete. The test results show that the failure patterns of the beam specimens are mostly flexural. The investigation also revealed that there were no beams failing due to rupture of the SS rebars. Only two beam exhibited combined shear and flexural failure where reinforcement ratio was high. No clear bond failure was observed during testing up to the cracking point. It is worthy to note that the flexural cracks observed at the l/3 point for SS and l/2 for MS reinforced beam.
2) The load displacement relationship reflected that the ultimate capacity of the beams increase as the reinforcement ratio increases. Subsequently, compressive strength of concrete also influences the ultimate capacity expectedly.
3) The cracking moment of tested beams and the theoretical values are quite close.

4) The specimens having medium longitudinal reinforcement ratios exhibited both of the largest deflection and ultimate capacity. This can be explained by the fact that high strength renders the beams more rigid and less ductile as expected.
5) For high steel ratio, the ultimate capacity of SS reinforced beams was found to be 25-40% less than the code specified values. The results indicate that the Stainless-Steel concrete beams were comparatively less stiff than the MS reinforced beams. This happens due to the fact that the strength of SS rebars are higher than the MS rebars but the modulus of elasticity is just opposite. Therefore, high strength and low stiffness of SS rebar leads to early deformation and reduced ultimate moment capacity of the beams.

CHAPTER 5

NUMERICAL MODELING

5.1 General

In this study, Finite Element (FE) modelling of MS and SS reinforced concrete beams were performed using the finite element software- ABAQUS v14.1. The FE modeling using Abaqus has been proven to be an effective tool, especially for such type of concrete beam analyses. The FEM for RC beams have been generally developed based on the replacing of composite continuum by an assembly of elements representing the concrete and the steel reinforcement. This chapter includes the modeling consideration, modeling technique, material model for concrete and steel, assembly of the different parts, materials and geometric nonlinearity, analysis approximations and analysis output of concrete beams reinforced with MS and plain SS rebars.

5.2 FE Modeling

The FE method is a widely acknowledged numerical technique for solving physical problems. Typical problem areas of interest in engineering and mathematical physics that are solvable by the use of the FE method more preferably the problems related structural analysis, heat transfer, fluid flow, mass transport and electromagnetic potential.

5.3 Specimen Detail

Overall cross sectional dimensions of the beams were kept constant in all specimens following exact geometry of the tested beams. All beams were designed and tested to achieve a minimum strain in the steel of 0.4 %. The reinforcement ratios for all beams satisfied the minimum and maximum value recommended by ACI 318. Two concrete compressive strengths were used in the design. They were 45 MPa and 55 MPa concrete. All beam specimens were loaded statically up to the failure point subjected to four-point

bending scheme. Beams having IDs MSL-1, MSL-2, MSH-1, MSH-2, SSL-1, SSL-2, SSM-1, SSM-2, SSM'-2, SSH-1, SSH-2, and SSH'-1 had reinforcement ratios of 0.59,0.59,1.60,1.60,0.59,0.59,1.2,1.2,1.3,1.6,1.6,2.32% respectively. Beams MSL-1, MSL-2, MSH-1and MSH-2 were the only beams reinforced with Mild steel (MS) bars on the tension side as controlled beams. Beams SSL-1, SSL-2, SSM-1, SSM-2, SSM'-2, SSH-1, SSH-2 and SSH'-1 were constructed to observe and evaluate flexural performance of Stainless Steel rebars compared to that of conventional carbon steel bars in concrete. The test matrix has already been mentioned in Table 3.1 of the Chapter 3.

5.4 Element Types

Different type of 3D elements has been offered by nonlinear FE package, ABAQUS v14, to predict the complex behavior of RC structure. However, frequently used 3D elements for modelling of concrete material are:

- C3D20
- C3D8

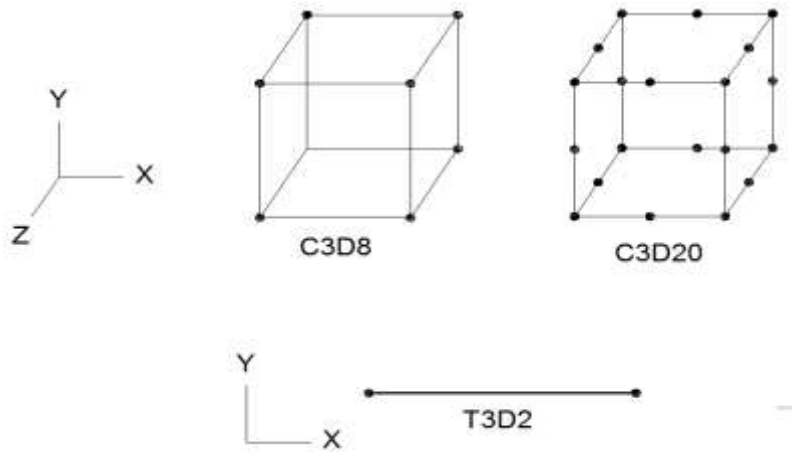

Fig 5. 1 **:** C3D20, C3D8, T3D2 elements used to model the concrete of the reinforced beams by ABAQUS v14

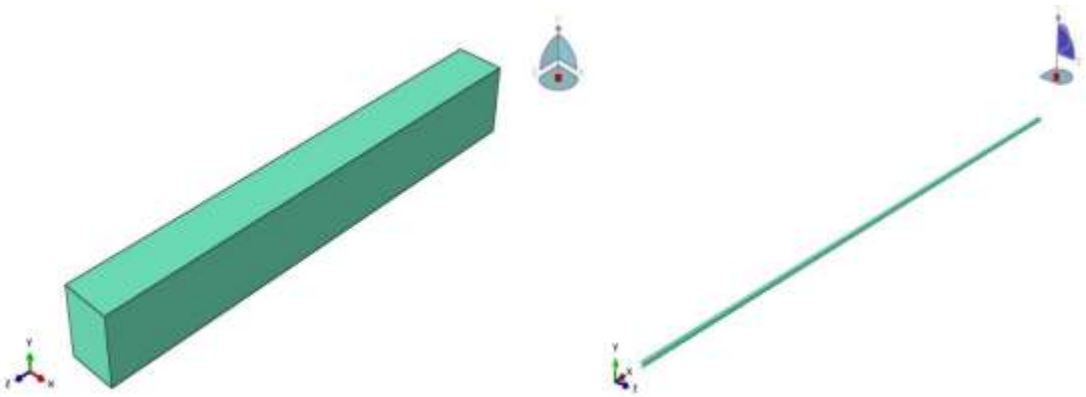

(a) (b)

Fig 5. 2 : (a) Beam model as 3D solid element (C3D8), (b) Longitudinal rebar model as 1D truss element (T3D2)

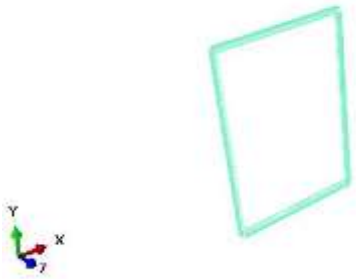

Fig 5. 3 : Stirrup model as 1D truss element (T3D2)

In the present study, C3D8 element has been employed to model concrete material of RC structure to avoid longer run time for the analysis. C3D8 element is simple linear continual solid brick element with 8 (2 x 2 x 2) integration points. On the other hand, ABAQUS v14 offer a range of two nodded link elements such as truss element T3D2. In the present study, T3D2 element has been employed to model reinforcement bars of RC beams.

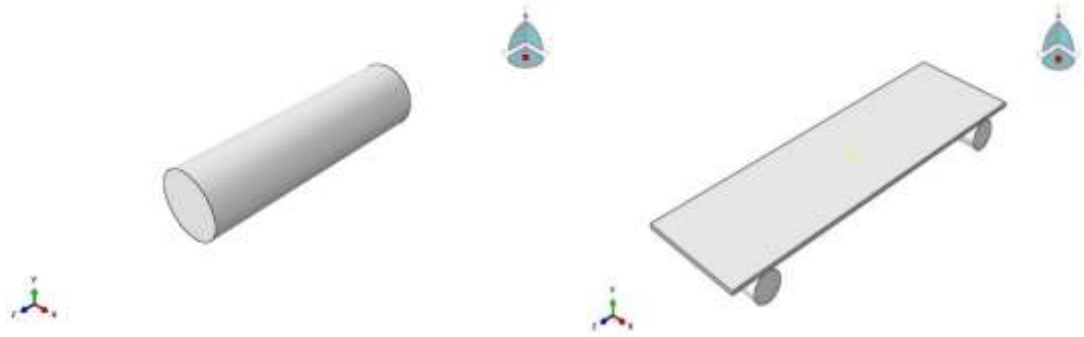

(a) (b)

Fig 5. 4 : (a) Bottom roller support of the beam model as 3D solid element, (b) Loading shell at the top of the beam model as 3D discrete rigid

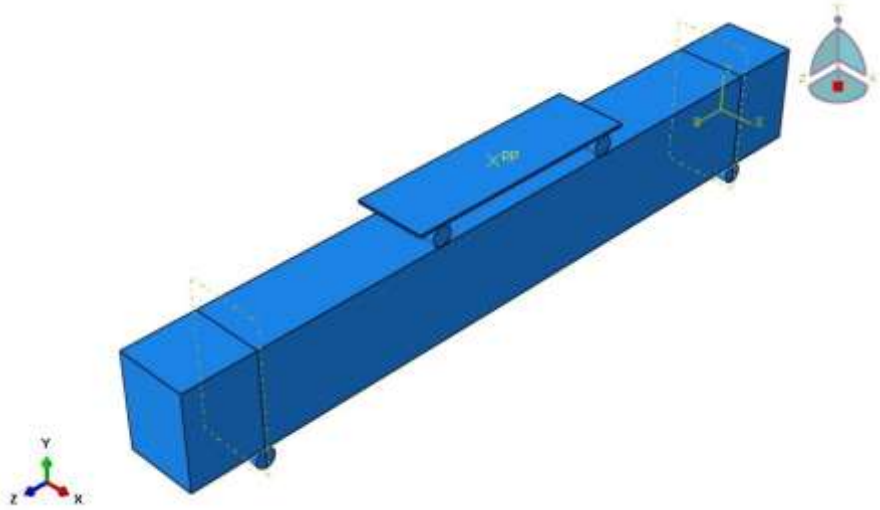

Fig 5. 5 : 3D view of overall geometry of numerical model

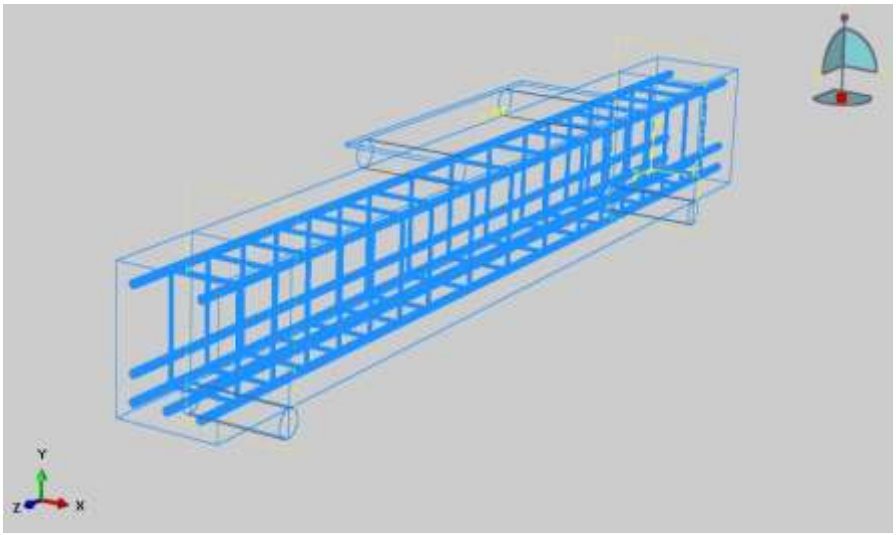

Fig 5. 6 : Reinforcement arrangement inside the numerical model

5.5 FE Modeling of Concrete Components

The explicit FE method has proven to be an effective tool, especially for transient impact analyses. The FEM for RC structures have generally been based on replacing the composite continuum by an assembly of elements representing the concrete and the steel reinforcement. From the literature, it has been observed that three techniques are mainly employed for modelling reinforcement in a 3D FEM of a concrete structure: smeared model, embedded model, and discrete model. In this study, embedded element technique is chosen depending on the application and the degree of detail in which the model needs to be developed. However, most of the difficulties in modelling of RC behavior depend on the development of an effective and realistic concrete material formulation and not in the modelling of the reinforcement.

5.5.1 Rebar as Embedded Element

To overcome mesh dependency in the discrete model, the embedded formulation allows independent choice of concrete mesh, as shown in Fig. 5.7. In this approach, the stiffness of the reinforcement elements is evaluated independently from the concrete elements, but the element is built into the concrete mesh in such a way that its displacements are compatible with those of surrounding concrete elements. The concrete elements and their intersection points with each reinforcement segment are identified and used to establish the nodal locations of the reinforcement elements. The embedded formulation is generally used with higher-order elements. In concrete structures where reinforcement modelling is complex, the embedded representation is advantageous. However, the additional nodes required for the reinforcement increase the number of degrees of freedom (DOFS), and hence the solution time. Furthermore, researchers have found that analyses with the embedded representation are in general more computationally efficient than those with the discrete representation.

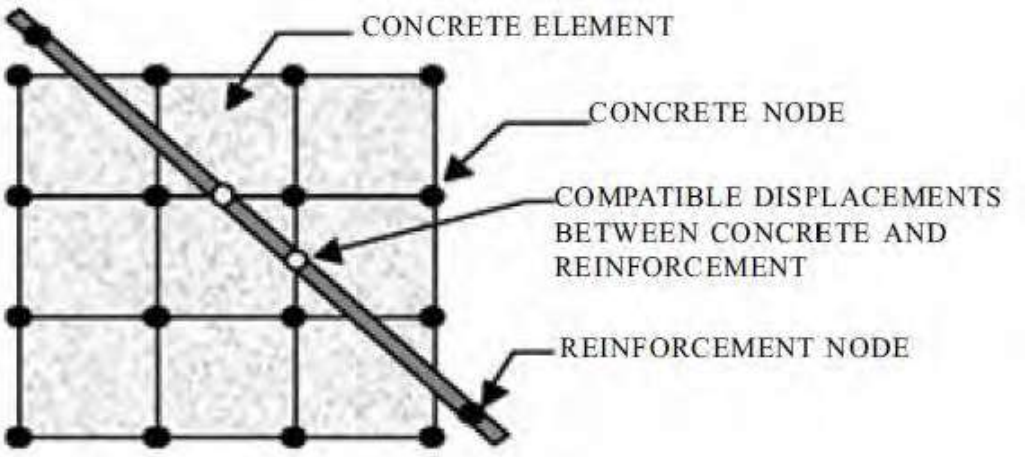

Fig 5. 7 **:** Embedded formulation for RC beams

5.6 Contact Zone Modeling

Several contact algorithms are available in the literature, namely, frictional sliding, single-surface contact, nodes impacting on a surface, tied interfaces, 1-D slide lines, rigid walls, material failure along interfaces, penalty and Lagrangian projection options for constraint enforcement and fully automatic contact. The strain compatibility is maintained at the contact zone since the reinforcement are modeled as the embedded element inside the concrete.

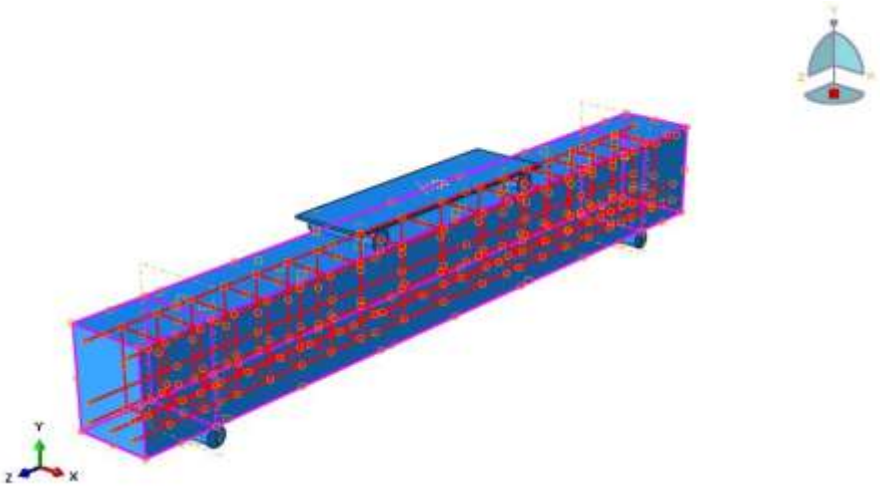

Fig 5. 8 : Embedded contact between 1D rebar to 3D solid elements

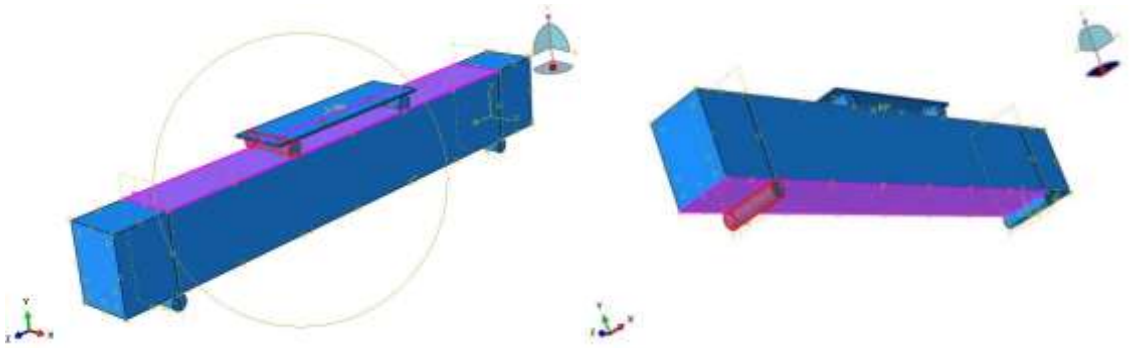

Fig 5. 9 : Surface to surface contact: (a) Rigid body to beam top surface, (b) Support (solid element) to beam bottom surface

This algorithm uses a penalty method to model the contact interface between the different parts particularly the surface between loading apparatus and top surface of the beams. In this approach, the slave and master surfaces are generated separately. An example of this approach is illustrated in Fig. 5.10. The internal forces added to the slave nodes are a function of the penetrated distance and a calculated stiffness for the master surface. The stiffness is computed as a function of the bulk modulus, volume, and surface area of the elements in the master surface. Friction less, tangential and hard normal behavior between different parts in contact has been used in the present study. The top roller is considered as the master surface where the beam top is the slave as the force transmits from roller to beams.

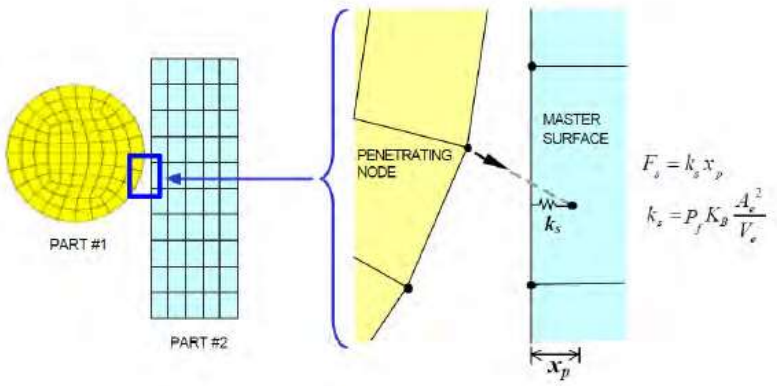

Fig 5. 10 **:** Penalty method for contact algorithm

5.7 Boundary Condition

In the model, two cylinders are placed beneath the beam as the bottom supports. The lower outer surfaces of two of the beams are made to confirm the pinned support condition i.e. no translation and rotation allowed. Moreover, x-directional and z-directional movements of the plate and cylinders are restrained.

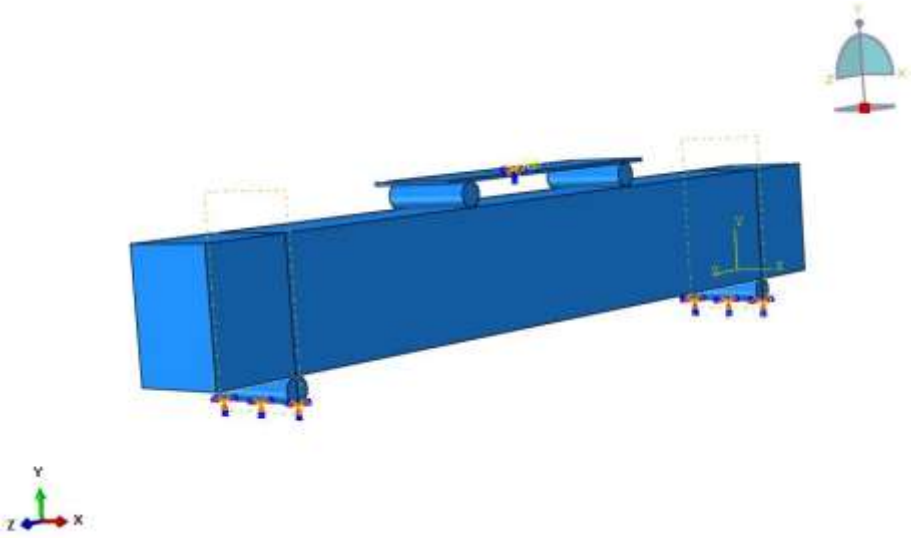

Fig 5. 11 : Boundary Conditions at the supports

5.8 Material Modeling

In material library of ABAQUS software, there is a wide range of tools that helps to model materials using the constitutive relationship. There are several material models to represent concrete and steel, which have been implemented in this commercial software used for simulation of concrete structures. For example, the Concrete Damage Plasticity (CDP) model, Concrete Smeared Crack model, and Modified Drucker-Prager/Cap model are widely acceptable and popular material models for modelling of concrete in ABAQUSv.14. In the present study, concrete damage plasticity (CDP) model has been employed to model concrete material of RC structure and elasto plastic non-linear behavior of reinforcing steel is considered in the material model of RC beams.

5.8.1 Concrete Damage Plasticity

The concrete damaged plasticity model in ABAQUS.v14 provides a general capability for modelling concrete and other quasi-brittle (rock, brick etc.) materials in all types of structures (beams, trusses, shells, and solids). CDP model also uses concepts of isotropic damaged elasticity in combination with isotropic tensile and compressive plasticity to represent the inelastic behavior of concrete. The uniaxial properties of concrete is presented in Fig. 5.12.

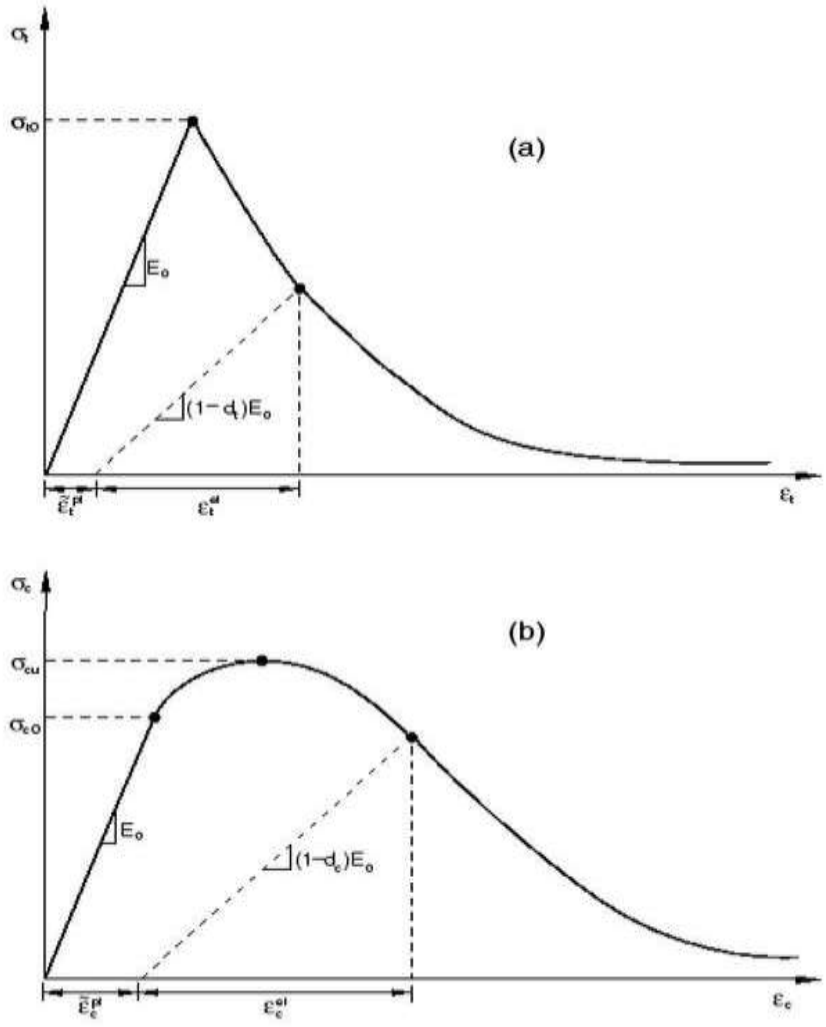

Fig 5. 12 **:** Response of Concrete to Uniaxial Loading in Tension (a) and Compression (b), Adopted from ABAQUS/Standard User's Manual, (2002).[73]

The model is a continuum of plasticity-based damage model for concrete. It assumes that the main two failure mechanisms are tensile cracking and compressive crushing of the concrete material. According to CEB-FIP 2010, the material model of concrete follows the relationship as shown in 5.13 and 5.14 which are accommodated in this study.

Table 5.1: Concrete Damage Plasticity (Example for, f'c = 50 Mpa)

Density, ρ (N-sec2/mm4)	2.40455E-09	Modulus of Elasticity, E (N/mm2)	32092.88
Poison's Ratio, ν	0.15		
Dilation angle, Ψ	38°	Eccentricity	0.1
fbo/fco	1.16	K	0.67

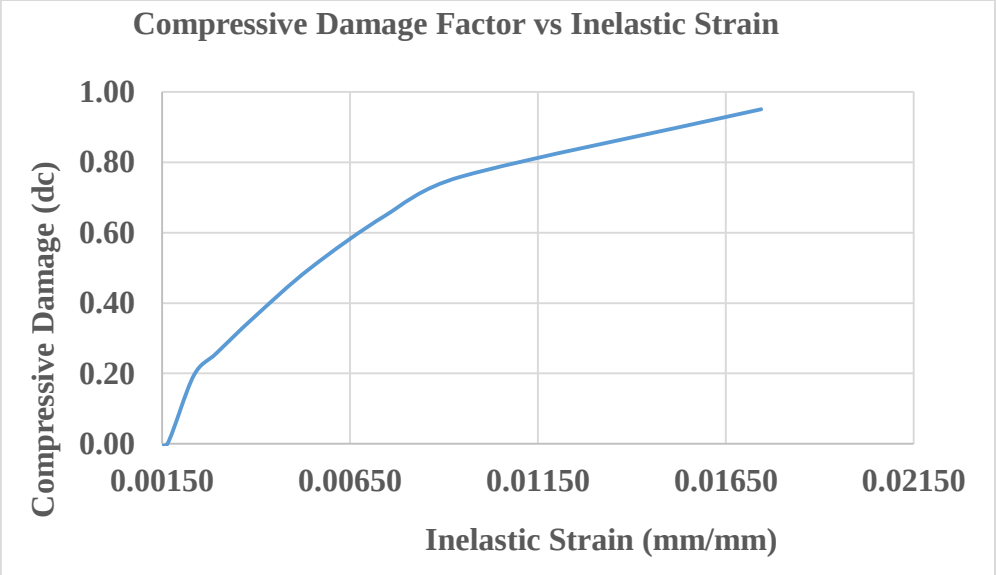

Fig 5. 13: Compressive Damage Factor vs Inelastic Strain

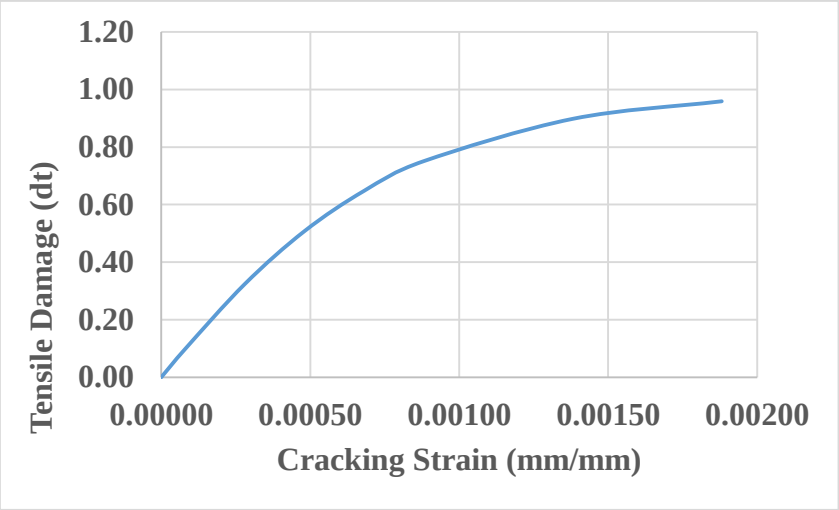

Fig 5. 14 : Tensile Damage Factor vs Cracking Strain

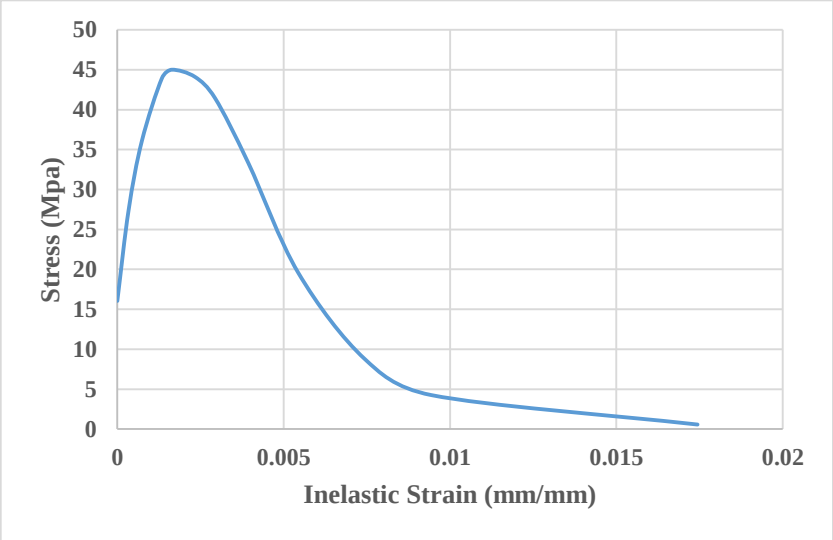

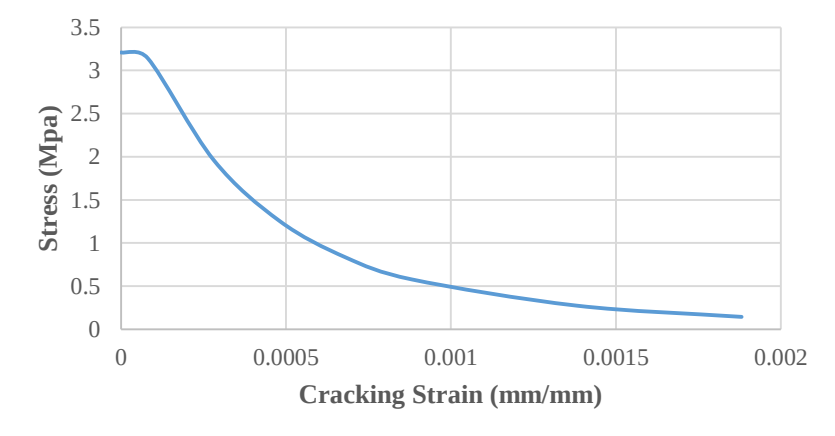

Fig 5. 15 : Tensile Stress vs Inelastic and cracking Strain

5.8.2 Material model for Stainless Steel:

The simplified Ramberg-Osgood model ware used for two different diameter (10mm and 12mm) stainless steel reinforcement as given in chapter 3 Fig 3.4. As stated previously, the stress-strain behavior of stainless steel is quite different from that of carbon steel as shown in Fig: 3.6. Carbon steel has a linear elastic response with a well-defined yield point and yield plateau, followed by a moderate degree of strain hardening. On the other hand, stainless steel exhibits a predominantly non-linear and continuous stress-strain response without a clearly-defined yield point as well as significant levels of strain hardening.

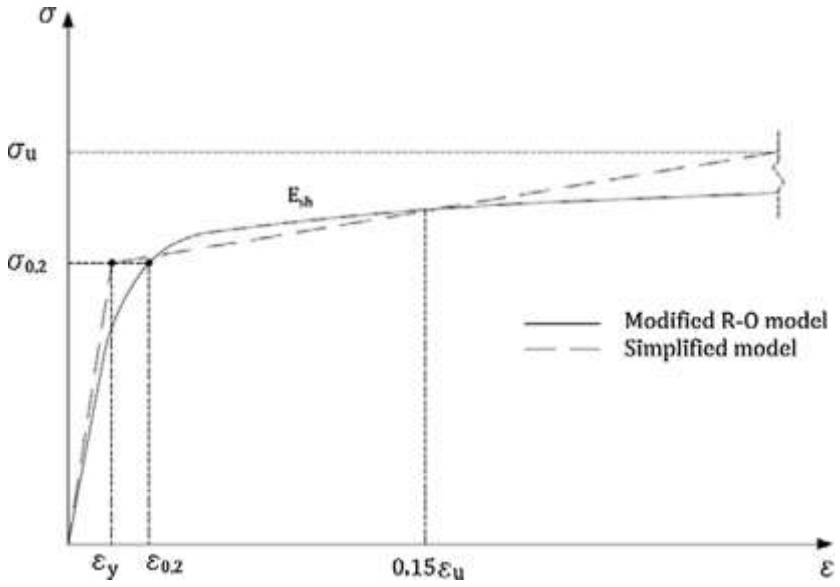

Fig 5. 16: (a) Adopted from Ramberg and Osgood 1943, Adopted from Ramberg and Osgood (1943) [21]

In the absence of a visible yield point, the typical value adopted is the 0.2% proof stress σ (0.2%) which is determined by drawing a line with a slope equal to the elastic modulus (E) between 0.2% strain on the x-axis and the stress-strain curve. The analysis employs the modified Ramberg-Osgood stainless steel material model [22, 58], as depicted in Fig. 5.16.

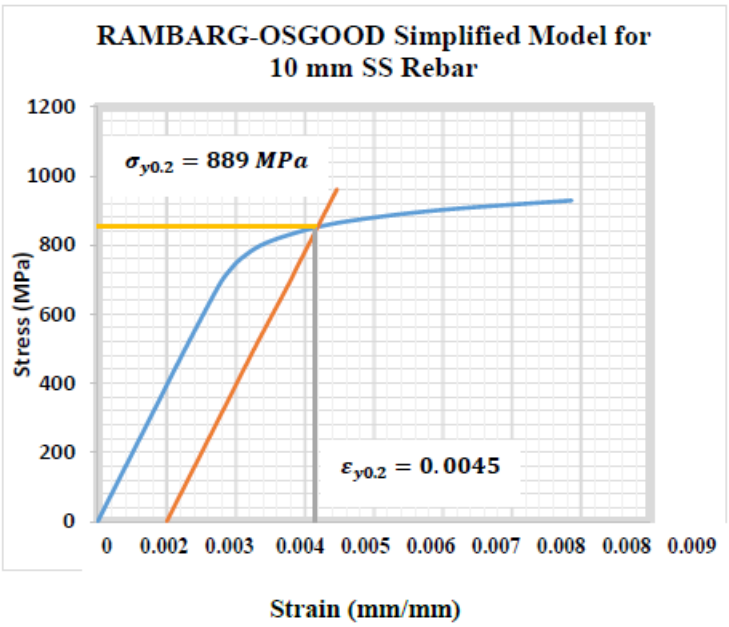

Fig 5.16: (b)

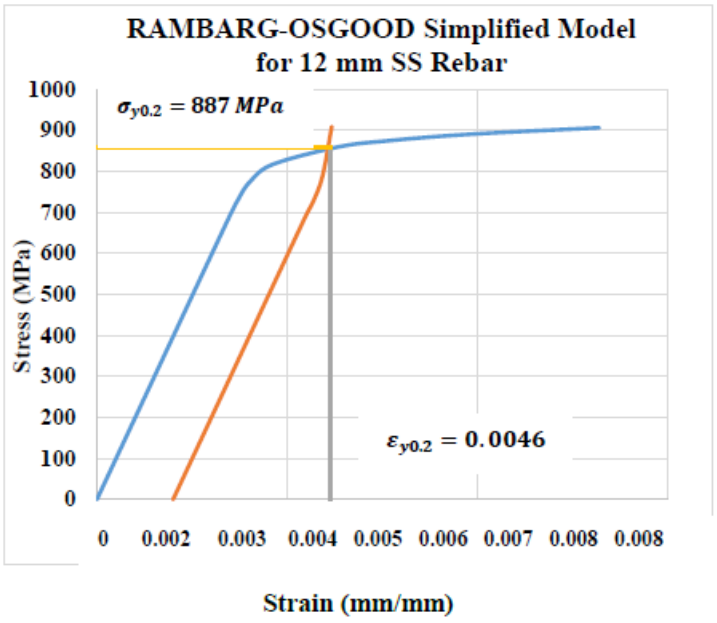

Fig: 5.16: (c)

Fig 5. 17 : (a)The simplified material model for stainless steel with reference to the modified R-O model, 5.19(b) R-O Model for 10 mm SS rebar, 5.19(c) R-O Model for 12 mm SS rebar

5.9 Loading Protocol

In the present study, the loading protocol used is displacement-controlled method. Here, a downward displacement in a rate of 1mm/min (as imposed in the experiment) was applied on the top surface of the plate placed over the cylinders. This system generates a load vs. displacement graph which is used to determine the flexural properties of the RC beams.

5.10: Selection of Meshes

The ABAQUS mesh module tools allow generating meshes on the part element or assembled parts model created within ABAQUS software. In the numerical model, meshing of structural elements was performed using uniform element size. Mesh module within ABAQUS software provides control over the element meshing to create particular mesh model topologies and also optimizes the size of mesh to obtain reliable results.

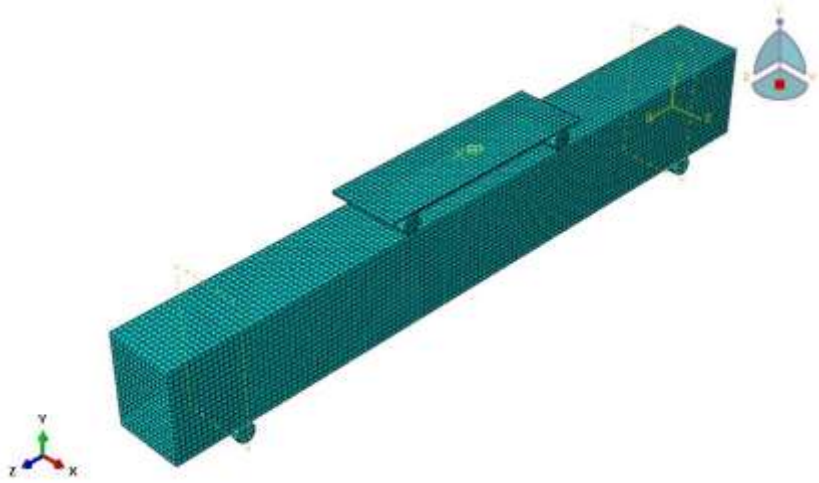

Fig 5. 18 : Solid elements

- Mesh size: 12 mm
- Geometric order: Linear
- Family: 3D stress
- Element Library: Explicit
- Hexagonal, Reduced integration
- C3D8R: An 8-node linear brick, reduced integration, hourglass control

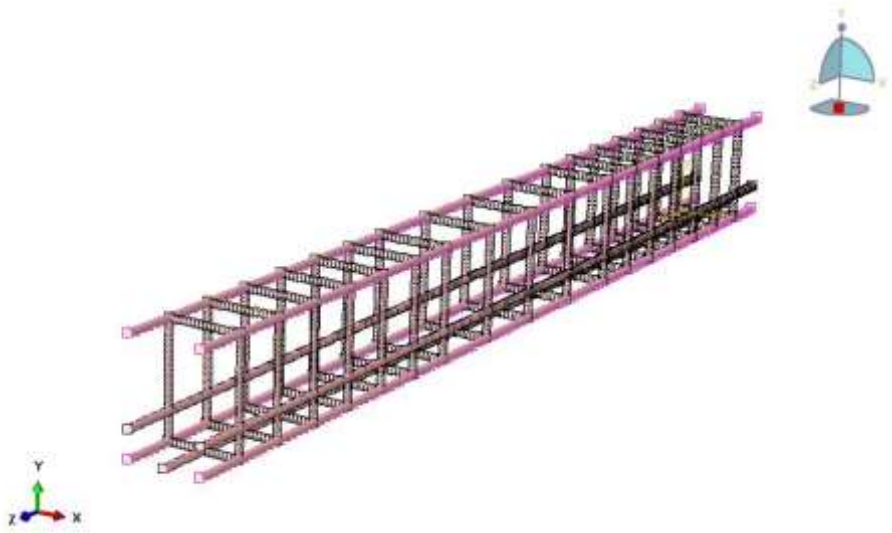

Fig 5. 19 : Truss elements to emulate the reinforcements

- ❖ Mesh size : 12 mm
- ❖ Geometric order: Linear
- ❖ Family: Truss
- ❖ Element Library: Explicit
- ❖ T3D2: A 2-node linear 3-D truss

After finalizing the model definitions, the model is run and analyzed by ABAQUS Job module. The ABAQUS Job module allows the submitted job to be monitored during the analysis progress.

5.11 Solution Strategy

In the model, both material and geometric non-linearity are considered to determine the accurate flexural capacity of reinforced beams. The explicit FE analysis performs the incremental procedure and at the end of each increment updates the stiffness matrix based on geometry change (if applicable) and material changes (if applicable). Then a new stiffness matrix is constructed and the next increment of load or displacement is applicable to the system. In this type of analysis, the hope is that if the increments are small enough the results will be accurate.

5.12 Experimental Validation

5.12.1 Comparison between experimental and numerical results

Primarily, comparisons were made for the beams reinforced with MS rebars. Later, a comparative study between experimental and numerical results for both SS reinforced concrete beams and MS reinforced concrete beams was done.

In Figure 5.20, load-displacement curves for MS reinforced concrete beam developed from experiment and numerical models are presented. The figure shows that the experimental load displacement response is quite close to that of the numerical analysis. The peak load obtained from the numerical beam analysis was 61.83kN with the corresponding maximum displacement of 4.00 mm and the peak load obtained for experimental beam was 62.17kN with corresponding displacement of 14.16 mm. The experimental result shows that the peak load is obtained at a relatively larger displacement than that of the numerical model. The reason for the experimental beam to show higher displacement is mainly due to the application of geotextile in the experimental set-up that was placed under the loading apparatus to fix it with the beam. The geo-textile has a very low stiffness and displaced easily at the start of the test on its own and thus shows more displacement than the ABAQUS numerical model curve. The crack pattern and failure at ultimate load as observed in the experiment also quite similar to that in numerical output.

Mild Steel Reinforced Concrete Beam (MSL-2)

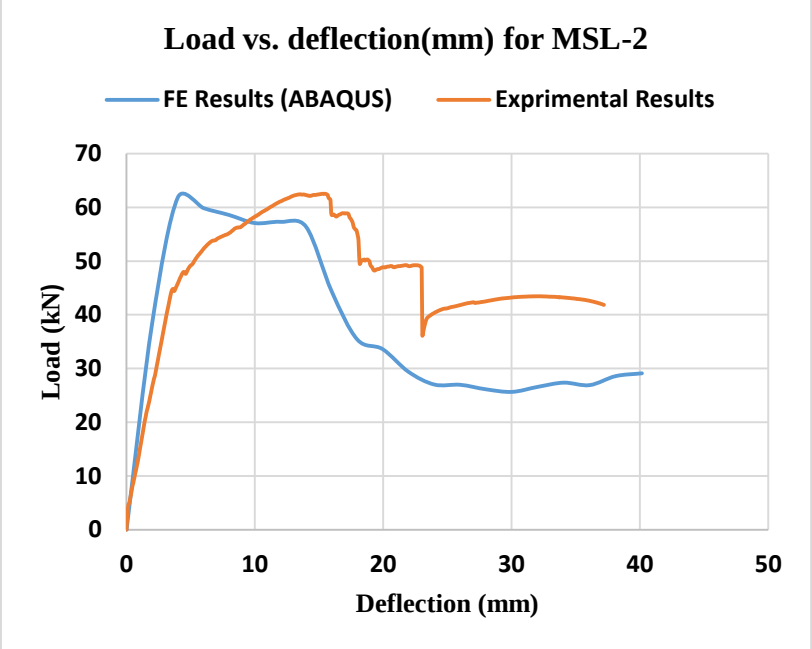

Fig 5. 20 **:** Load vs. displacement of experimental and numerical model of mild steel reinforced concrete beam (MSL-2)

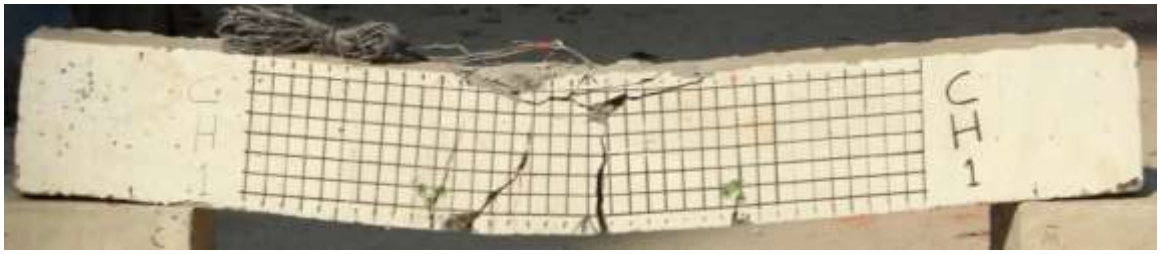

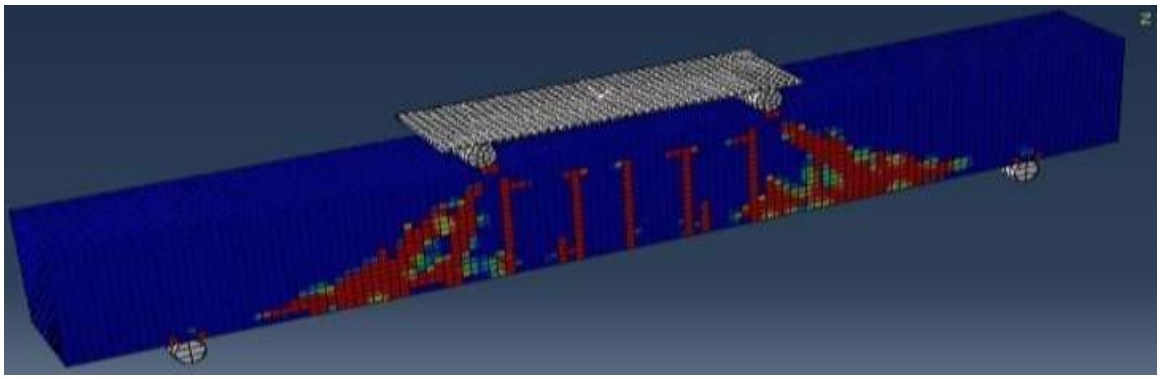

Fig 5. 21 : Response of experimental and numerical model (a-b) of mild steel reinforced concrete beam (MSL-2)

Mild Steel Reinforced Concrete Beam (MSL-1)

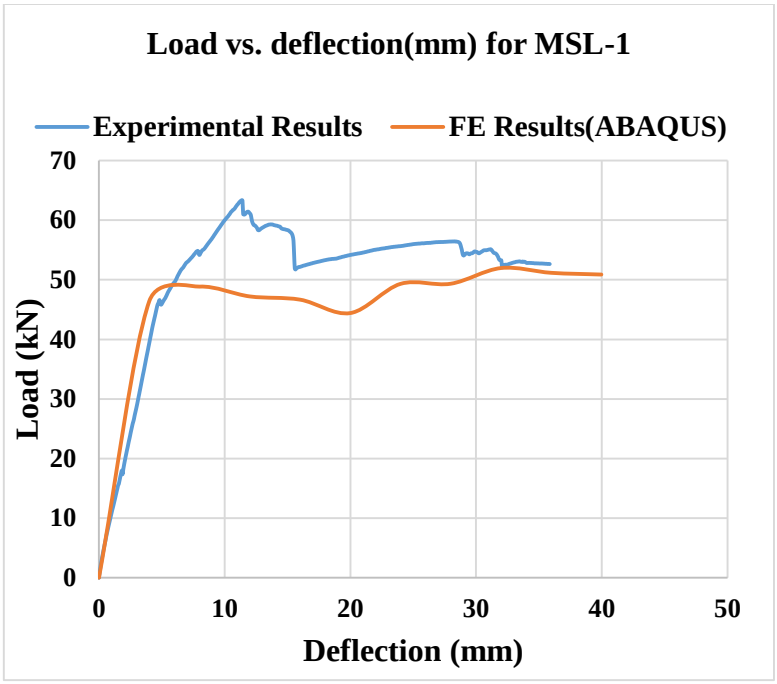

Fig 5. 22: Load vs. displacement of experimental and numerical model of mild steel reinforced concrete beam (MSL-1)

(a) Observed beam specimen

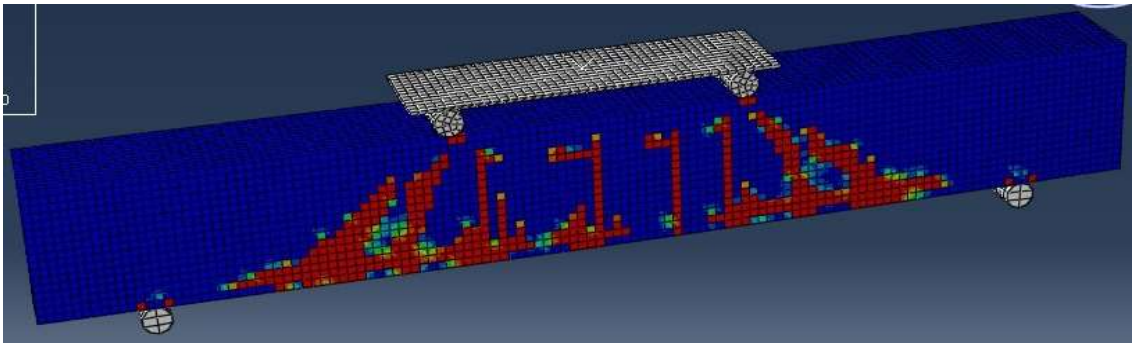

(b) Damage tension

Fig 5. 23 : Response of experimental and numerical model (a-b) of mild steel reinforced concrete beam (MSL-1)

In Figure 5.22, the figure shows that load displacement response obtained from experimental investigation is quite close to that of the numerical analysis for mild steel at low reinforcement ratio. The peak load obtained for numerical beam model was 48.86kN with corresponding displacement of 8.00 mm and the peak load obtained for experimental beam was 60.75kN with corresponding displacement of 10.30 mm. The experimental curve shows that the peak load is obtained at a greater displacement than that of the numerical model curve. The main variation in behavior between the predicted and the observed results can be viewed after the peak load has reached, where ABAQUS v.14 found that the beam lost its capacity at 48.86 KN as the peak load, whereas the actual beam sustained up to 60.75 kN load. The result is quite similar to the other MS reinforced beams as observed in the existing literature.

Mild Steel Reinforced Concrete Beam (MSH-2)

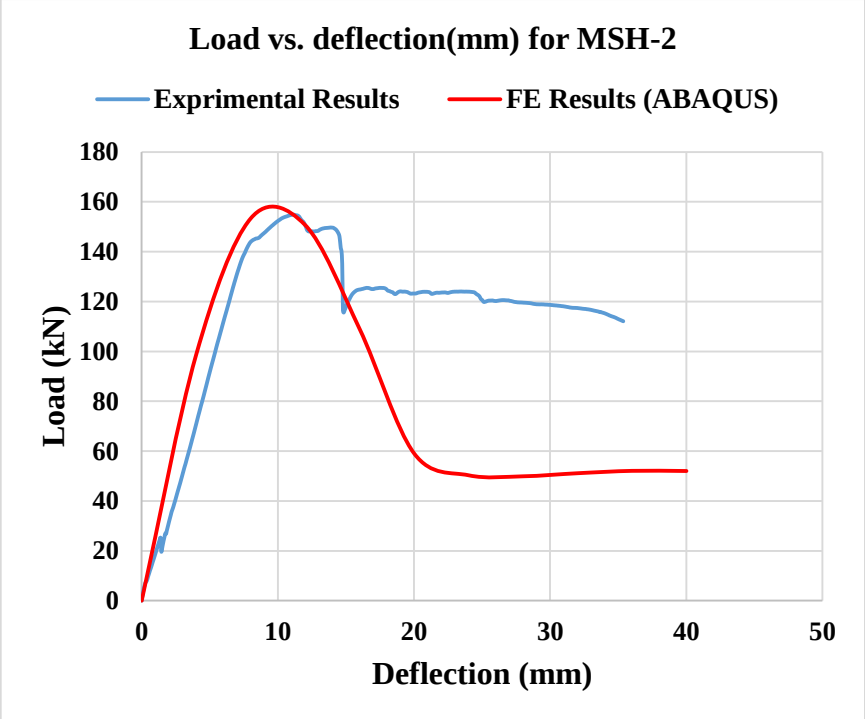

Fig 5. 24 **:** Load vs. displacement of experimental and numerical model of mild steel reinforced concrete beam (MSH-2)

(a) Observed beam specimen

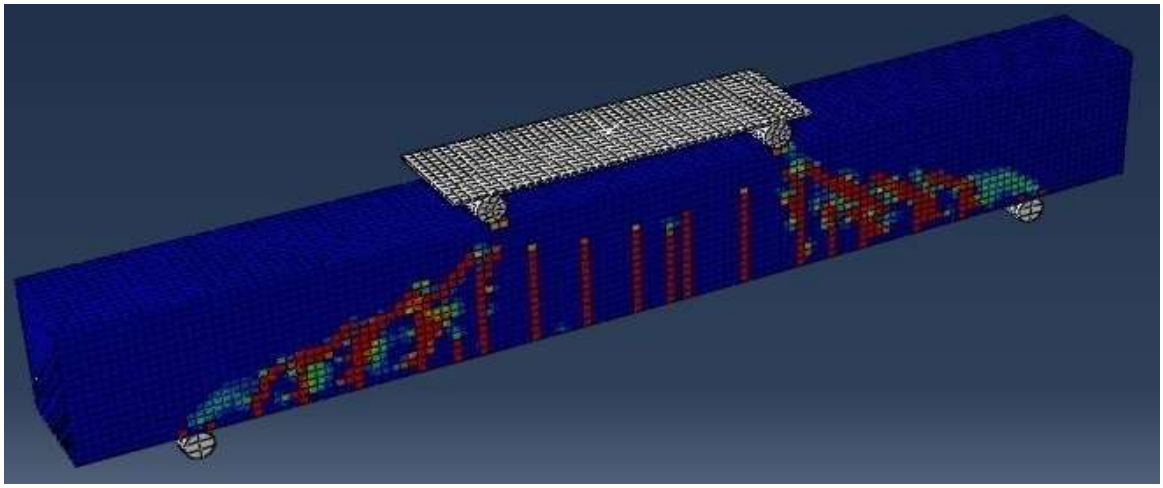

(b) Damage tension

Fig 5. 25 : Response of experimental and numerical model (a-b) of mild steel reinforced concrete beam (MSH-2)

It is obtained from the Figure 5.26, the load-displacement relationship obtained from experimental investigation and numerical analysis are very close. The peak load obtained for numerical beam model was 153.3kN with corresponding displacement of 8.00 mm and the peak load obtained for experimental beam was 153.82kN with corresponding displacement of 10.46 mm. In addition, the crack patterns of experimental beam and numerical cracking profile are also apparently similar.

Mild Steel Reinforced Concrete Beam **(MSH-1)**

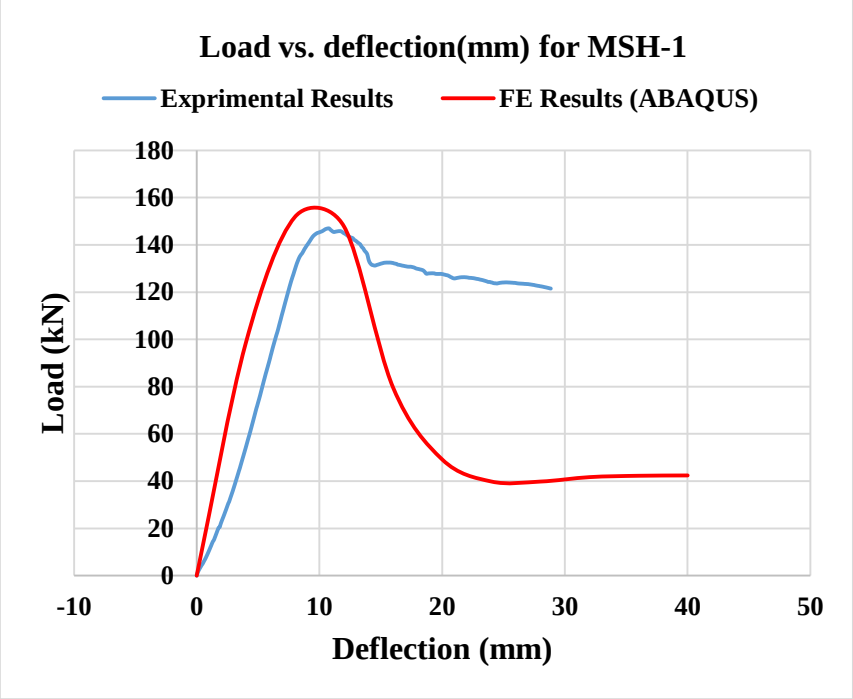

Fig 5. 26 **:** Load vs. displacement of experimental and numerical model of mild steel reinforced concrete beam (MSH-1)

(a) Observed beam specimen

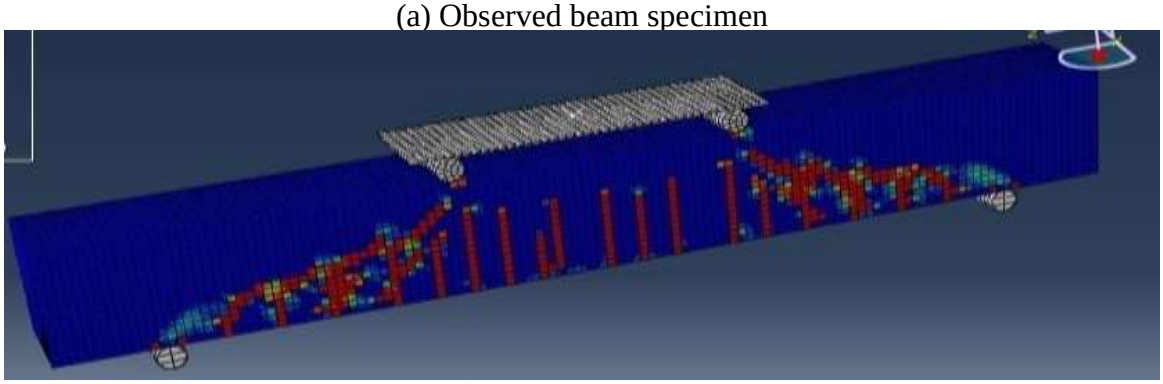

(b) Damage tension

Fig 5. 27 : Response of experimental and numerical model (a-b) of mild steel reinforced concrete beam (MSH-1)

In Figure 5.26 the load of both the curves are observed to be close and hence showed a good agreement with that of the experimental results. The peak load obtained for numerical beam model was 151.80kN with corresponding displacement of 8.00 mm and the peak load obtained for experimental beam was 146.98kN with corresponding displacement of 10.76 mm. The experimental curve shows that the peak load is obtained at a greater displacement than that of the numerical model curve.

Stainless Steel Reinforced Concrete Beam **(SSL-2)**

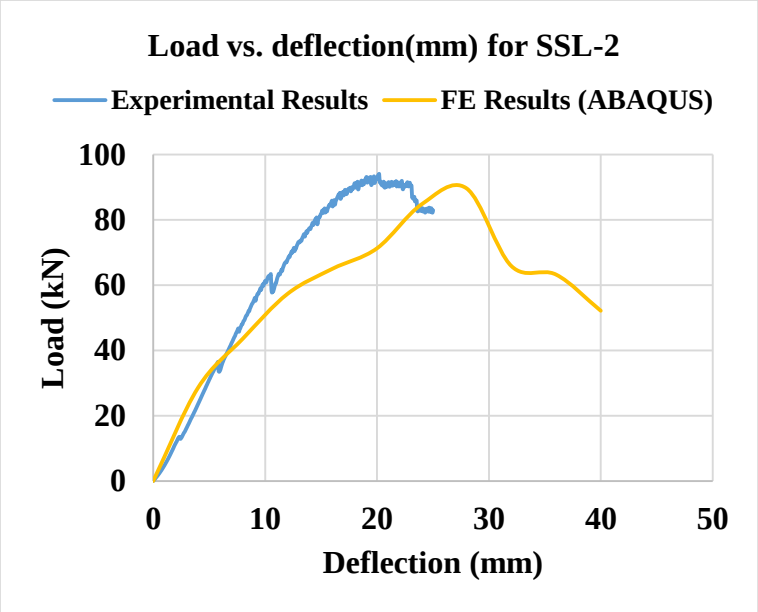

Fig 5. 28 **:** Load vs. displacement of experimental and numerical model of mild steel reinforced concrete beam (SSL-2)

(a) Observed beam specimen

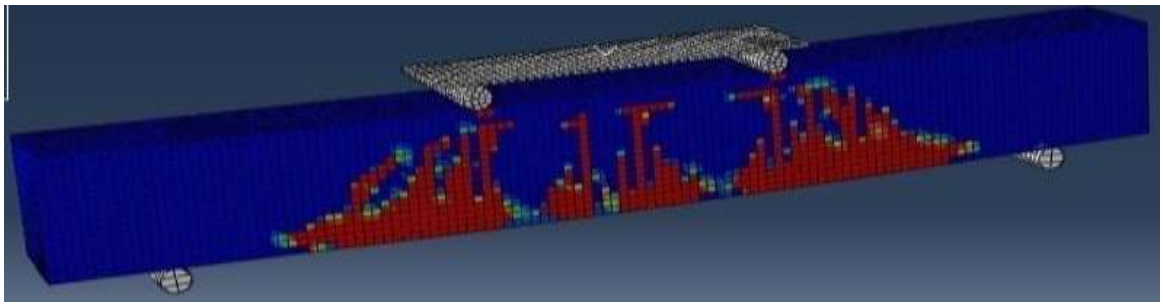

(b) Damage tension

Fig 5. 29 **:** Response of experimental and numerical model (a-b)of mild steel reinforced concrete beam (SSL-2)

In Figure 5.27 the load displacement curve is also observed to be close that ultimately declares the validation experimental results. The peak load obtained for numerical beam model was 89.67kN with corresponding displacement of 27.99mm and the peak load obtained for experimental beam was 91.93kN with corresponding displacement of 19.17 mm. The experimental curve shows that the peak load is obtained at a less displacement than that of the numerical model curve. The crack patterns particularly the flexural crack at middle of the beam is quite similar to the experimental test beam and numerical analysis output.

In the relationship as presented in Figure 5.30, shows that that load displacement response obtained from experimental investigation is quite close to that of the numerical analysis for stainless steel at low reinforcement ratio. The peak load obtained for numerical beam model was 84.81kN with corresponding displacement of 28.00 mm and the peak load obtained for experimental beam was 70.05kN with corresponding displacement of 17.66 mm. The experimental curve shows that the peak load is obtained at a greater displacement than that of the numerical model curve. The reason for the experimental beam to show more displacement is due to the use of geotextile in the experimental beam. The geotextile has a

greater displacement of its own and thus shows more displacement than the ABAQUS numerical model curve.

Stainless Steel Reinforced Concrete Beam **(SSL-1)**

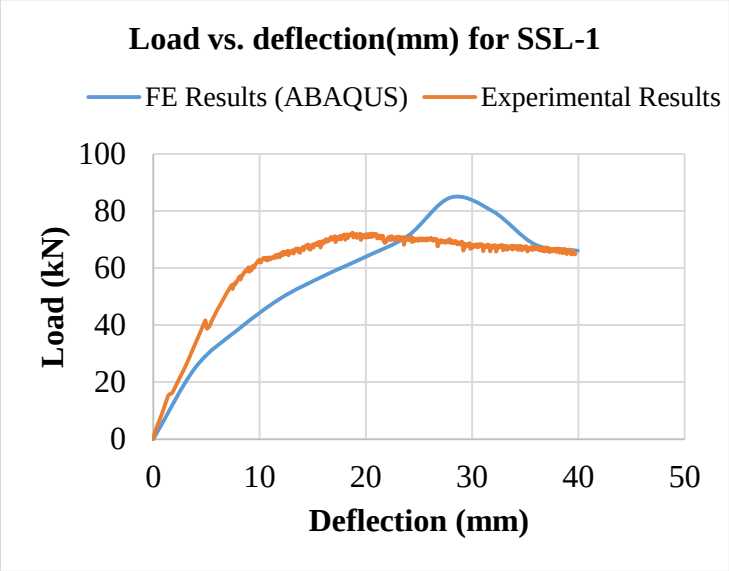

Fig 5. 30 **:** Load vs. displacement of experimental and numerical model of mild steel reinforced concrete beam (SSL-1)

(a) Observed beam specimen

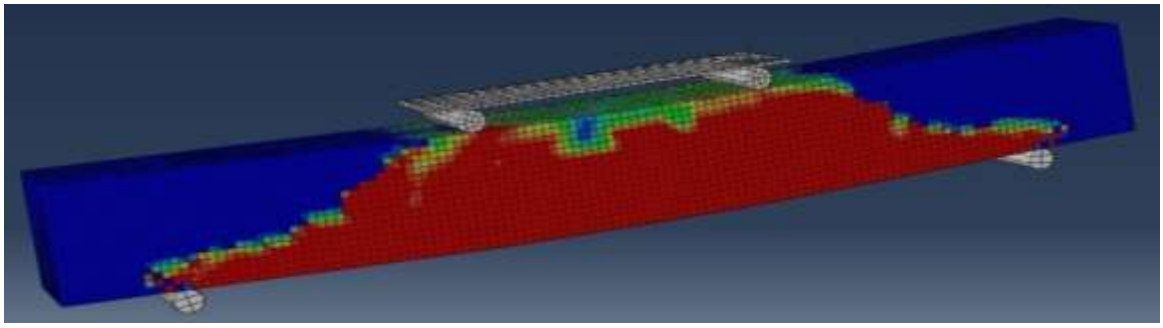

(b) Damage tension

Fig 5. 31**:** Response of experimental and numerical model (a-b) of mild steel reinforced concrete beam (SSL-1)

Stainless Steel Reinforced Concrete Beam **(SSM-1)**

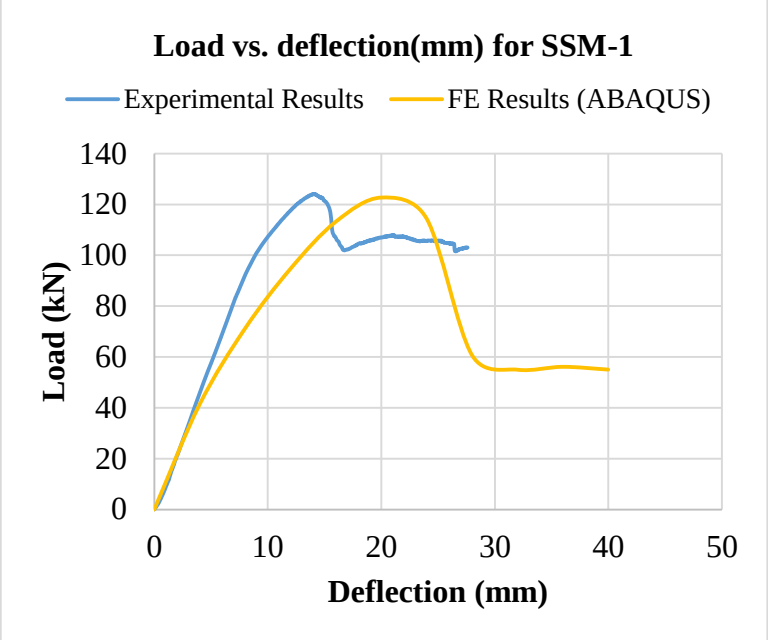

Fig 5. 32 **:** Load vs. displacement of experimental and numerical model of mild steel reinforced concrete beam (SSM-1)

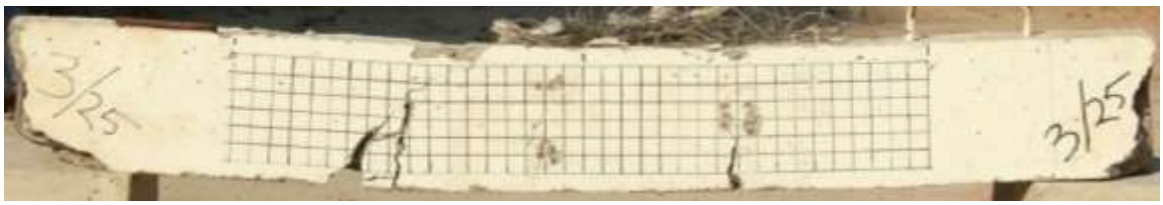

(a) Observed beam specimen

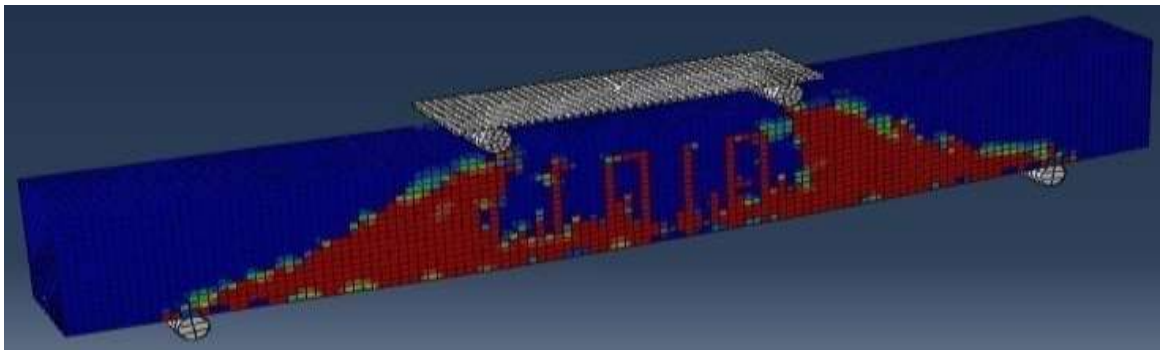

(b) Damage tension

Fig 5. 33**:** Response of experimental and numerical model (a-b) of mild steel reinforced concrete beam (SSM-1)

In Figure 5.32, that load displacement response obtained from experimental investigation is quite close to that of the numerical analysis for stainless steel at low reinforcement ratio. The peak load obtained for numerical beam model was 121.89kN with corresponding displacement of 13.13 mm and the peak load obtained for experimental beam was 114.407kN with corresponding displacement of 23.99 mm. The experimental curve shows that the peak load is obtained at a greater displacement than that of the numerical model curve. The main variation in behavior between the predicted and the observed results can be viewed after the peak load has reached, where ABAQUS (2014) found that the beam lost its capacity at 121.89 kN as the peak load, whereas the actual beam sustained up to 114.40 kN load.

Stainless Steel Reinforced Concrete Beam **(SSM-2)**

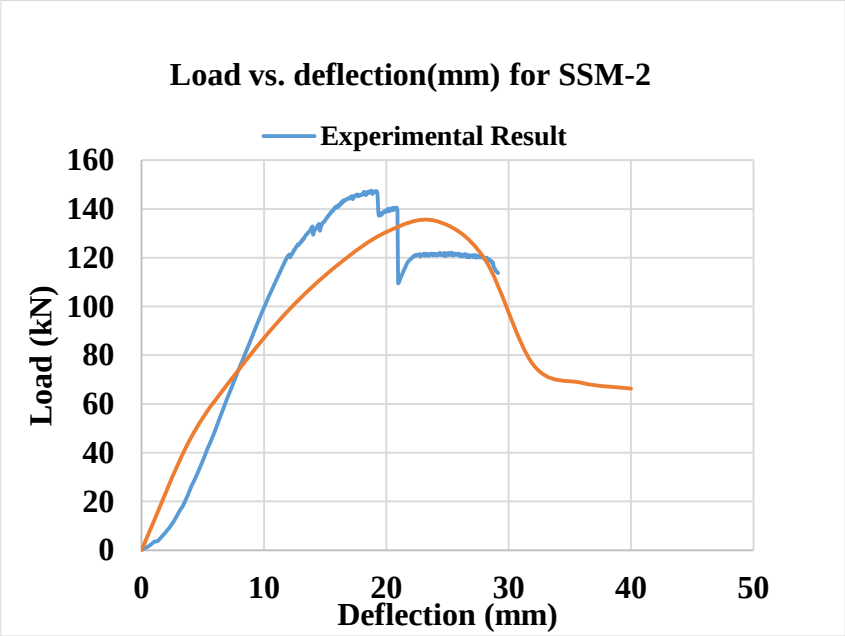

Fig 5. 34**:** Load vs. displacement of experimental and numerical model of mild steel reinforced concrete beam (SSM-2)

(a) Observed beam specimen

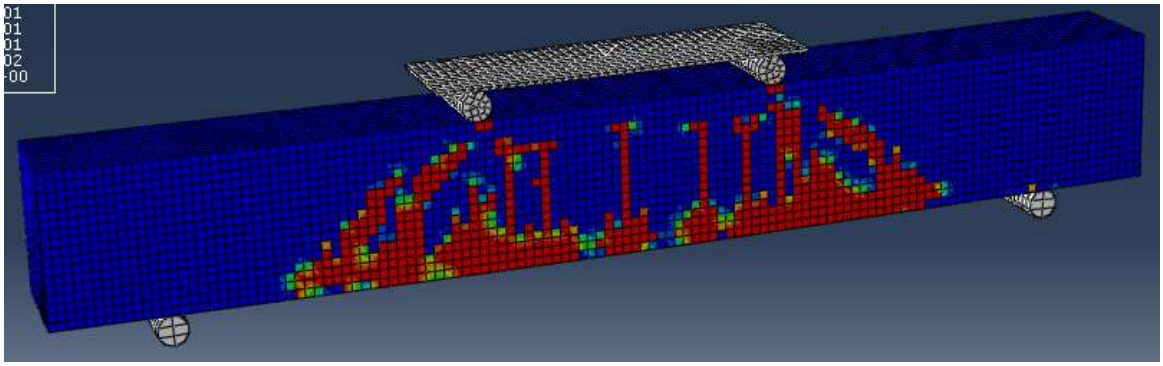

Fig 5. 35 : Response of experimental and numerical model (a-b)of mild steel reinforced concrete beam (SSM-2)

Similar to the previous FE output, for medium steel ratio, experimental results of SS reinforced beam shows a very close result with the numerical model as shown in Figure 5.34. The peak load obtained for numerical beam model was 135.16 kN with corresponding displacement of 23.99 mm and the peak load obtained for experimental beam was 145.66kN with corresponding displacement of 17.86 mm. The experimental curve shows that the peak load is obtained at a less displacement than that of the numerical model curve.

Stainless Steel Reinforced Concrete Beam (SSH-2)

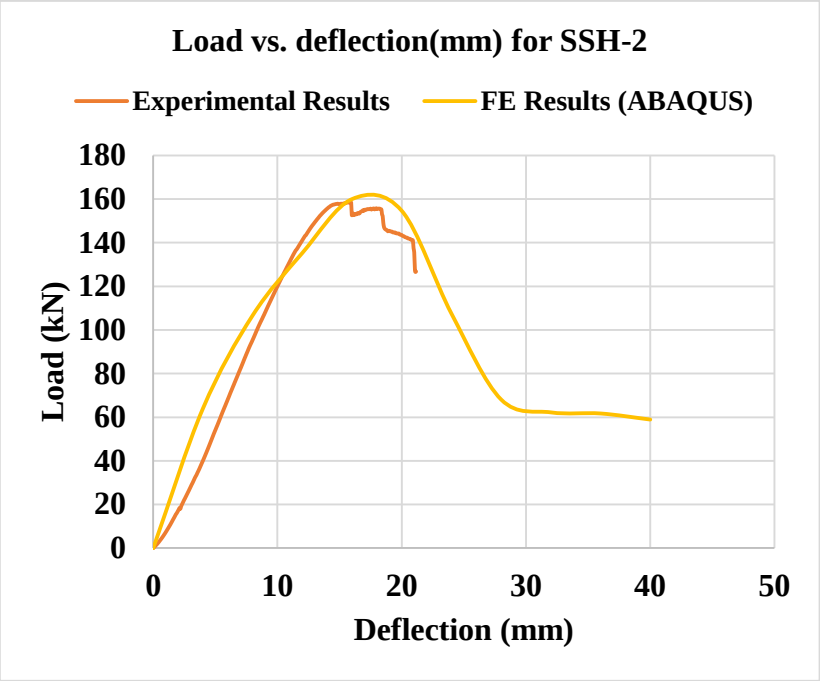

Fig 5. 36 **:** Load vs. displacement of experimental and numerical model of mild steel reinforced concrete beam (SSH-2)

(a) Observed beam specimen (Experiment)

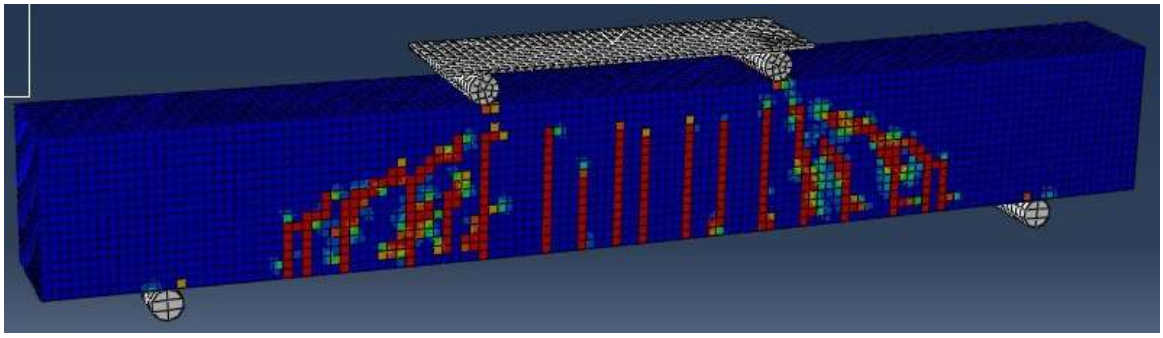

(b) Damage tension (FE Model)

Fig 5. 37 **:** Response of experimental and numerical model (a-b)of mild steel reinforced concrete beam (SSH-2)

In Figure 5.35 that load displacement response obtained from experimental investigation is quite close to that of the numerical analysis for stainless steel at high reinforcement ratio. The peak load obtained for numerical beam model was 154.64kN with corresponding displacement of 20.004 mm and the peak load obtained for experimental beam was 159.99kN with corresponding displacement of 16.00 mm. The main variation in behavior between the predicted and the observed results can be viewed after the peak load has reached, where ABAQUS (2014) found that the beam lost its capacity at 154.64 kN as the peak load, whereas the actual beam sustained up to 159.99 kN load.

Stainless Steel Reinforced Concrete Beam **(SSH-1)**

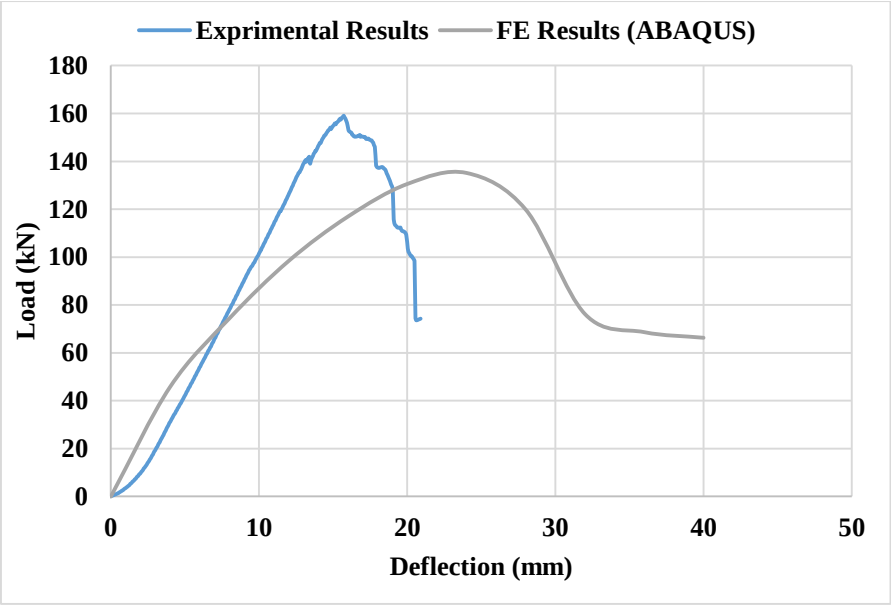

Fig 5. 38 **:** Load vs. displacement of experimental and numerical model of mild steel reinforced concrete beam (SSH-1)

(a) Observed beam specimen

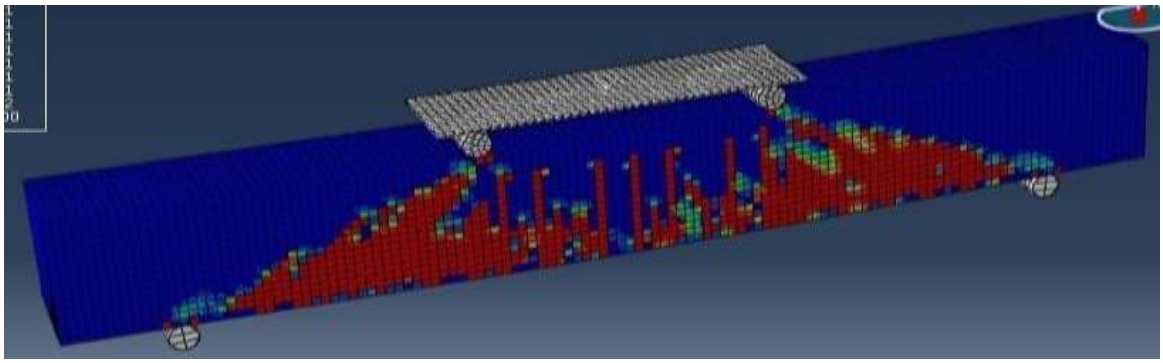

(b) Damage tension

Fig 5. 39 **:** Response of experimental and numerical model (a-b)of mild steel reinforced concrete beam (SSH-1)

Similar observation is finding in Fig:5.37 for SSH-1 reinforced beams except at higher load. The peak load obtained for numerical model was 135.16kN with corresponding displacement of 24.00 mm and the peak load obtained for experimental beam was 155.09kN with corresponding displacement of 15.02 mm. The experimental curve shows that the peak load is obtained at a less displacement than that of the numerical model curve.

In Figure 5.39, the peak load obtained for numerical beam model was 98.34kN with corresponding displacement of 23.99 mm and the peak load obtained for experimental beam was 126.12kN with corresponding displacement of 12.52 mm. This may happen due to the fact that concrete crushes at high steel ratio that results premature failure of the beam without yielding the steel rebars.

Stainless Steel Reinforced Concrete Beam (SSM'-2)

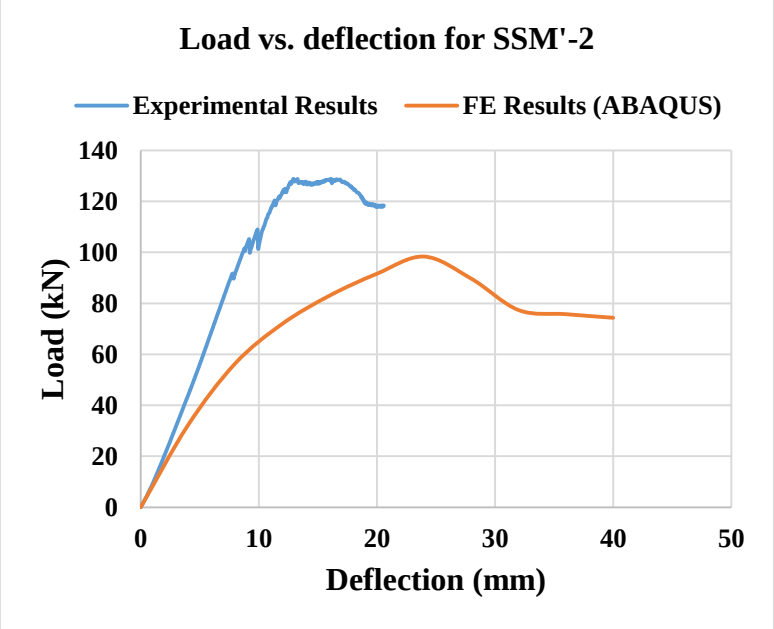

Fig 5. 40 **:** Load vs. displacement of experimental and numerical model of mild steel reinforced concrete beam (SSM'-2)

(a) Observed beam specimen

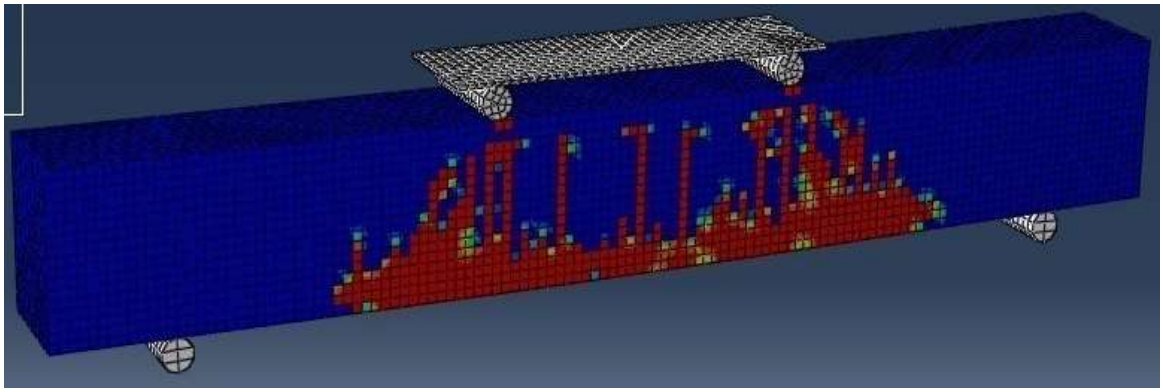

(b) Damage tension

Fig 5. 41 **:** Response of experimental and numerical model (a-b)of mild steel reinforced concrete beam (SSM'-2)

Stainless Steel Reinforced Concrete Beam (SSH' -1)

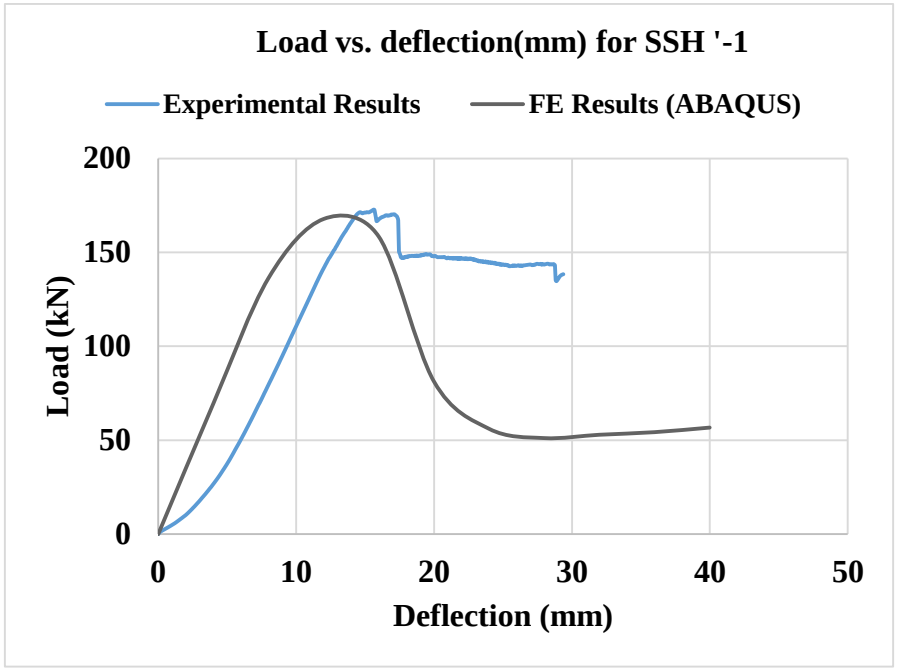

.

Fig 5. 42 **:** Load vs. displacement of experimental (CH1) and numerical model of mild steel reinforced concrete beam (SSH' -1)

(a) Observed beam specimen

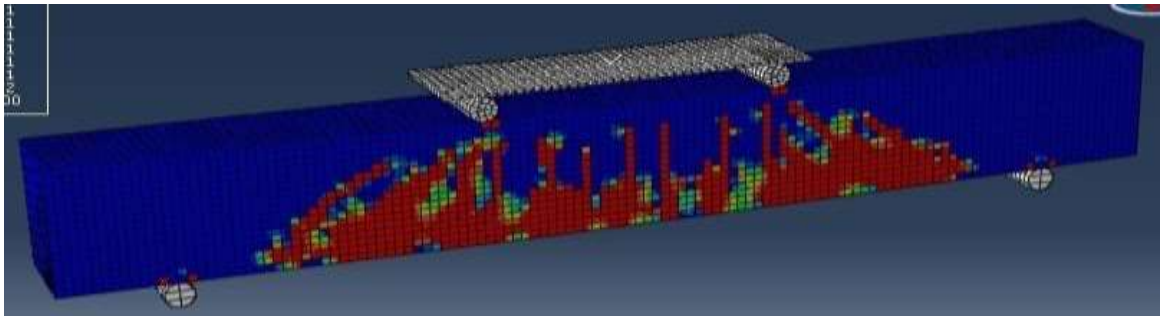

(b) Damage tension

Fig 5. 43 **:** Response of experimental and numerical model (a-b)of mild steel reinforced concrete beam (SSH' -1)

In Figure 5.41, the load displacement response obtained from experimental investigation is quite close to that of the numerical analysis for stainless steel at high reinforcement ratio. The peak load obtained for numerical beam model was 167.79kN with corresponding displacement of 11.99mm and the peak load obtained for experimental beam was 170.96kN with corresponding displacement of 14.86 mm. The experimental curve shows that the peak load is obtained at a greater displacement than that of the numerical model curve. The crack patterns of the actual beam shows similar behavior of the numerical analysis out particularly at the 1/3 point of the beam.

5.13 Conclusion

In this chapter, FE modeling procedure, assumption, analysis scheme and output extractions are discussed first. In addition, the FE results are compared with the experimental output as discussed in chapter 4. The results extracted from the numerical models were compared with that obtained from the experimental tests. The load verses mid span deflection of the beams has been compared and investigated. The responses of FE analysis has been found to be relatively similar to the actual response as observed in the test nearly for all beam specimens. In the current study, it is obtained from the results that the peak loads for experimental and numerical beam models are satisfactorily close enough though there are some differences in the initial stiffness. This difference can be described by the fact that minor mis-fit at the experimental test may change the displacement corresponding to the load. Besides, the concrete strength uncertainty may differ the actual ultimate capacity. Otherwise it may be concluded that the outcome from the numerical models were able to predict the ultimate capacity quiet accurately and the approach is successful for stainless steel reinforced concrete beams. The most accurately simulated model showed that 98.5% accuracy in predicting the ultimate load. The crack patterns and failure modes are also observed to be quite similar for both experiments and FE models.

CHAPTER 6

CONCLUSIONS

6.1 General

The research program presented in this thesis was investigated to study the flexural behavior of concrete beams reinforced with smooth Stainless Steel rebars. This experimental program included a total twelve reinforced concrete beams subjected four points bending test. Eight of them are SS reinforced concrete beams and remaining four beams are reinforced by carbon steel (CS) as control specimens. All beams were tested under static loading conditions up to failure in order to investigate the behavior during the cracking, ultimate capacities, and modes of failure. All beams were fully instrumented to monitor midspan deflection, steel strain, and crack propagation, and the flexural behavior of each beam. The experimental results and analysis conducted in this research are steered toward the development of reinforcement recommendation, which will address the use of SS rebars as reinforcements for structural concrete. Finally, a series of FE models are developed to simulate all twelve experimental beam following exact geometry, loading and boundary condition considering both geometric and material non-linearity.

6.2 Conclusions

Based on observed behavior, experimental results, theoretical prediction, and Finite Element analysis, the following conclusions can be made:

1) Mechanical properties of SS rebar shows that yield and ultimate strength of the SS rebars are observed to be 888 and 1015 MPa respectively which are higher than that of the normal CS/MS rebars. However, the modulus of elasticity of SS is approximately 195 MPa is smaller than the MS rebars.

2) From the load displacement response, the experimental results shows that SS reinforced beams shows larger deflection than that of the MS beams. This happens due to the fact that SS rebars has low stiffness than the MS rebars as we observed the rebar tests (as discussed in 1). Therefore, it can be concluded from the experimental results that Stainless Steel concrete beams were found less stiffer than mild steel reinforced beam.

3) For both of SS and MS reinforced concrete beams SSL-1, MSL-1 were similar steel ratio is 0.59 %, but the ultimate capacity for SS is significantly higher. The results indicate that the stainless steel concrete beams is around 38% higher ultimate capacity then MS concrete beam. Therefore, it can be concluded that the SS reinforced beam shows improved performance in low steel ratio.

4) SS rebars shows high deformability in rebar test and in the beam test. No rebar yielding is observed in case of beam test. SS reinforced beams shows higher performance in terms of ultimate capacity for low to medium steel ratio. The specimens with the medium longitudinal reinforcement ratio was 1.20% exhibited both of the largest deflection and ultimate capacity than low steel ratio.

5) All SS reinforced beams exhibit ductile flexural failure. The mode of failure was mostly classified as a ductile flexural failure, which is evident from the significant straining of reinforcement followed by concrete crushing in the compression zone.

6) FE models are developed to validate the experimental results which shows a very good agreement between them in terms of pick load and cracking patterns. For some cases, minor deviations are observed in initial stiffness which mainly arises from the test setup.In case of stainless steel reinforced concrete beam, the numerical

models predicted the peak loads with an accuracy of 96.86% of that observed in experimental test for concrete beam having id of SSH-2.

7) The outcome of this study opens the door to investigate local SS rebars so that they can be utilised as the reinforcement in structural components. The research outcome may be added in the national and international guideline to commercialize the SS grade 201 as rebar.

6.3 Limitations of the Study

To fulfill the objective of the experiment, there are scope to improve from the existing study. The limitations are stated below

1) Stainless steels are comparatively expensive than the MS. Although stainless steel is undoubtedly more expensive than carbon steel in terms of initial costs, over the life time of a structure if maintenance and rehabilitation works can be avoided through the use of more durable materials, then stainless steel provides a very competitive.

2) It is also important that the SS rebars that are available in local market are mostly smooth. Deformed SS rebar may improve the capacity of the concrete beam and hence other performances as well.

6.4 Recommendations for Future Study

The current research work has contributed to understanding of the behavior of reinforced concrete beam flexural behavior with SS rebars under static loading and to the implementation of a suitable design guidelines. However, several topics have been unveiled for investigation and some propositions require further validation. Several suggestions are given hereafter,

1) The data which is attended after the experimental work provide a base for any future study related with Stainless Steel Rebar. Additional tests must be performed to

evaluate the consistency of SS steel modified model in design. Such as cyclic fatigue tests should be pursued in order to provide fatigue strength results.

2) Future experimental programs on SS reinforcing beams subjected to severe environmental conditions should be done to verify the highly corrosion-resistant nature claimed by the manufacturer and taking into account the effect of surrounding concrete in corrosion of SS rebars.
3) Various studies on related topics, such as slabs, pre-stressed beams and columns should be carried out to develop a complete guideline on the use of SS rebars as reinforcements for structural concrete applications.

REFERENCES

[1] El-Mogy, M., A. El-Ragaby, and E. El-Salakawy, Behavior of continuous concrete beams reinforced with FRP Bars, in Advances in FRP Composites in Civil Engineering. 2011, Springer. p. 283-286.

[2] Issa, M.S., I.M. Metwally, and S.M.J.E.S. Elzeiny, Influence of fibers on flexural behavior and ductility of concrete beams reinforced with GFRP rebars. 2011. **33**(5): p. 1754-1763.

[3] Rasheed, H.A., R. Nayal, and H.J.C.S. Melhem, Response prediction of concrete beams reinforced with FRP bars. 2004. **65**(2): p. 193-204.

[4] Okelo, R., Development and splice lengths criteria for straight fiber reinforced polymer composite bars in tension. 2003.

[5] Uomoto, T. and S.J.S.P. Misra, Behavior of concrete beams and columns in marine environment when corrosion of reinforcing bars takes place. 1988. **109**: p. 127-146.

[6] Nanni, A., A. De Luca, and H.J. Zadeh, Reinforced concrete with FRP bars: Mechanics and design. 2014: CRC Press.

[7] Castro, H., et al., Mechanical properties and corrosion behaviour of stainless steel reinforcing bars. 2003. **143**: p. 134-137.

[8] García-Alonso, M., et al., Corrosion behaviour of new stainless steels reinforcing bars embedded in concrete. 2007. **37**(10): p. 1463-1471.

[9] Duarte, R., et al., Corrosion behavior of stainless steel rebars embedded in concrete: an electrochemical impedance spectroscopy study. 2014. **124**: p. 218-224.

[10] Medina, E., et al., Evaluation of mechanical and structural behavior of austenitic and duplex stainless steel reinforcements. 2015. **78**: p. 1-7.

[11] Yang, L., et al., Flexural buckling behavior of welded stainless steel box-section columns. 2016. **104**: p. 185-197.

[12] Gardner, L. and M.J.J.o.C.S.R. Theofanous, Discrete and continuous treatment of local buckling in stainless steel elements. 2008. **64**(11): p. 1207-1216.

[13] Wang, Y., et al., Experimental study of lateral-torsional buckling behavior of stainless steel welded I-section beams. 2014. **14**(2): p. 411-420.

[14] Hassanein, M. and N.J.J.o.C.S.R. Silvestre, Flexural behavior of lean duplex stainless steel girders with slender unstiffened webs. 2013. **85**: p. 12-23.

[15] Rabi, M., K. Cashell, and R.J.E.S. Shamass, Flexural analysis and design of stainless steel reinforced concrete beams. 2019. **198**: p. 109432.

[16] McGurn, J. Stainless steel reinforcing bars in concrete. in Proceedings of the International Conference of Corrosion and Rehabilitation of Reinforced Concrete Structures, Orlando, FL, FHWA. 1998. Citeseer.

[17] Cramer, S., et al., Corrosion prevention and remediation strategies for reinforced concrete coastal bridges. 2002. **24**(1): p. 101-117.

[18] Pérez-Quiroz, J., et al., Assessment of stainless steel reinforcement for concrete structures rehabilitation. 2008. **64**(11): p. 1317-1324.

[19] Afshan, S. and L.J.T.-W.S. Gardner, The continuous strength method for structural stainless steel design. 2013. **68**: p. 42-49.

[20] Huang, Y. and B.J.J.o.S.E. Young, Design of cold-formed lean duplex stainless steel members in combined compression and bending. 2015. **141**(5): p. 04014138.

[21] Ramberg, W. and W.R. Osgood, Description of stress-strain curves by three parameters. 1943.

[22] Rasmussen, K.J.J.J.o.c.s.r., Full-range stress–strain curves for stainless steel alloys. 2003. **59**(1): p. 47-61.

[23] Gardner, L.J.P.i.S.E. and Materials, The use of stainless steel in structures. 2005. **7**(2): p. 45-55.

[24] Li, Q., et al., Experimental and Theoretical Studies on Flexural Performance of Stainless Steel Reinforced Concrete Beams. 2020. **2020**.

[25] Davis, J.R., Stainless steels. 1994: ASM international.

[26] ÜBERBLICK, N.B.E. and A.E.A.I.U.J.O.-G.-J. APERÇU, Stainless steel reinforcement–a survey. 2005. **16**: p. 111.

[27] Cunat, P.-J.J.I., Paris, Alloying elements in stainless steel and other chromium-containing alloys. 2004.

[28] Alonso, M.C., et al., Corrosion behavior of duplex stainless steel reinforcement in ternary binder concrete exposed to natural chloride penetration. 2019. **199**: p. 385-395.

[29] Briz, E., et al., Stress corrosion cracking of new 2001 lean–Duplex stainless steel reinforcements in chloride contained concrete pore solution: An electrochemical study. 2018. **192**: p. 1-8.

[30] Rivera-Corral, J., et al., Corrosion behavior of steel reinforcement bars embedded in concrete exposed to chlorides: Effect of surface finish. 2017. **147**: p. 815-826.

[31] ASTM, S.J.A.A.A.M.-b., Standard specification for deformed and plain carbon-steel bars for concrete reinforcement. 2009.

[32] Cochrane, D.J.C.J., March issue, Success for stainless steel. 2003: p. 26-28.

[33] Lollini, F., et al., Corrosion behavior of stainless steel in chloride-contaminated carbonated concrete. 2019. **8**(2): p. 79-95.

[34] Rong, Y., Acoustic Emission Evaluation and Mechanical Property Characterization of Stainless Steel Specimens Manufactured by Powder Based 3-D Printer. 2015, University of Pittsburgh.

[35] Ali, M.A. and F.J.A.J.o.M.S. Ying, An Empirical finding of entrepreneurial factors & issues on stainless steel industry: a business case study of Outokumpu AB, Finland. 2014. **2**(4): p. 142.

[36] Virmani, Y. and G.J.F.-R.-.-. Clemena, FHWA, Corrosion Protection-concrete Bridges, Report No. 1998. **18**.

[37] Lee, H. and K. Neville, Handbook of epoxy resins. 1967.

[38] Clear, K.C. and Y.P.J.P.R. Virmani, Corrosion of nonspecification epoxy-coated rebars in salty concrete. 1983. **47**(1): p. 1-10.

[39] Schiessl, P.J.C.S.H.R.P., Ottawa, ON, Review of the KC, Inc., reports on effectiveness of epoxy-coated reinforcing steel. 1992.

[40] Smith, J.L. and Y.P. Virmani, Performance of epoxy coated rebars in bridge decks. 1996, United States. Federal Highway Administration.

[41] Weyers, R.E., et al., Field investigation of corrosion-protection performance of bridge decks constructed with epoxy-coated reinforcing steel in Virginia. 1997. **1597**(1): p. 82-90.

[42] Nanni, A., 1 Composites: Coming on Strong. 1999.

[43] Derias, M. and R. El-Hacha. Flexural and shear strengthening of masonry walls with FRP composite materials: State-of-art. in Proceedings Asia-Pacific Conference on FRP in Structures (APFIS 2007). 2007. Citeseer.

[44] Bank, L.C., Composites for construction: structural design with FRP materials. 2006: John Wiley & Sons.

[45] Fico, R.J.U.o.N.F.I., PH. D. Thesis, Limit states design of concrete structures reinforced with FRP bars. 2007.

[46] Zemajtis, J., R.E. Weyers, and M.M. Sprinkel, Performance evaluation of corrosion inhibitors and galvanized steel in concrete exposure specimens. 1999, Virginia Transportation Research Council.

[47] Manning, D., E. Escalante, and D.J.W. Whiting, DC, Panel Report—Galvanized Rebars as Long-Term Protective System. 1982.

[48] Record, C.U.I.S.J.R.I.F.P., Méthode rapide de caractérisation des roches mètres, de leur potentiel pétrolier et de leur degré d'évolution. 1977. **32**(1): p. 23-42.

[49] Frick, C.P., et al., Thermal processing of polycrystalline NiTi shape memory alloys. 2005. **405**(1-2): p. 34-49.

[50] Mast, R.F., et al., Flexural strength design of concrete beams reinforced with high-strength steel bars. 2008. **105**(5): p. 570.

[51] Kondubhairi, P.H. and M. Nagendra, EXPERIMENTAL ANALYSIS OF FLEXURAL BEHAVIOR OF RC BEAMS BY USING HIGH STRENGTH STEEL. 2019.

[52] ASTM, C., Test method for sieve analysis of fine and coarse aggregates. 2006.

[53] Lepech, M. and V.C. Li. Durability and long term performance of engineered cementitious composites. in Proceedings of the International Workshop on HPFRCC in Structural Applications. 2005.

[54] ASTM, C.J.S.p.f.m. and c.c.t.s.i.t. laboratory, 192-90a. 1990.

[55] Committee, A. and I.O.f. Standardization. Building code requirements for structural concrete (ACI 318-08) and commentary. 2008. American Concrete Institute.

[56] Bentz, E.C. and M.P.J.C.J.o.C.E. Collins, Development of the 2004 Canadian Standards Association (CSA) A23. 3 shear provisions for reinforced concrete. 2006. **33**(5): p. 521-534.

[57] Narayanan, R. and A. Beeby, Designers' Guide to EN 1992-1-1 and EN 1992-1-2. Eurocode 2: Design of Concrete Structures: General Rules and Rules for Buildings and Structural Fire Design. Vol. 17. 2005: Thomas Telford.

[58] Mirambell, E. and E.J.J.o.C.S.R. Real, On the calculation of deflections in structural stainless steel beams: an experimental and numerical investigation. 2000. **54**(1): p. 109-133.

[59] Castro, H., et al., Mechanical properties and corrosion behaviour of stainless steel reinforcing bars. 2003. **143**: p. 134-137.

[60] García-Alonso, M., et al., Corrosion behaviour of new stainless steels reinforcing bars embedded in concrete. 2007. **37**(10): p. 1463-1471.

[61] Duarte, R., et al., Corrosion behavior of stainless steel rebars embedded in concrete: an electrochemical impedance spectroscopy study. 2014. **124**: p. 218-224.

[62] Issa, M.S., I.M. Metwally, and S.M.J.E.S. Elzeiny, Influence of fibers on flexural behavior and ductility of concrete beams reinforced with GFRP rebars. 2011. **33**(5): p. 1754-1763.

[63] Rasheed, H.A., R. Nayal, and H.J.C.S. Melhem, Response prediction of concrete beams reinforced with FRP bars. 2004. **65**(2): p. 193-204.

[64] Okelo, R., Development and splice lengths criteria for straight fiber reinforced polymer composite bars in tension. 2003.

[65] Ansley, M.H.J.F.D.o.T., Investigation into the structural performance of MMFX reinforcing. 2002.

[66] Wibowo, L.S.B. ANALITICAL STUDY OF FLEXURAL STRENGTH AND DRIFT CAPACITY OF RC BEAMS UNDER MONOTONIC LOADING. in PROCEEDING International Conference Technopreneur and Education 2018. 2018.

[67] Pérez-Quiroz, J., et al., Assessment of stainless steel reinforcement for concrete structures rehabilitation. 2008. **64**(11): p. 1317-1324.

[68] Weyers, R.E., et al., Field investigation of corrosion-protection performance of bridge decks constructed with epoxy-coated reinforcing steel in Virginia. 1997. **1597**(1): p. 82-90.

[69] https://www.google.com.bd/search?q=plain+stainless+steel+bar&tbm=isch&ved

[70] Derias, M. and R. El-Hacha. Flexural and shear strengthening of masonry walls with FRP composite materials: State-of-art. in Proceedings Asia-Pacific Conference on FRP in Structures (APFIS 2007). 2007. Citeseer.

[71] Li, Q., et al., Experimental and Theoretical Studies on Flexural Performance of Stainless Steel Reinforced Concrete Beams. 2020. **2020**.

[72] ASTM, C., Test method for sieve analysis of fine and coarse aggregates. 2006.

[73] ABAQUS, ABAQUS/Standard User's Manual, 2002.